

**NASA CONTRACTOR  
REPORT**



**NASA CR-**



**NASA CR-2614**

**EVALUATION OF DISPERSION STRENGTHENED  
NICKEL-BASE ALLOY HEAT SHIELDS FOR  
SPACE SHUTTLE APPLICATION**

*R. Johnson, Jr. and D. H. Killpatrick*

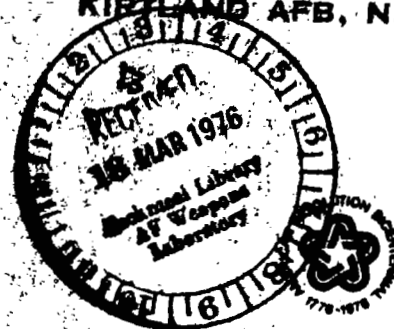
*Prepared by*

**MCDONNELL DOUGLAS ASTRONAUTICS COMPANY**

**Huntington Beach, Calif. 92647**

*for Langley Research Center*

**LOAN COPY: RETURN TO  
AFWL TECHNICAL LIBRARY  
KIRTLAND AFB, N. M.**



**NATIONAL AERONAUTICS AND SPACE ADMINISTRATION • WASHINGTON, D. C. • MARCH 1976**



0061540

1. Report No. NASA CR-2614		2. Government Accession No.	
4. Title and Subtitle  Evaluation of Dispersion Strengthened Nickel - Base Alloy Heat Shields for Space Shuttle Application		5. .... March 1976	
		6. Performing Organization Code	
7. Author(s)  R. Johnson Jr. and D. H. Killpatrick		8. Performing Organization Report No.	
		10. Work Unit No.	
9. Performing Organization Name and Address McDonnell Douglas Astronautics Company Huntington Beach, California 92647		11. Contract or Grant No. NASI - 11654	
		13. Type of Report and Period Covered Contractor Report	
12. Sponsoring Agency Name and Address National Aeronautics and Space Administration, Washington, D. C.		14. Sponsoring Agency Code	
15. Supplementary Notes Langley Technical Monitor - W. B. Lisagor Final Report			
16. Abstract The results obtained in a program to evaluate dispersion-strengthened nickel-base alloys for use in a metallic radiative thermal protection system operating at surface temperatures to 1477 K (2200 F) for the Space Shuttle are presented. Vehicle environments having critical effects on the thermal protection system are defined; TD Ni-20Cr characteristics of material used in the current study are compared with TD Ni-20Cr produced in previous development efforts; cyclic load, temperature, and pressure effects on TD Ni-20Cr sheet material residual strength are investigated; the effects of braze reinforcement in improving the efficiency of spotwelded joints are evaluated through tests of joint samples and through simulated mission tests of a braze reinforced heat shield; parametric studies of metallic radiative thermal protection systems are reported; and the design, instrumentation, and testing of full scale subsize heat shield panels in two configurations are described. Initial tests of full scale subsize panels included simulated meteoroid impact tests; simulated entry flight aerodynamic heating in an arc-heated plasma stream; programed differential pressure loads and temperatures simulating mission conditions; and acoustic tests simulating sound levels experienced by heat shields during boost flight. Based on full scale			
17. Key Words (Suggested by Author(s)) TD Ni - 20 Cr, Metallic Thermal Protection Systems, Heat Shields, Multiparameter Testing		18. Distribution Statement  Unclassified, Unlimited  Subject Category 26	
19. Security Classif. (of this report) Unclassified	20. Security Classif. (of this page) Unclassified	21. No. of Pages 147	22. Price* \$5.75

16. Abstract (Continued)

subsize panel tests, design, fabrication, and testing of a single configuration of a full-size, full scale TD Ni-20Cr heat shield test array was conducted. The design and fabrication of two additional full-size, full scale test arrays to be tested in flowing gas test facilities at the NASA Langley Research Center is also described. Cost and reusability evaluations of TD Ni-20Cr heat shield systems are presented, and weight estimates of a TD Ni-20Cr heat shield system for use on a Shuttle Orbiter vehicle are made.

## CONTENTS

Section 1	INTRODUCTION AND SUMMARY	1
Section 2	STUDY VEHICLE SELECTION AND THERMAL PROTECTION SYSTEM ENVIRONMENT	5
	2.1 Trajectory and Test Simulation	5
	2.2 TPS Performance Requirements	14
Section 3	MATERIAL PROPERTIES	17
	3.1 Cyclic Multiple Parameter Tests	18
	3.2 Braze-Reinforced Joint Tests	30
Section 4	DESIGN CONCEPT SELECTION	39
Section 5	SUBSIZE HEAT SHIELD PANEL DESIGN AND TESTING	43
	5.1 Design Criteria	44
	5.2 Meteoroid Impact Panel Tests	45
	5.3 Plasma Arc Tests	46
	5.4 Simulated Joint Tests	52
	5.5 Full-Scale Subsize Panel Tests	58
Section 6	FULL-SIZE HEAT SHIELD TEST ARRAY DESIGNS	83
	6.1 Heat Shield Array for Contractor Tests	84
	6.2 Test Array for the High Temperature Structures Tunnel	99
	6.3 Test Array for the Thermal Protection System Test Facility	103
Section 7	FULL-SIZE THERMAL PROTECTION SYSTEM TESTS	109
	7.1 TPS Array Instrumentation	109
	7.2 Preliminary Tests	112
	7.3 Simulated Mission Cyclic Tests	120
	7.4 Cost Studies	132
	7.5 Design Adequacy and Life Expectancy	137
	7.6 Installation and Inspection Evaluations	138
Section 8	CONCLUSIONS	143
	REFERENCES	147



# EVALUATION OF DISPERSION STRENGTHENED NICKEL-BASE ALLOY HEAT SHIELDS FOR SPACE SHUTTLE APPLICATION

By R. Johnson, Jr. and D. H. Killpatrick  
McDonnell Douglas Astronautics Company

## Section 1 INTRODUCTION AND SUMMARY

The objective of this program was to evaluate TD Ni-20Cr material for application in reusable radiative metallic heat shields as part of a Space Shuttle thermal protection system (TPS). The evaluations conducted in the program encompassed analytical and experimental efforts designed to assess the potential of TD Ni-20Cr heat shields in terms of reuse capability, refurbishment requirements, TPS weight, and TPS costs.

TD Ni-20Cr, a dispersion-strengthened metal for which production techniques were recently improved (Reference 1), was selected for this evaluation program because it extends the service temperature limits for uncoated metallic structures by 111°K to 333°K (200°F to 600°F) above those of current superalloys. A maximum reuse temperature of 1477°K (2,200°F) has been projected for TD Ni-20Cr heat shields.

The work conducted under this program is part of an overall effort by the NASA to evaluate advanced thermal protection systems for application in reusable space vehicles capable of entry from earth-orbital missions, maneuvering flight after entry, and horizontal landing. Such advanced thermal protection systems are also projected as being applicable to vehicles capable of sustained hypersonic flight within the earth's atmosphere at speeds ranging from Mach 6 to 12. A reusable space vehicle having the capabilities mentioned above is currently under development as a key part of the NASA Space Shuttle Program (SSP). This vehicle, designated the Orbiter, will be capable of at least 100 missions to earth orbit followed by entry flight and return to a designated landing site.

The Orbiter TPS has been recognized as a key system in determining the vehicle weight. Durability of the TPS will also be a significant factor in refurbishment requirements; hence, costs associated with refurbishment will be directly affected by the TPS performance in terms of reuse capability. A third design goal, TPS reliability, is a primary requirement for successful operational service of the Space Shuttle. The goal of improving these key TPS performance requirements - weight, cost, and reliability - resulted in establishment of this program to evaluate TD Ni-20Cr heat shields. The evaluations undertaken in this two-phase program were based upon a coordinated analytical and experimental approach that led to demonstration tests to determine the performance and behavior of a full-size, full-scale TD Ni-20Cr heat shield array when tested under simulated Space Shuttle TPS environmental conditions.

Phase I efforts (Reference 2) were devoted to (1) a definition of Shuttle Orbiter environments critical for its TPS, (2) material evaluations of TD Ni-20Cr sheet material to be used in this program, (3) parametric studies of TPS designs, and (4) tests of full-scale subsize TPS panel designs.

Results of TD Ni-20Cr material evaluations showed current sheet material used in this program to have essentially the same properties and characteristics as material produced in earlier development programs, with the exception that the current material exhibits lower elongation at failure in the temperature range of 921°K (1,200°F) to 1,368°K (2,000°F). Parametric studies of six different heat shield designs resulted in the selection of two TPS configurations for competitive tests in Phase I. The two designs were (1) a corrugation-stiffened single-face heat shield panel with packaged insulation underneath it and (2) a zee-stiffened single-face panel with the same type of insulation package.

Full-scale subsize panels were used in several tests to evaluate the two designs selected from parametric studies, to evaluate two panel edge joint designs, and to evaluate simulated meteoroid impact effects on the TD Ni-20Cr panel designs. Panels with full-scale cross sections but subsize in

planform area were designed and fabricated into test components having a 45.7-cm (18-in.) length and a width of approximately 17.3-cm (6.8-in.). Panels of this size, the largest fabricated for Phase I tests, were subjected to cyclic tests consisting of programmed differential pressure loads, temperature profiles, and environmental pressures that simulated boost and entry flight environments applicable to TD Ni-20Cr metallic radiative heat shields. Acoustic exposures were interspersed at intervals to simulate critical acoustic loads imposed on the TPS during boost flight.

Panel edge joint designs subjected to cyclic exposures in a plasma-arc stream simulating repeated entry flights showed that either of the two designs tested was effective in preventing severe ingestion of hot gases at the panel edges. One of the edge closeouts was a simple overlap design, and the second utilized a closure strip that covered both edges of adjoining panels.

Phase I simulated mission tests using the selected heat shield designs showed the TD Ni-20Cr heat shields to be capable of sustaining 100 simulated mission profiles. However, reinforcement of heat shield attach points was required to complete the full 100 test cycles. Simulated meteoroid impact tests with sample panels showed that, with the criteria used, penetration occurred when impact was made on a single 0.0254-cm (0.010-in.) thick sheet, but impact in the region of a double thickness of 0.0254-cm (0.010-in.) material resulted in cratering of the outer sheet without penetration. Subsequent exposures in a plasma-arc stream that simulated entry airflow conditions resulted in no additional degradation of either type of impact point.

As a result of Phase I evaluations, a corrugation-stiffened single-face panel design was selected for the full-scale, full-size TPS test arrays tested in Phase II (Reference 3). The Phase I tests of two panel edge closure designs in simulated entry flow conditions led to the selection of a closure strip design to cover the space between panels.

During Phase II three full-size TD Ni-20Cr heat shield arrays were designed and fabricated, one for cyclic simulated mission tests in the McDonnell Douglas Space Simulation Laboratory and two for testing in flowing gas

facilities at the NASA Langley Research Center. All three test arrays used the same basic heat shield panel design, a corrugation-stiffened single-face panel with nominal planform dimensions of 48.2-cm by 46.0-cm (19-in. by 18.1-in.). When the interpanel closure strip dimensions are accounted for, the nominal heat shield module size is 50.4-cm by 50.4-cm (20-in. by 20-in.). The full size heat shield arrays for Phase II tests included surface panels, panel closeouts, a simulated substructure, panel supports and attachments, and insulation packages between the panels and the substructure. Differences in test fixture planform sizes, depths, and attachment requirements caused differences in each test array, particularly in the closeout panels, the edge details, and in the insulation depth between the heat shields and the simulated substructure.

The program was managed by Read Johnson, Jr. under the direction of Dr. J. F. Garibotti, Chief Structures Engineer, Research and Development, Structures, Development Engineering. Major contributions were made to the program by Dr. D. H. Killpatrick, Material and Process, Development Engineering. Others who contributed to the program and to the preparation of this report are: B. G. Fitzgerald, coordination of tests conducted at the McDonnell Douglas Research Laboratories; Ralph Lilienkamp, in charge of Space Simulation Chamber tests; John Hill and John McDaniels, Simulation Test Engineers; W. B. Shelton, Acoustic Test Engineer; W. A. Rinehart, in charge of Plasma Arc Tunnel tests; B. A. Cramer, analysis of cumulative creep effects.

## Section 2

### STUDY VEHICLE SELECTION AND THERMAL PROTECTION SYSTEM ENVIRONMENT

The initial program efforts were devoted to (1) selection of a representative Shuttle Orbiter configuration, (2) selection of a typical location on the Orbiter for application of a TD Ni-20Cr TPS, and (3) review of critical trajectories, TPS environments, and simulation requirements for use in material and panel tests. Results of the initial work are summarized in this section, and more detailed discussions of entry trajectories and TPS criteria are presented in Reference 2.

#### 2.1 TRAJECTORY AND TEST SIMULATION EVALUATION

A review of the Orbiter boost, entry, and cruise flight trajectories was conducted with the objectives of establishing TPS performance requirements for vehicle regions where TD Ni-20Cr may be utilized effectively and to establish simulation requirements to be used in material characterization tests and TPS component tests.

The Shuttle Orbiter configuration selected as the baseline vehicle for heat shield evaluations is shown in Figure 2-1 in the launch configuration in which the orbiter is mated with the external tank and solid rocket motors (SRM). The delta-winged Orbiter configuration is typical of those designed to orbit a 27,250 kg (60,000 lb) payload and to have a cross-range on entry of approximately 2,040 km (1,100 nm). Dimensions of the baseline Orbiter are shown in greater detail in Figure 2-2.

##### 2.1.1 Boost, Entry, and Cruise Trajectories

The basic design pressures and temperatures experienced by the TPS surface panels were determined by the vehicle trajectories during boost, entry, and terminal approach phases of the mission. To define the TPS panel pressure and temperature histories, the trajectories for the baseline Orbiter were reviewed and a critical set of boost, entry and cruise trajectories were selected. From the selected trajectories critical flight parameters were defined as shown in Figure 2-3.

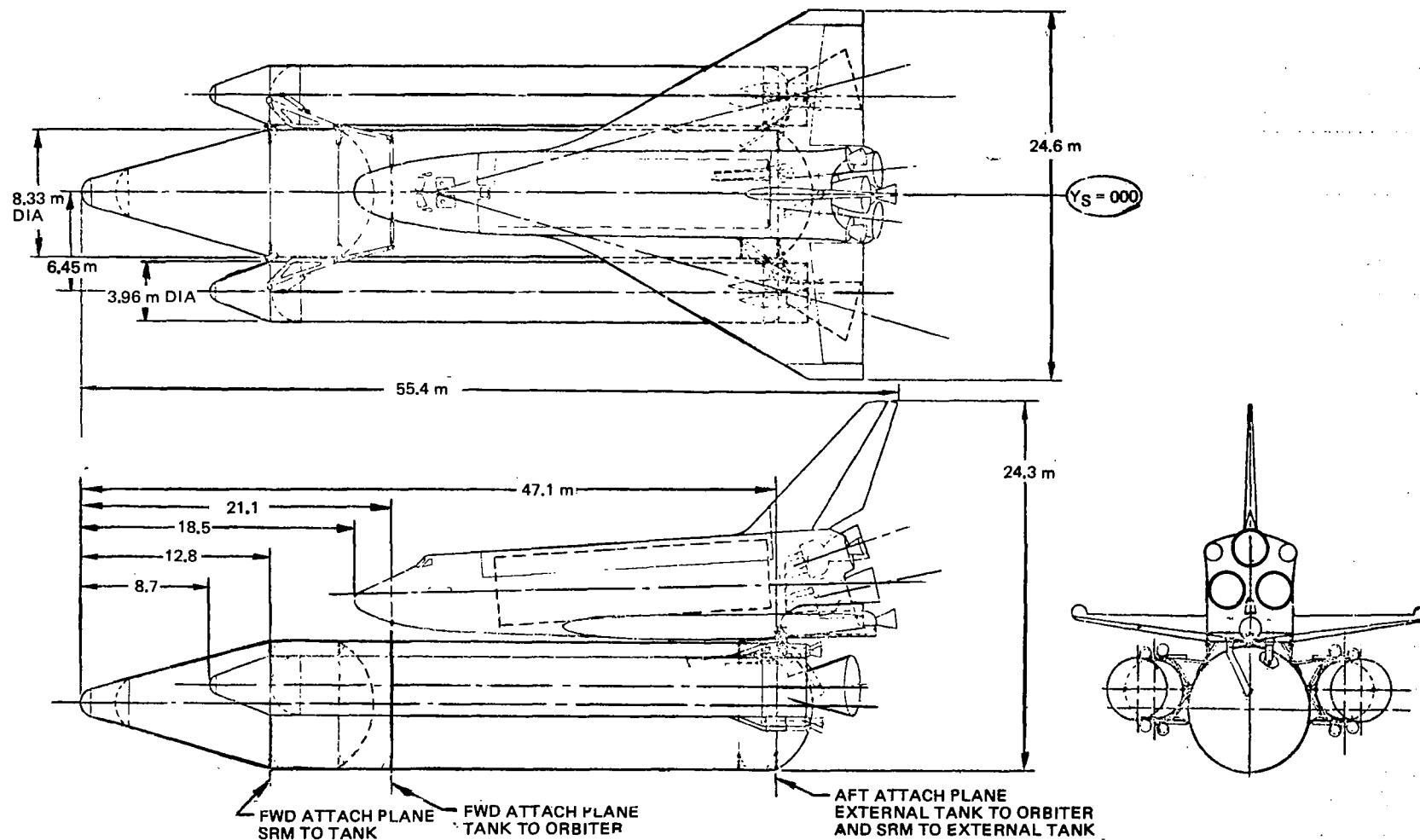


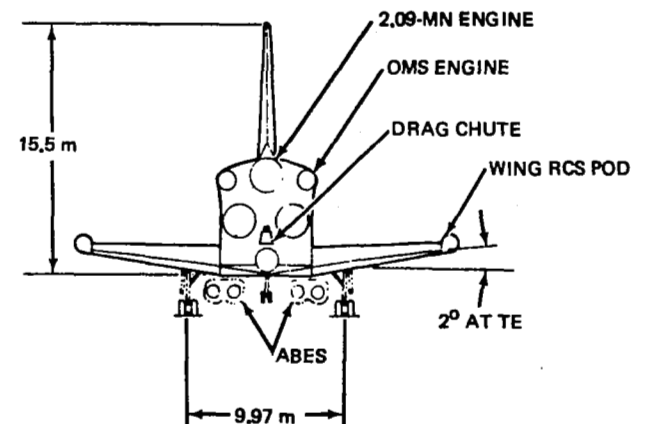
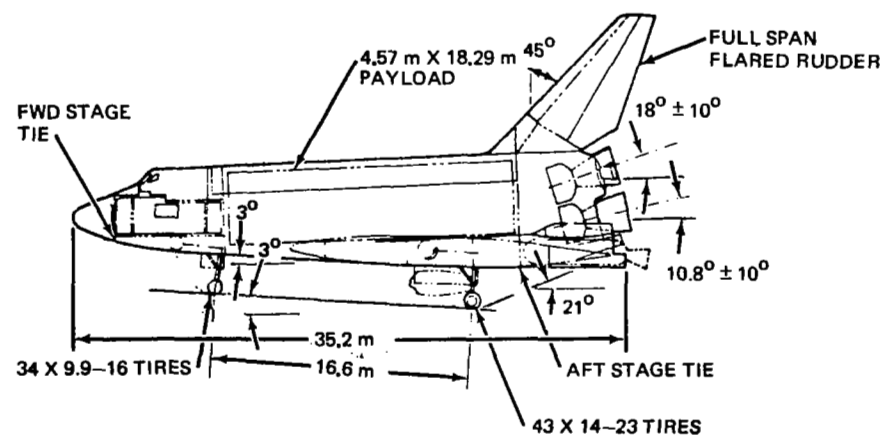
Figure 2-1. Shuttle Mated Configuration

THEO AREA	353	m <sup>2</sup>
EXPOSED AREA	224	m <sup>2</sup>
AR	1.71	
ELEVON AREA	50.9	m <sup>2</sup>
WETTED AREA W PODS	471	m <sup>2</sup>
WING BODY INTERSECTION	42.9	m <sup>2</sup>
ML VOLUME W PODS	169.6	m <sup>3</sup>
AIRFOIL	NACA 0008-64	

THEO AREA	41.8 m <sup>2</sup>
EXPOSED AREA	40.1 m <sup>2</sup>
ASPECT RATIO	1.74
RUDDER AREA	15 m <sup>2</sup>
WETTED AREA	82.5 m <sup>2</sup>
TAIL BODY INTERSECTION	2.8 m <sup>2</sup>
ML VOLUME	11.6 m <sup>3</sup>

WETTED AREA	1,232	m <sup>2</sup>
PROJECTED PLANFORM	409	m <sup>2</sup>
ML VOLUME	1,154	m <sup>3</sup>

WETTED AREA	
FWD	128 m <sup>2</sup>
MID	413 m <sup>2</sup>
AFT W OMS AND BODY FLAP	147.2 m <sup>2</sup>
BASE	34.5 m <sup>2</sup>
TOTAL	724 m <sup>2</sup>
ML VOLUME	972.6 m <sup>3</sup>
PROJECTED PLANFORM	184.9 m <sup>2</sup>



**Figure 2-2. Baseline Orbiter Configuration**

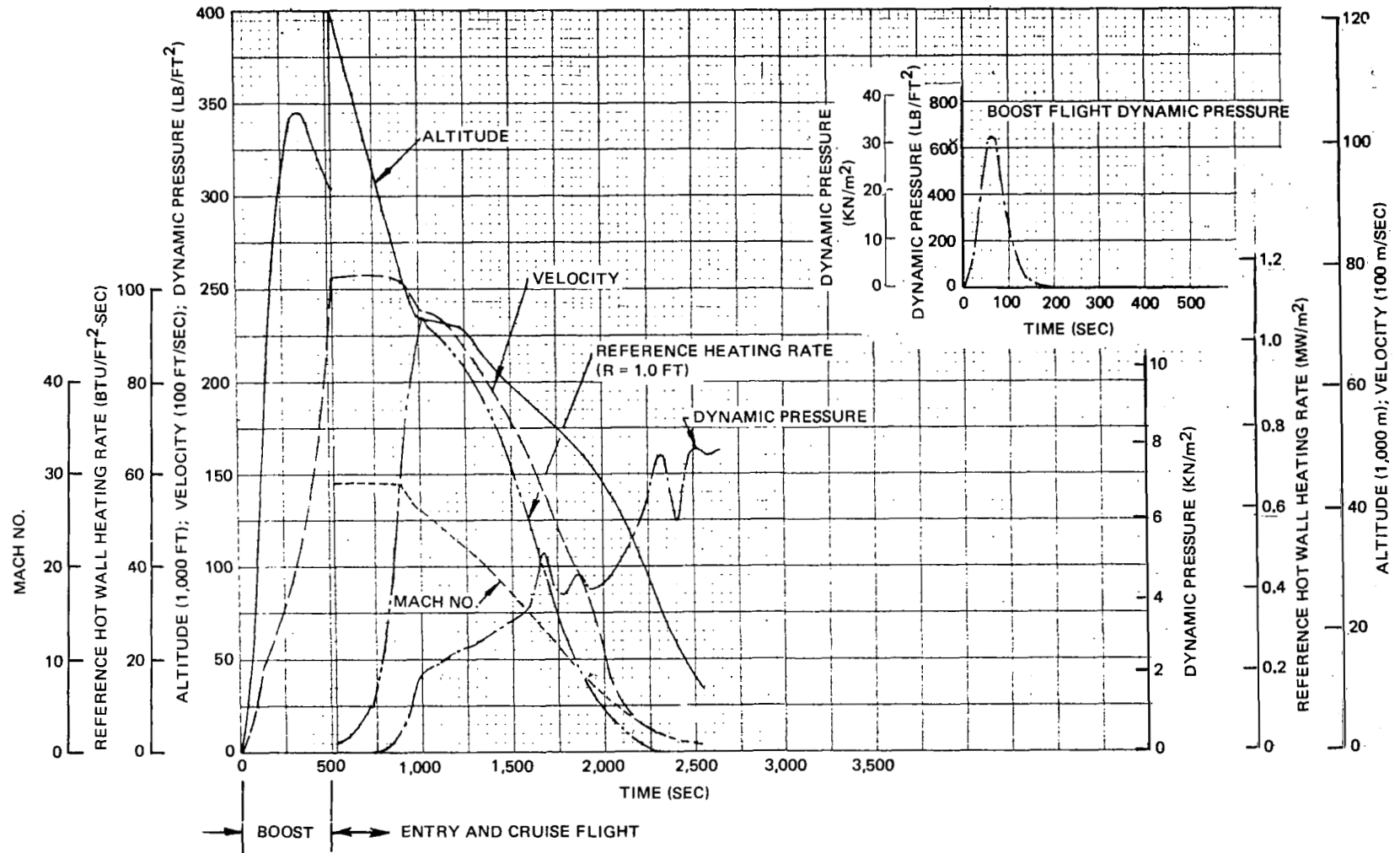


Figure 2-3. Baseline Orbiter Flight Parameters



After selecting critical trajectory parameters, a typical TD Ni-20Cr heat shield area on the lower surface of the Orbiter was chosen for the purpose of deriving specific time-histories of TPS temperatures, differential pressures, and static pressures to be used in Phase I studies and in subsequent Phase II designs of full-scale, full-size TD Ni-20Cr heat shield arrays. As a criterion for initial selection of a typical surface area for a TD Ni-20Cr TPS, a maximum reuse temperature of 1,477°K (2,200°F) was chosen, along with 100 entry flights as the nominal number of missions. Thermal analyses of the baseline Orbiter showed maximum lower surface temperatures to range from 1,368°K to 1,699°K (2,000°F to 2,600°F) during entry flight. The maximum temperature isotherms for the Orbiter configuration are shown in Figure 2-4. From the isotherms shown in Figure 2-4, a position on the lower surface centerline at  $X/L = 0.35$  was chosen to define panel design parameters. The selected position sustains a maximum temperature of 1,477°K (2,200°F) and it is also subjected to maximum temperatures for a significant portion of the entry period due to the early initiation of turbulent flow. Figure 2-5 shows the selected position on the vehicle.

Using the flight parameters of Figure 2-3, the critical panel temperature and pressure environments for the selected lower surface position were established. The critical temperature and pressure conditions, shown in Figure 2-6, were then used to develop test profiles for programmed multiple-parameter cyclic tests of TD Ni-20Cr material samples and for load and temperature profiles used in the heat shield panel tests. Such test profiles are discussed subsequently in Sections 3, 5, and 6.

#### 2.1.2 Acoustic Environment

The overall sound pressure levels predicted for the baseline Orbiter configuration are shown in Figure 2-7 for launch and ascent conditions. The full-scale subsize panel designs developed for Phase I tests were analyzed for resistance to fatigue failures at a maximum overall sound pressure level (OASPL) of 160 db in accordance with the predicted values for the Orbiter forward lower surface shown in Figure 2-7. The acoustic fatigue analysis conducted for the Phase I test panels (Reference 2, Appendix D) was reviewed during Phase II and the analytical results were found to be valid

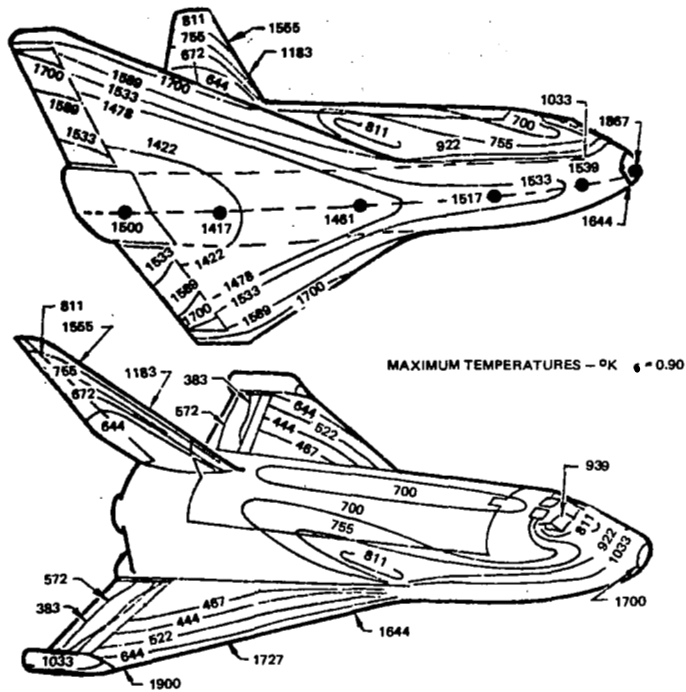


Figure 2-4. Maximum Temperatures During Entry

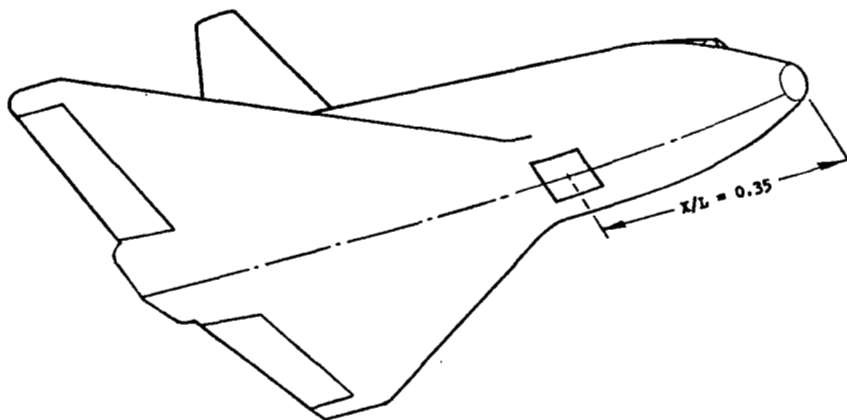


Figure 2-5. Orbiter Surface Area for TPS Parametric Study

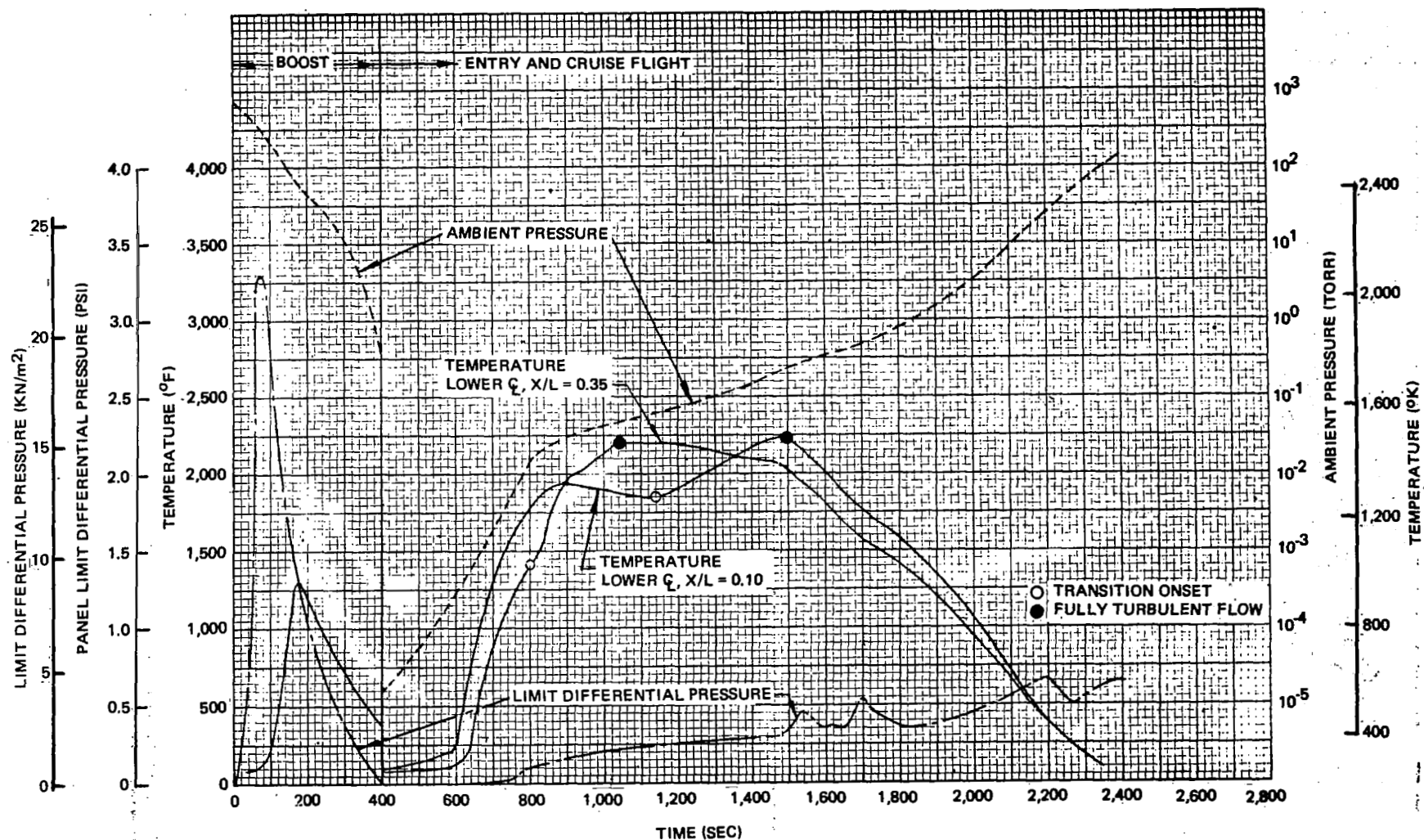
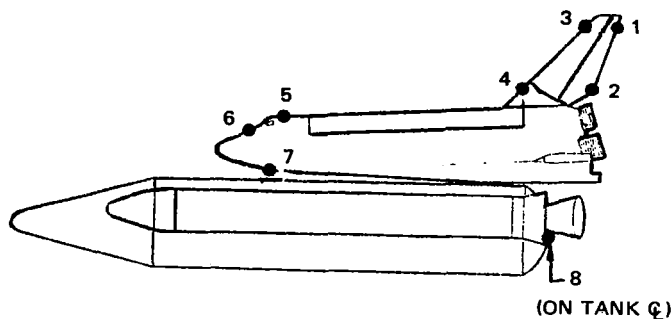


Figure 2-6. Temperature, Panel Differential Pressure, and Ambient Pressure Time-Histories



OVERALL SOUND PRESSURE LEVEL (dB)			
	LAUNCH*	ASCENT**	
1	164.6	161	*BASED ON TEST FIRINGS OF SATURN J-2 ENGINES AT NASA-MSFC
2	165.9	161	
3	163.6	155	
4	163.3	146	
5	158.2	161	
6	157.6	148	**BASED ON AMES WIND TUNNEL TEST DATA
7	158.0	160	
8	165.0	153	

Figure 2-7. Orbiter Overall Sound Pressure Levels

for Phase II panels due to similarity of design and test conditions (Reference 3). A duration of 30 seconds at 160 db during liftoff was selected as being the critical acoustic environment. Fatigue analyses, presented in Reference 2, Appendix D, were based on the 160 db level for 100 missions with a life factor of 10.

### 2.1.3 Meteoroid Environment

The meteoroid environment selected for use in determining simulated meteoroid impact test conditions was taken from Reference 4. References 4 and 5 formed the basis for selecting criteria for the meteoroid environment in the near-earth and cislunar regions and for penetrations of metallic TPS panels. In Reference 4, a model of the average cumulative total meteoroid flux-mass was developed for the region of 1 astronomical unit (1 A. U.) from the sun near the ecliptic plane. This model is shown in Figure 2-8, which also shows data from various sources in comparison to the adopted model. The probability-velocity distribution developed in Reference 4 gives an average velocity of 20 km/s for sporadic meteoroids in the near-earth region.

The meteoroid environment criteria specified in Reference 5 were also reviewed, and meteoroid environments specified therein were found to agree with those of Reference 4. The meteoroid flux-mass model shown in Figure 2-8 is taken from Reference 4, this model being expressed by the equations:

$$\left. \begin{aligned} 10^{-6} \leq m \leq 10^0: \log N_t &= -14.37 - 1.213 \log m \\ 10^{-12} \leq m \leq 10^{-6}: \log N_t &= -14.339 - 1.584 \log m - 0.063 (\log m)^2 \end{aligned} \right\} (1)$$

where

$m$  = meteoroid mass, g

$N_t$  = particles of mass,  $m$ , or greater per square meter per second

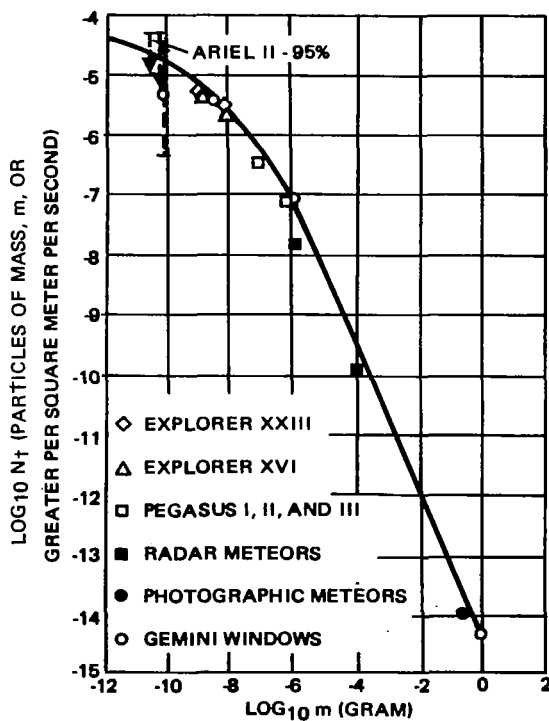


Figure 2-8. Meteoroid Flux-Mass Model

Also, Reference 7 specifies an average meteoroid velocity of 20 km/s and a mass density of  $0.5 \text{ g/cm}^3$ . The criteria of Reference 6 stipulate that the Space Shuttle shall be designed for at least a 0.95 probability of no puncture during the maximum total time (100 to 500 missions) in orbit using the meteoroid model defined in Figure 2-8 combined with the mass and velocity values quoted above from Reference 7. The penetration criterion of a 0.95 probability of no puncture was reviewed in greater depth during full-scale subsize panel design efforts. Findings from that review are discussed in Section 5 and in Reference 2, Appendix E.

## 2.2 TPS PERFORMANCE REQUIREMENTS AND DESIGN CRITERIA

A review of the Space Shuttle requirements (Reference 6) was also made to determine additional performance requirements for the Orbiter TPS. A summary of the pertinent requirements for TPS designs is presented in Table 2-1. The basic set of requirements given in Table 2-1 was used in analytical comparisons of candidate designs, in design of all TD Ni-20Cr heat shields and TPS test components, and as a guide in determining objectives in tests of TPS designs.

Table 2-1  
SUMMARY OF HEAT SHIELD DESIGN CRITERIA

Mission Phase	Limit Differential Pressure ( $\text{kN/m}^2$ )	Overall Sound Pressure Level	Panel Flutter	Meteoroid Impact	Cumulative Creep In 100 Missions cm (in.)	Factor of Safety(1)
Boost Flight	+22.75 (Collapse) -6.89 (Burst)	160 db	No flutter at 1.5 times local dynamic pressure.	--	--	1.50
Orbital Mission	--	--	--	Designed for a 0.95 probability of one or less puncture in a 7-day mission.	--	--
Entry Flight	+3.45 (Collapse) -3.45 (Burst)	--	Same as Boost Flight	--	$\delta = 0.254 + 0.0254 L$ ( $\delta = 0.10 + 0.01L$ ) (See Section 2)	1.50

(1) See Reference 2, Appendix A for detailed factors used in combined loads.

Heat shield creep limits were also examined in establishing design criteria. Previous criteria have specified that materials shall not exhibit cumulative creep strain leading to rupture, detrimental deformation, or creep buckling during their service life. However, a specific amount of allowable deformation in metallic TPS panels was not stipulated; in lieu of such a specified amount, the following equation for maximum cumulative panel deformation during the life of the vehicle was used in initial sizing studies:

$$\delta = 0.25 + 0.025L \text{ (cm)}$$

(2)

$$(\delta = 0.1 + 0.01L \text{ (in.)})$$

where

$\delta$  = maximum normal panel deflection, cm (in.)

L = distance between panel supports, cm (in.)

Equation (2) was used in the initial sizing of heat shield panel cross sections; however, a more detailed analysis was conducted as a part of the parametric studies of various designs presented in Reference 2, Appendix D. Other criteria presented in Reference 2, Appendix A are specific with respect to flight conditions, loads, design factors of safety, internal temperatures that are to be maintained, and duration of missions. Those criteria were used in parametric studies and in the design of test components.





### Section 3

#### MATERIAL PROPERTIES

A majority of TD Ni-20Cr sheet characterization tests to evaluate current material properties were conducted under separate or recently completed contracts sponsored by the Lewis Research Center (LeRC) of the NASA. The two evaluation programs sponsored by LeRC are (1) NAS3-15558, Characterization of TD NiCr Material, and (2) NAS3-15567, Forming and Joining of TD NiCr. The program for characterization of material properties (NAS3-15558) provided all necessary material property data with the exception of cumulative creep and residual strength characteristics after mission simulation cycles. The latter properties were evaluated in this program through multiple-parameter tests of tensile samples. Such tests were conducted using a modified Astrofurnace chamber in which the samples were subjected to programmed cycles of stress, temperature, and pressure that simulated critical Orbiter mission conditions for a metallic radiative heat shield. In addition to the multiple-parameter tests, single lap-shear joint specimens were tested to evaluate the improvements in joint efficiency resulting from braze-reinforcement of spot-welded, spot diffusion-bonded, and seam-welded joints. Braze-reinforcement of joint areas in thin-gage heat shields was considered a promising technique to improve both panel fatigue strength under boost flight acoustic loads and panel resistance to joint degradation from long-term thermal and load conditions of repeated entry flights. A braze-reinforced spot welded closeout panel was later included in the contractor test array during Phase II tests. Results of such tests are presented in Section 6. The multiple-parameter tests of tensile samples and the braze-reinforced joint tests are discussed in the remainder of this section while the results from material property tests conducted under NAS3-15558 are presented in Reference 2, Appendix B.

Strength levels used for design of the full-scale subsize panels were selected from the data contained in Reference 2, Appendix B which were then modified to account for degradation effects of exposure to the elevated-temperature, low-pressure environment projected for Orbiter entry flights. The analysis used in reducing strength levels to account for such environmental degradation is

presented in Reference 2, Appendix C, which also contains comparisons of the analytical values with results obtained in residual strength tests of TD Ni-20Cr samples subjected to simulated mission environments. Results of the cyclic multiparameter tests were also reviewed and compared with the computed strength degradations used to obtain design allowables.

### 3.1 CYCLIC MULTIPLE-PARAMETER TESTS

The multiple-parameter test series consisted of repeated cycles of stress, static pressure, and temperature profiles that were designed to simulate mission conditions on a Shuttle Orbiter metallic heat shield. Prior to the start of testing, all TD Ni-20Cr specimens were oxidized at 1,451°K (2,150°F) for 1 hour at 1 atmosphere air pressure to produce a dark, high-emittance surface oxide. The basic test profile of chamber pressure, temperature, and stress are shown in Figure 3-1. Temperature and chamber pressure profiles were maintained as shown in Figure 3-1 for all test samples, but the stress profiles were ratioed for different sets of test specimens. The ratios used in varying the stress profiles are given in Table 3-1, which also shows the peak stress

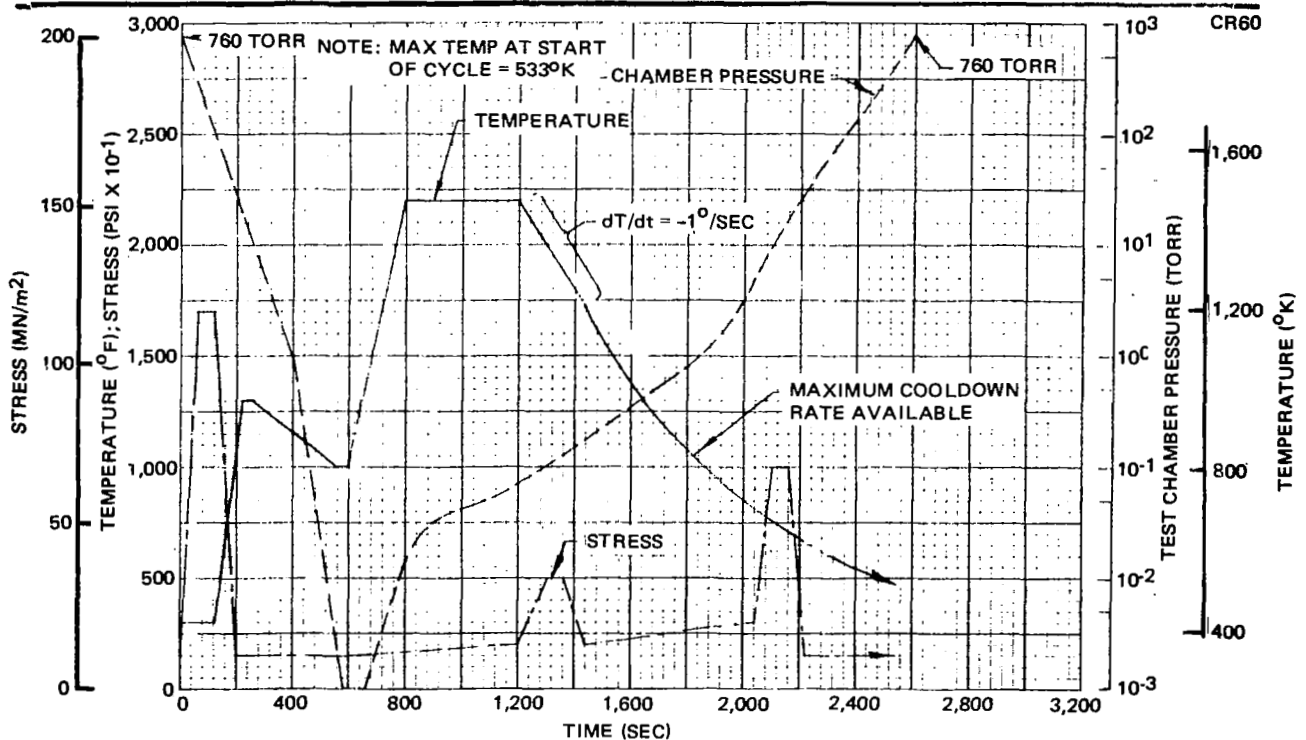


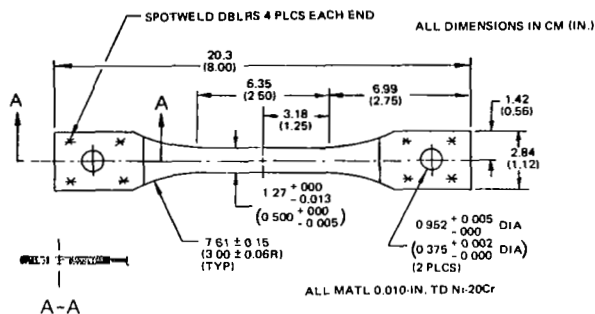
Figure 3-1. Cyclic Multiple Parameter Test Profiles

Table 3-1

TEST MATRIX FOR CYCLIC CREEP STRAIN SPECIMENS

Test Set No.	Specimen Number	Specimen Orientation	Stress Profile	Max. Stress At 1,368°K; MN/m <sup>2</sup> (psi)	No. of Cycles
I	1	L (1)	Basic (3)	34.4 (5,000)	100
	2	L	Basic	34.4 (5,000)	
II	3	T(2)	0.8 x Basic	27.6 (4,000)	100
	4	T	0.8 x Basic	27.6 (4,000)	
III	5	L	0.9 x Basic	31.0 (4,500)	100
	6	L	0.9 x Basic	31.0 (4,500)	
IV	7	T	0.7 x Basic	24.1 (3,500)	100
	8	T	0.7 x Basic	24.1 (3,500)	
V	9	L	0.8 x Basic	27.6 (4,000)	75
	10	L	0.8 x Basic	27.6 (4,000)	
VI	11	T	0.7 x Basic	24.1 (3,500)	75
	12	T	0.7 x Basic	24.1 (3,500)	

- (1) Longitudinal  
 (2) Transverse  
 (3) See Figure 3-1



applied to the samples at 1,368°K (2,000°F) during simulated entry flight. The tensile sample configuration used in the tests is also shown in Table 3-1. A sheet thickness of 0.0254-cm (0.010-in.) was used for all samples since it is representative of the thin sheet that would be characteristic of those used in radiative metallic heat shields.

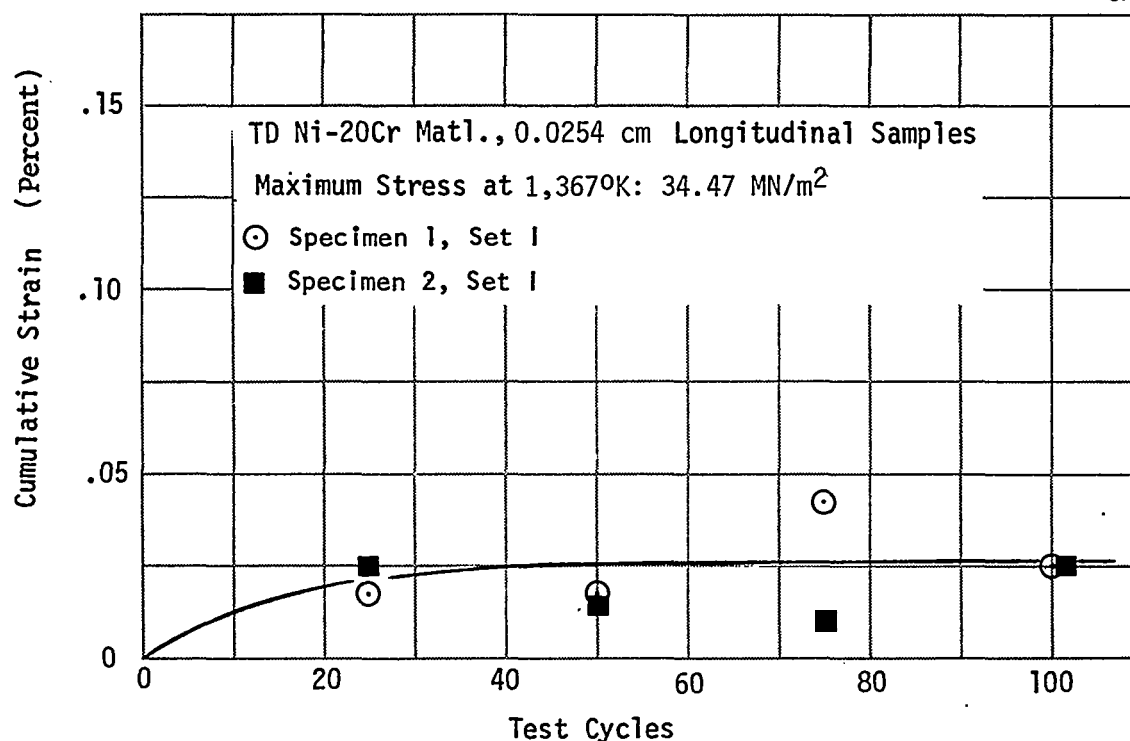
The multiple-parameter tests were conducted in a modified Astrofurnace unit at the McDonnell Douglas Research Laboratories at St. Louis. An extension to the furnace chamber permits force transducers to be located inside the chamber. This modification uses a force transducer for each test specimen. Such an arrangement provides direct measurement of the load in each specimen and, by locating the transducers internally, avoids unaccounted-for pressurization effects on the sample caused by pressure differences between the low chamber pressure and the one-atmosphere pressure outside the chamber.

A maximum stress level of  $34.4 \text{ MN/m}^2$  (5,000 psi) was selected for the longitudinal samples at elevated temperature conditions based on a review of data from Reference 7 that defines cumulative creep at 100 hr as a function of stress. As a result of the review of cumulative creep data, it was judged that  $34.4 \text{ MN/m}^2$  was an upper stress limit at  $1,368^\circ\text{K}$  ( $2,000^\circ\text{F}$ ) beyond which large creep deformations and an accompanying severe strength degradation might be expected for 0.0254-cm (0.010-in.) thick TD Ni-20Cr material. Similarly, a stress level of  $27.6 \text{ MN/m}^2$  (4,000 psi) was selected as a peak stress at elevated temperatures for transverse samples. To obtain data over a range of stresses, the samples were divided into three sets each for longitudinal and transverse samples (Table 3-1). Maximum stresses were reduced to  $30.9 \text{ MN/m}^2$  (4,500 psi) and  $27.6 \text{ MN/m}^2$  (4,000 psi) for the additional sets of longitudinal samples, while a similar reduction to  $24.1 \text{ MN/m}^2$  (3,500 psi) was made for the remaining sets of transverse samples.

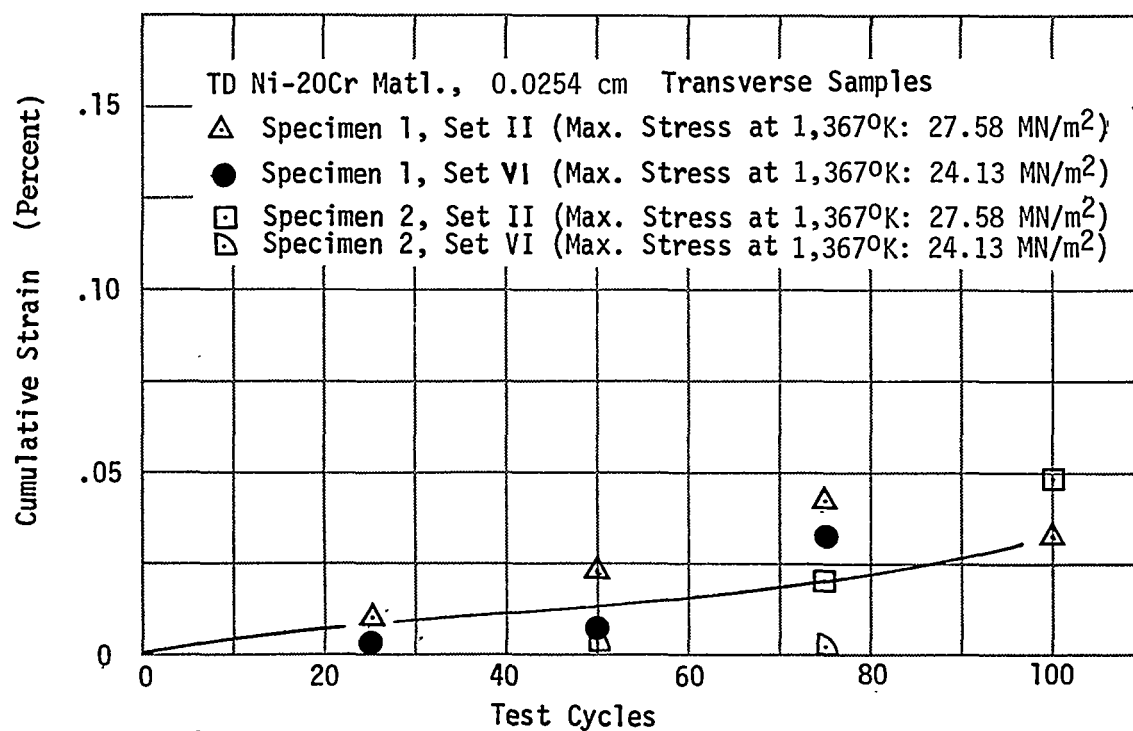
### 3.1.1 Cumulative Creep Strains

A total of 100 cycles was applied to each tensile sample in test sets I, II, III, and IV while each sample of sets V and VI received 75 cycles (Table 3-1). The cumulative creep strain of each specimen was determined at 25-cycle intervals. Cumulative strain was determined by using a Unitron Measuring Microscope to measure the change in distance between reference marks placed on each specimen in the center of the gage length.

Typical cumulative strain data are shown in Figure 3-2 as a function of number of test cycles. The very low strains experienced by the samples, combined with the accuracy limits of the measuring technique, yielded scatter in the data that is especially evident in Figures 3-2d and 3-2e. The maximum average cumulative strain developed from tensile stresses in the cyclic tests was approximately 0.04 percent, a magnitude that is not expected to be critical in design of TD Ni-20Cr heat shields. However, permanent deformations may also occur from cyclic thermal stresses occurring in buildup heat shields; deformations from thermal cycles are discussed subsequently in Sections 5 and 6.

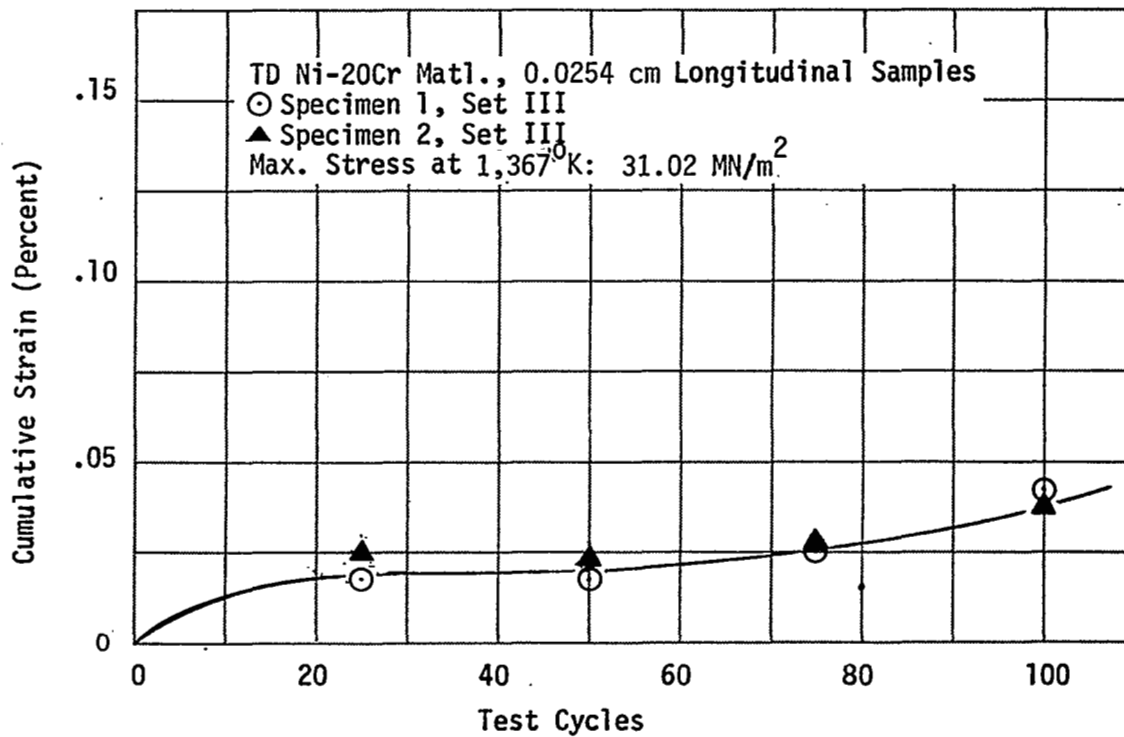


a. SET I, LONGITUDINAL SAMPLES

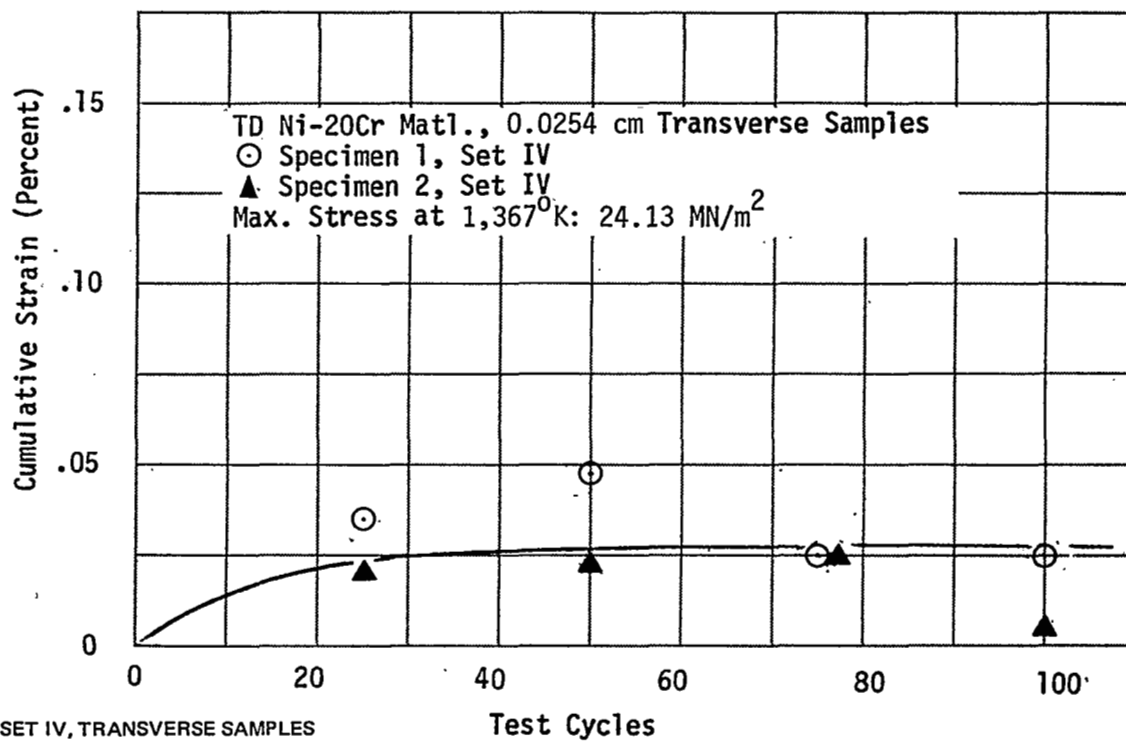


b. TRANSVERSE SAMPLES

Figure 3-2. Cumulative Average Strain Versus Test Cycles (Page 1 of 3)



c. SET III, LONGITUDINAL SAMPLES



d. SET IV, TRANSVERSE SAMPLES

Figure 3-2. (Page 2 of 3)

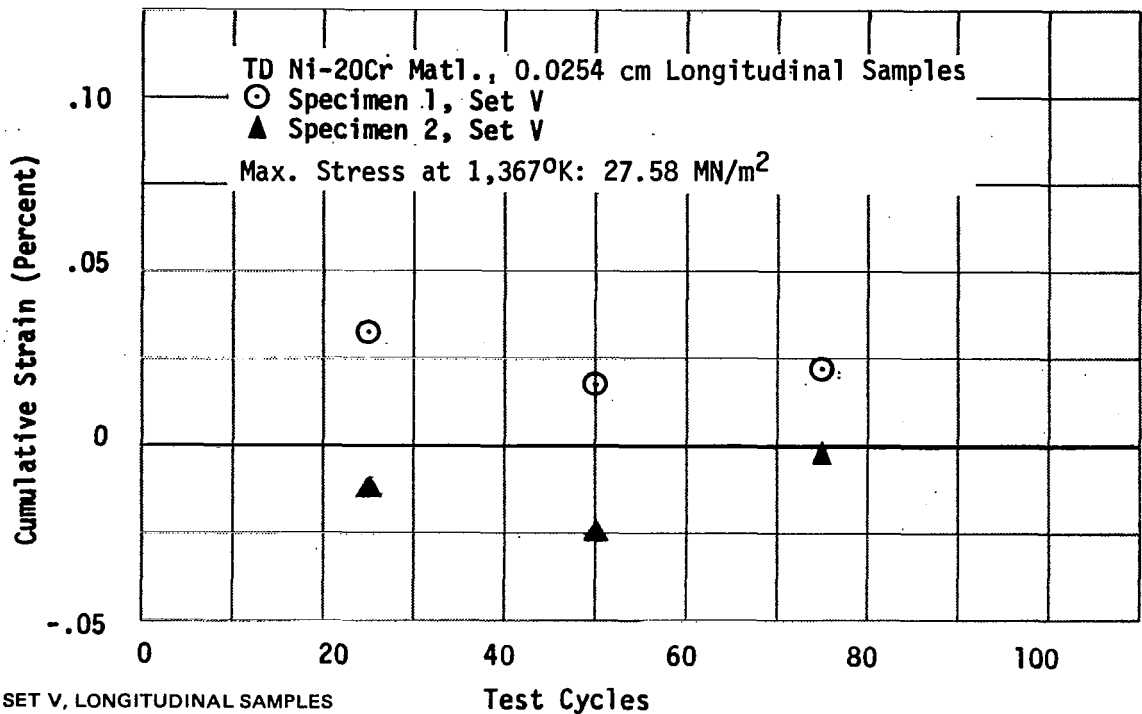


Figure 3-2. (Page 3 of 3)

Cumulative strains generated in the multiple-parameter cyclic tests are compared in Figure 3-3 with strains recorded on other samples tested in constant-load and temperature tests that are reported in Reference 7. The stress levels used for the cyclic test points plotted in Figure 3-3 were the maximum stresses at elevated temperature (Figure 3-1), and as such represent a somewhat shorter total time at those stresses than shown for the constant-load specimens reported in Reference 7. Despite the differences in stress and temperature histories between the two test series, relatively low total strains are shown by the TD Ni-20Cr samples subjected to either cyclic multiple-parameter tests or to constant-load and temperature tests at maximum stress levels in the range of 24.1 to 31.0 MN/m<sup>2</sup> (3,500 to 4,500 psi).

Figure 3-3 illustrates the typical elevated temperature characteristic of TD Ni-20Cr in which strains are exceptionally low ( $\epsilon \leq 0.1$  percent) in either cyclic or constant tensile load conditions until a critical stress level is applied, such a level being dependent on direction of applied stress (longitudinal or transverse) and temperature. Stresses above the critical level produced rapidly increasing cumulative strains and the samples generally

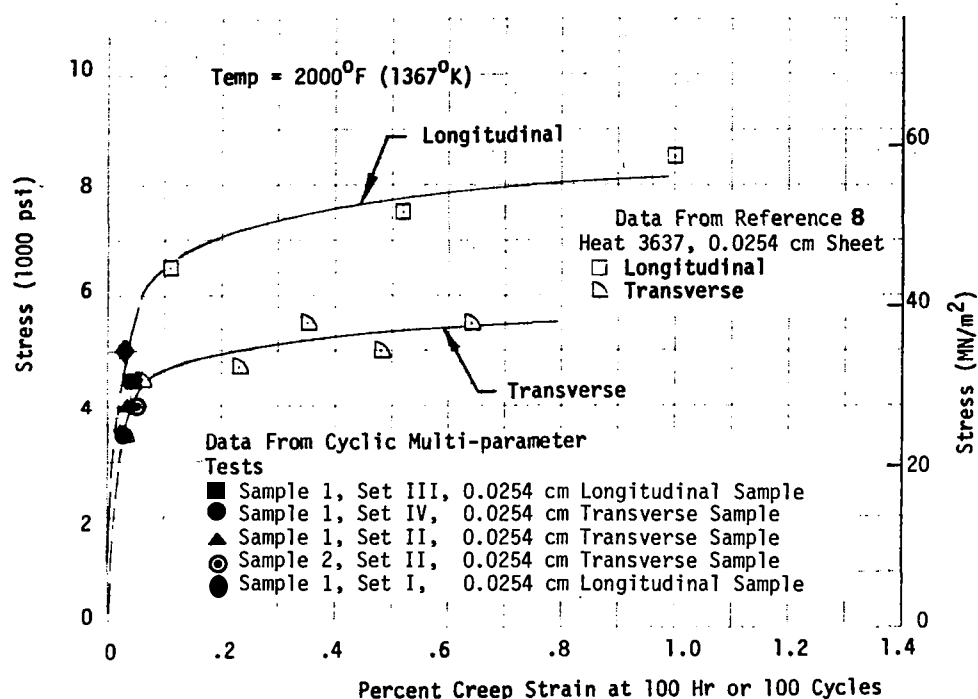


Figure 3-3. Strain Comparison Between Cyclic and Constant Load Tests

failed at total strains ranging from 1 to 2 percent. Such behavior is further reflected in the data of Reference 2, Appendix B.

None of the cyclic test samples was stressed above the critical level, and consequently maximum cumulative strains were less than 0.05 percent. Also, none of the test samples failed and all were available for residual strength evaluations.

### 3.1.2 Residual Strength Tests

Residual strength characteristics were evaluated at room temperature and 1,368°K (2,000°F), half the samples being tested at room temperature and the remainder at 1,368°K (2,000°F). Ultimate tensile strength, yield strength, and elongation at failure were measured during residual strength tests.

Results of all residual strength tests conducted with cyclic creep samples are summarized in Table 3-2. Test results showed a significant loss of elongation at room temperature as well as reductions in ultimate and yield strengths.



Table 3-2  
RESIDUAL STRENGTH OF CYCLIC CREEP SPECIMENS

Specimen Number	Specimen Orientation	Stress Profile	Max. Stress at 1,368°K; MN/m <sup>2</sup> (psi)	Residual Strength					
				Room Temperature			1368°K (2,000°F)		
				F <sub>tu</sub> <sup>i</sup> MN/m <sup>2</sup> (psi)	F <sub>ty</sub> <sup>i</sup> MN/m <sup>2</sup> (psi)	ε <sup>(4)</sup>	F <sub>tu</sub> <sup>i</sup> MN/m <sup>2</sup> (psi)	F <sub>ty</sub> <sup>i</sup> MN/m <sup>2</sup> (psi)	ε <sup>(4)</sup>
1	L <sup>(1)</sup>	Basic <sup>(3)</sup>	34.4 (5,000)	600 (87,000)	490 (71,100)	2.0			
2	L	Basic	34.4 (5,000)				99.9 (14,500)	—	1.0
3	T <sup>(2)</sup>	0.8 x Basic	27.6 (4,000)	308 (44,700)	—	—			
4	T	0.8 x Basic	27.6 (4,000)				48.8 (7,100)	—	1.0
5	L	0.9 x Basic	31.0 (4,500)	497 (72,100)	472 (68,500)	1.0			
6	L	0.9 x Basic	31.0 (4,500)				91.8 (13,300)	—	—
7	T	0.7 x Basic	24.1 (3,500)	237 (34,400)	—	—			
8	T	0.7 x Basic	24.1 (3,500)				54.4 (7,900)	—	1.0
9	L	0.8 x Basic	27.6 (4,000)	730 (106,000)	492 (71,400)	7.0			
10	L	0.8 x Basic	27.6 (4,000)				93.7 (13,600)	—	1.0

It was desired to compare the degradation effects of low pressures and elevated temperatures only with the effects of stress cycles combined with pressure and temperature cycles. Thus, data from residual strength tests of both types of samples were used in comparisons of ultimate strength levels obtained from TD Ni-20Cr sheet material in these conditions. Such comparisons of average ultimate strengths are shown in Figure 3-4 for (1) as-received TD Ni-20Cr sheet, (2) samples tested after exposure to temperature and reduced pressure environments, and (3) the multiple-parameter creep strain samples that were subjected to programmed stress, temperature, and reduced pressure cycles. The results of the three types of tests showed that

- A. For 0.0254-cm (0.010-in.) thick material tested as longitudinal specimens, exposure without stress produced nearly the same degradation as exposure with stress.
- B. Transverse specimens were more severely affected than longitudinal specimens in residual room temperature testing.
- C. The same trend in directionality (i.e., transverse specimens showed more degradation) was noted in tests at 1,368°K (2,000°F), but not to the extent observed at room temperature.

From data obtained in the cyclic multiple-parameter tests, it was concluded that stress levels of 24.1 to 27.6 MN/m<sup>2</sup> (3,500 to 4,000 psi) in the transverse direction can produce a strength degradation of approximately 50 percent at room temperature for 0.0254-cm (0.010-in.) thick TD Ni-20Cr sheet. Ductility at room temperature was also shown to be severely reduced.

Despite the strength degradations noted in the multiple-parameter tests, subsequent design and testing of candidate heat shield configurations showed the noted strength reductions to have a minimum impact on panel weights and on overall TPS weights. The lessening of strength degradation effects on weight resulted from: (1) the relatively low tensile stresses that accompany critical compressive buckling loads at low temperature conditions where degradation was most severe, (2) the isotropic panel designs can

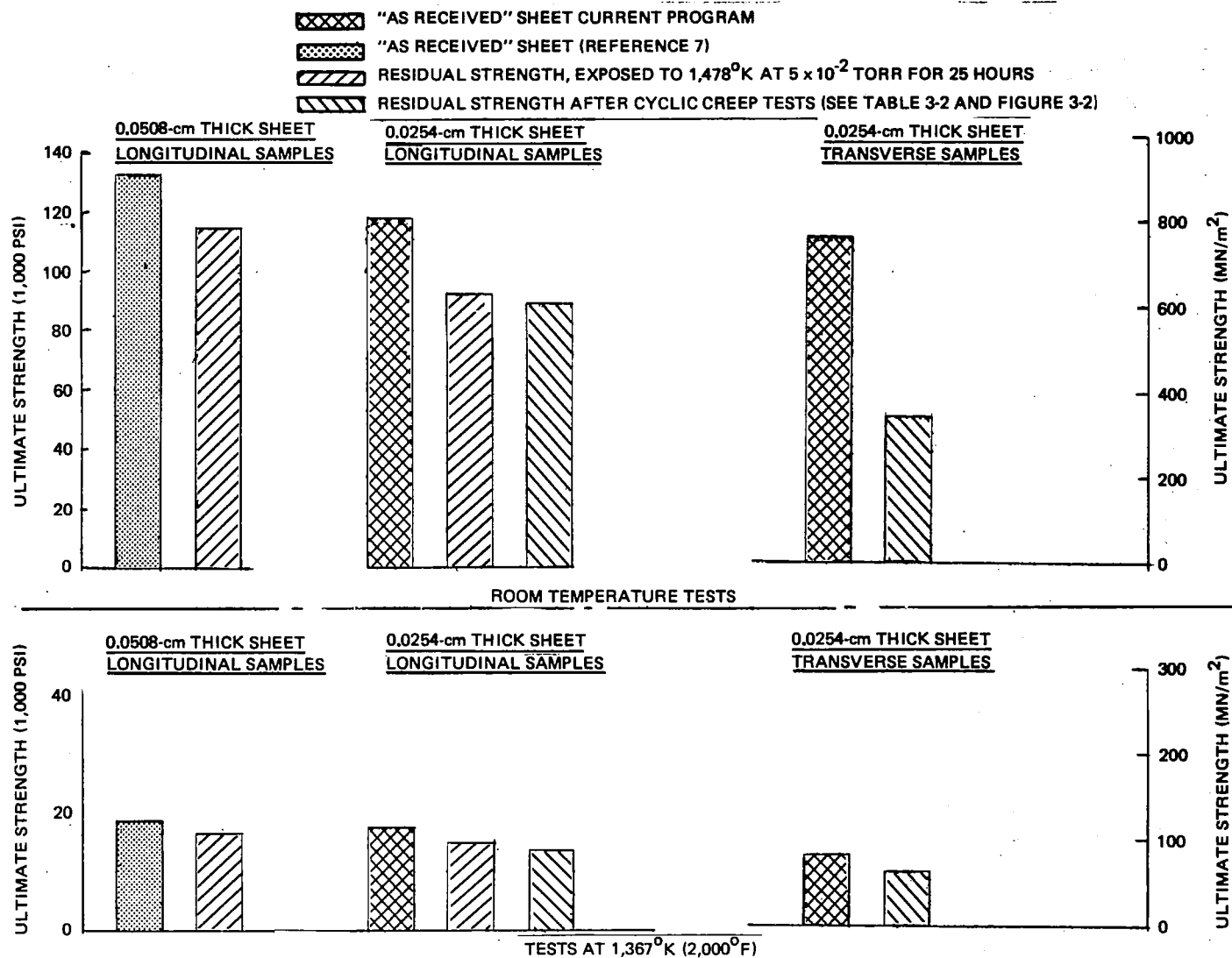


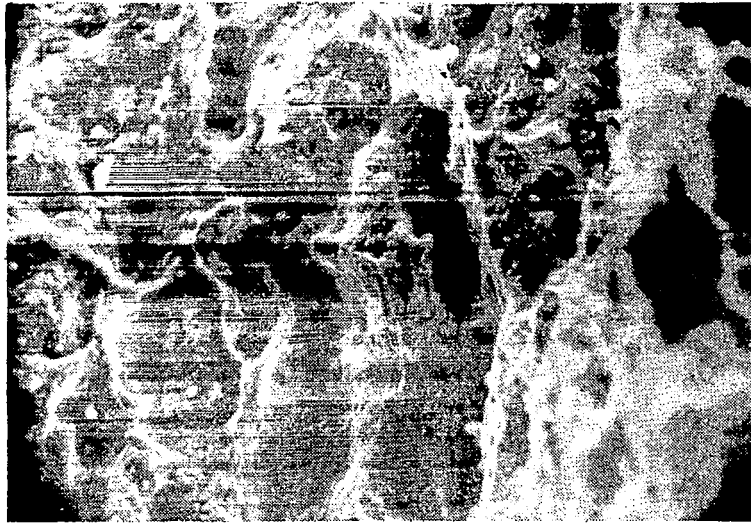
Figure 3-4. Average Ultimate Strength Comparisons of Basic TD Ni - 20 Cr Sheet and Residual Strength Samples

utilize the greater strength and lower degradations observed in the longitudinal direction, and (3) both the Phase I and Phase II panel tests showed critical areas on the heat shields to be near attach points and near panel edges rather than panel midspan areas where maximum stresses from static design loads were computed. The impact on overall TPS weights was also minimal because panel weights were computed to be less than 35 percent of the overall TPS weight. The latter effect is shown in parametric studies (Section 4) and in actual TPS weight breakdowns in Section 6.

### 3.1.3 Metallurgical Evaluations

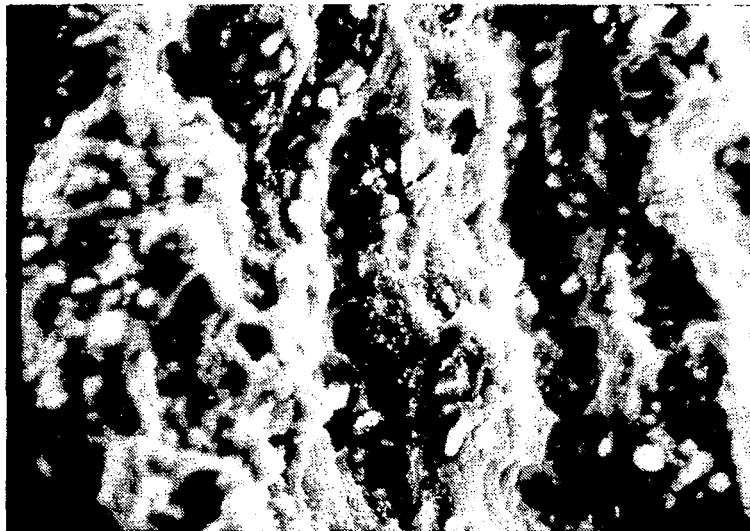
Metallurgical evaluations were also conducted on sections removed from the cyclic creep samples. Several samples showed visual evidence of surface oxidation on the fracture edge where final failure and sample separation occurred during residual strength tests. The oxidized appearance was evident on only a portion of the fracture edge, an appearance that suggested initial cracking may have occurred during elevated-temperature creep strain cycles applied in the Astrofurnace test chamber. Microstructure studies were conducted on two of the failed samples to determine whether internal oxidation could be detected in the samples.

Photomicrographs were first taken with a scanning electron microscope (SEM) at two positions along the fracture edge of specimen No. 7, a cyclic creep sample with a transverse orientation. The two areas photographed are shown in Figure 3-5, where the difference in appearance is evident. Cyclic creep specimen No. 7 was tested for residual strength at room temperature (Table 3-2) and showed severe loss in ultimate tensile strength. Since the residual strength test of specimen No. 7 was conducted at room temperature, any oxidation of the fracture edge could have occurred only during elevated-temperature portions of the creep strain test cycles. The latter fact, combined with the low ultimate stress of  $237.5 \text{ MN/m}^2$  (34,400 psi) recorded in residual strength tests, indicates that initial intergranular cracks may have occurred during the cyclic creep strain tests.



1600X

A. FRACTURE SURFACE WITHOUT OXIDATION.



1820X

B. FRACTURE SURFACE WITH APPARENT SURFACE OXIDATION.

**Figure 3-5** Photomicrographs of Fracture Edge Taken with Scanning Electron Microscope, Cyclic Creep Specimen No. 7

A set of photomicrographs was obtained with a light microscope on sections taken from specimens No. 5 and 7. The former sample had a longitudinal orientation. The two photomicrographs are shown in Figure 3-6 and 3-7, which also indicate the orientation of sections taken from the failed samples. The photomicrographs of Figures 3-6 and 3-7 showed no evidence of internal oxidation in either sample, and it was thus concluded that internal oxidation was not a significant factor in causing the strength degradation experienced by the cyclic creep samples.

### 3.2 BRAZE-REINFORCED JOINT TESTS

The use of thin-gage sheet material combined with the severe Shuttle acoustic environment indicated the possible requirement for an improved joining technique in which conventional spot-welds, spot diffusion-bonds, and resistance seam-welds are reinforced by a brazed area surrounding the nuggets or bond areas. Braze-reinforced spot-welded joints had a potential to increase the fatigue strength of simple lap-shear joints when compared to the fatigue strength levels of conventional unreinforced spot-welded joints of the same type. Thus, three types of standard joints used in thin-gage parts (spot-welds, diffusion-bonds, and seam-welds) were selected for evaluating the improved strength characteristics provided by braze reinforcement. Two gage combinations were evaluated, including 0.0254-cm (0.010-in.) joined to 0.0254-cm (0.010-in.) sheet and 0.0508-cm (0.020-in.) joined to 0.0508-cm (0.020-in.) sheet.

Four types of tests were conducted with braze-reinforced joints, (1) tensile-shear strength, (2) fatigue tests at room temperature and at 1,368°K (2,000°F), (3) stress-rupture tests at 1,368°K (2,000°F) and 1,477°K (2,200°F) and (4) residual strength at room temperature, 1,368°K (2,000°F), and 1,477°K (2,200°F). The test matrix and sample configuration are shown in Table 3-3.

The results of all braze-reinforced joint tests showed significant improvement when compared to results from similar tests with unreinforced joints. The tests conducted in this program indicated that full joint efficiency using realistic overlap could be obtained in designs similar to those used in full-scale TD Ni-20Cr heat shield panels.



UNETCHED

250X



Figure 3-6. Photomicrograph of Section at Fracture Edge, Cyclic Creep Specimen No. 5 (Longitudinal Sample)



UNETCHED

250X

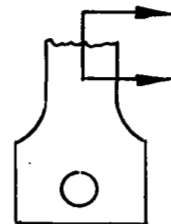


Figure 3-7 . Photomicrograph of Section at Fracture Edge, Cyclic Creep Specimen No. 7 (Transverse Sample)

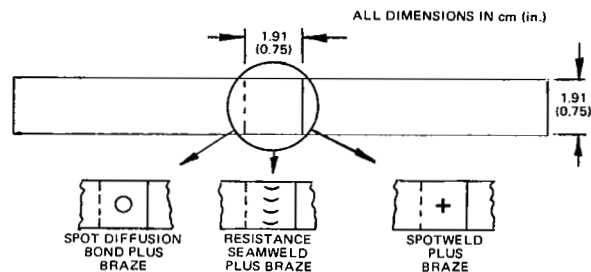
Table 3-3

BRAZE REINFORCED (BR) TD Ni-20Cr JOINT TESTS

Type of Joint		Type of Test and Number of Samples					
		Tensile-Shear	Fatigue		Stress Rupture		Residual Strength (1)
			RT	1,368°K	1,368°K	1,477°K	
BR Spotweld	0.0254-0.0254(2)	10	5	5	5	5	6
	0.0508-0.0508	10	5	5	5	5	6
BR Spot-Diffusion Bond	0.0254-0.0254	10	5	5	5	5	6
	0.0508-0.0508	10	5	5	5	5	6
BR Roll Seam Weld	0.0254-0.0254	10	5	5	5	5	6
	0.0508-0.0508	10	5	5	5	5	6

(1) Tests at room temperature, 1,368°K, and 1,477°K

(2) Sheet thicknesses in cm.



TD-6 braze alloy was selected for the tests, since it was the best available alloy for brazing TD Ni-20Cr. TD-6 alloy has approximately the same composition as Hastelloy C, with the exception of the addition of silicon, which has the effect of lowering the melting point to the range of 1,559 to 1,588°K (2,350 to 2,400°F).

### 3.2.1 Tensile-Shear Tests

The average ultimate strengths of the three types of braze-reinforced joints are compared in Figure 3-8 with the average strength of as-received TD Ni-20Cr sheet material at room temperature, 1,146°K, 1,368°K, and 1,477°K (1,600°F, 2,000°F, and 2,200°F). The joint stresses shown in Figure 3-8 were based on the cross-sectional area of the sheet strip outside of the joint and are therefore typical of the tensile stresses outside of the joint area. Strength differences in test data from both 0.0254-cm (0.010-in.) and 0.0508-cm (0.020-in.) joint samples are within the expected scatter for TD Ni-20Cr ultimate strength values, and the comparisons of Figure 3-8 indicate that joint efficiencies approaching 100 percent can be obtained at elevated



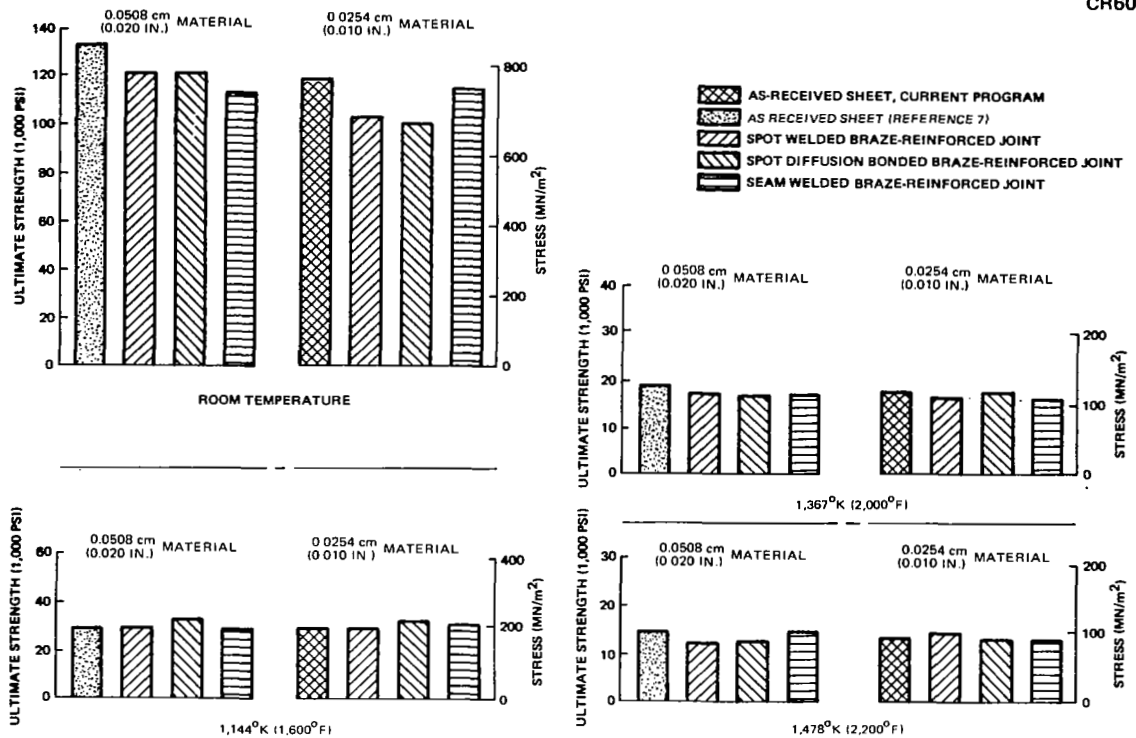


Figure 3-8. Comparison of Average Ultimate Tensile Strengths

temperatures in braze-reinforced joints of all three types tested with a joint overlap of 1.9 cm (0.75 in.).

Inspection of the tested specimens showed failure to occur in the parent metal of all of the tested joints. At room temperature, the data of Figure 3-8 indicate a decrease in joint efficiency of approximately 10 to 15 percent. The cause of the decrease was judged to be either the result of local stress increases near the joint caused by the eccentricity in the test samples (Table 3-3) or the result of degradation of the parent material caused by the braze cycle.

### 3.2.2 Fatigue Tests

Results of room-temperature fatigue tests conducted with 0.0254-cm (0.010-in.) and 0.0508-cm (0.020-in.) samples are compared in Figure 3-9 with parent metal fatigue strengths obtained from tests in this program and from Reference 7. Fatigue strengths exhibited by the joints are also compared with strength levels of unreinforced spot-welded samples (Reference 9). The

higher fatigue strength shown by the 0.0254-cm (0.010-in.) braze-reinforced joints in Figure 3-9 is attributed to the lower bending stresses induced in the thinner lap-joint specimens.

For the acoustic fatigue conditions of the Shuttle ascent flight, an improvement in joint fatigue strength of from 138 to 276 MN/m<sup>2</sup> (20,000 to 40,000 psi) could possibly be realized through use of braze-reinforced joining techniques. In terms of fatigue life for equally stressed joints, a fatigue life improvement by a factor of 10 could possibly be realized through use of braze-reinforced joints.

Results from fatigue tests of braze-reinforced joints conducted at 1,368°K (2,000°F) are shown in Figure 3-10. All of the braze-reinforced joints tested at that temperature showed reasonably close agreement whether made from 0.0254-cm (0.010-in.)-thick or 0.0508-cm (0.020-in.)-thick TD Ni-20Cr sheet.

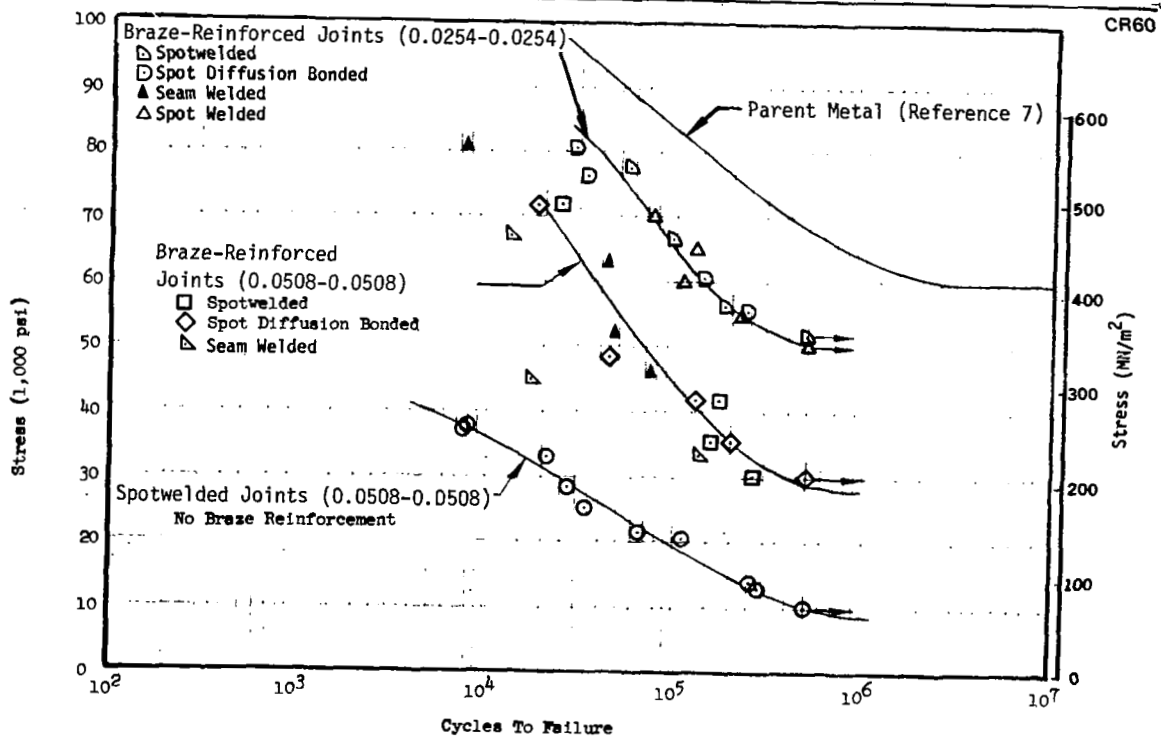


Figure 3-9. Room Temperature Fatigue Test Results for Braze-Reinforced Joints

This behavior was in contrast to the distinctly higher fatigue stress levels achieved by the 0.0254-cm (0.010-in.) thick samples in fatigue tests at room temperature (Figure 3-9). Also, the braze-reinforced joints tested at 1,368°K (2,000°F) exhibited high joint efficiencies that were comparable to parent metal values (Figure 3-10). Again, this behavior contrasted with the room temperature fatigue tests where none of the samples attained joint efficiencies near the parent metal strength levels. As in the tensile-shear tests of braze-reinforced joints, the cause of lowered fatigue strengths could be either stress increases from the eccentric single-lap configuration or degradation from the braze cycle.

### 3.2.3 Stress Rupture Tests

Typical stress-rupture test results are presented in Figure 3-11 for braze-reinforced joints tested at 1,368°K (2,000°F). The stress-rupture strengths of the joint samples were lower than parent metal strength (see Reference 2, Appendix B) of either 0.0254-cm (0.010-in.) or 0.0508-cm (0.020-in.) sheet thicknesses. Stress-rupture strength levels from tests of parent metal samples are shown in Figure 3-11 for comparison. All joint samples used material with a longitudinal orientation, and thus the parent metal values are also shown for longitudinal samples.

Similar stress-rupture test results are shown in Figure 3-12 for braze-reinforced joints tested at 1,477°K (2,200°F). In contrast to samples tested at 1,368°K (2,000°F), the joints tested at 1,477°K (2,200°F) exhibited a difference in stress-rupture strengths recorded for the two different sheet gages used in the samples. Joint samples made from 0.0254-cm (0.010-in.) sheet had higher stress-rupture strengths by approximately  $13.8 \text{ MN/m}^2$  (2,000 psi) when compared to 0.0508-cm (0.020-in.) samples. Again, the parent metal stress-rupture strength levels at 1,477°K (2,200°F) were higher than joint strengths throughout the range of tests.

All of the stress-rupture samples failed in the parent metal, a majority of the failures occurring immediately adjacent to the joint area. Thus, for the configuration used in the braze-reinforced joint tests (Table 3-2), the joint efficiencies were high when compared to the parent metal.

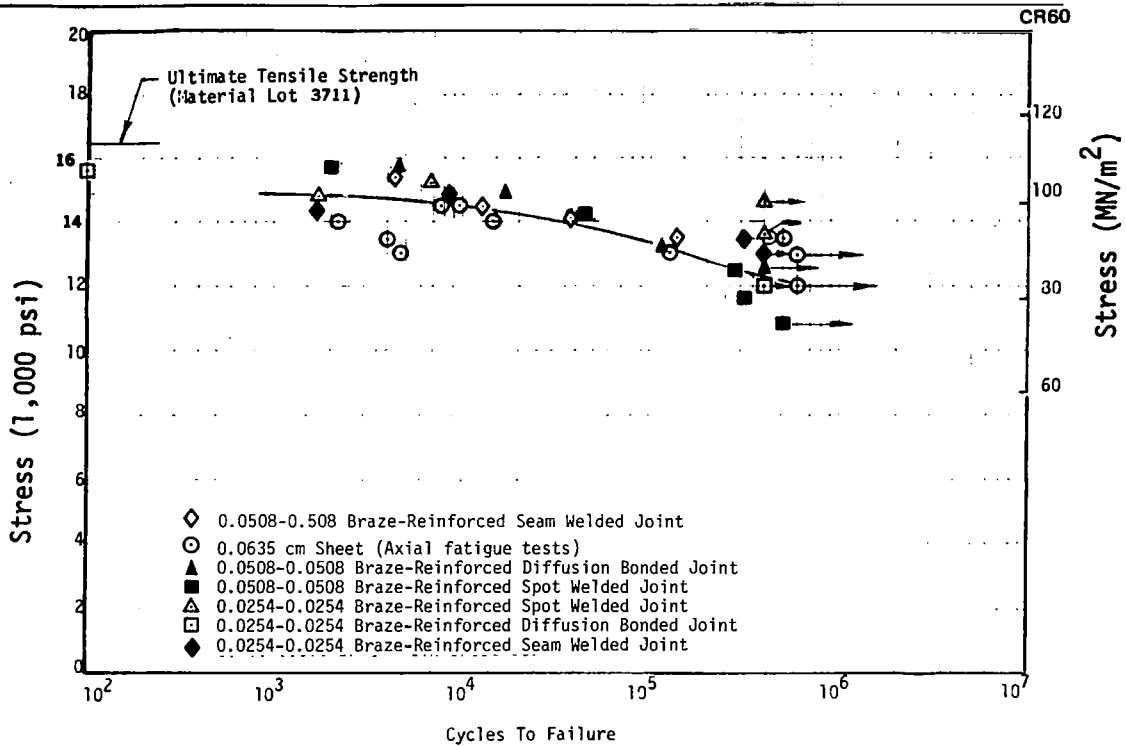


Figure 3-10. Fatigue Tests of Braze-Reinforced Joints at 1,367°K (2,000°F)

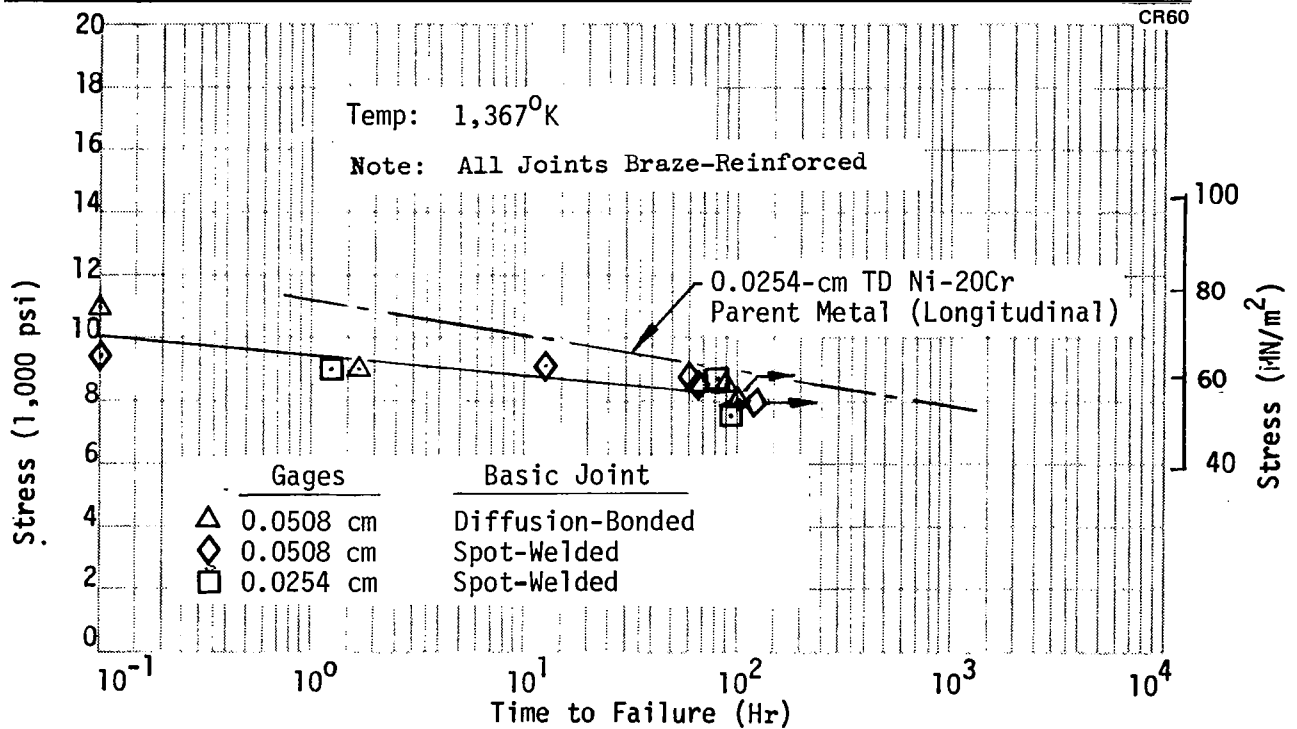


Figure 3-11. Stress Rupture Tests of Braze-Reinforced Joints at 1,367°K

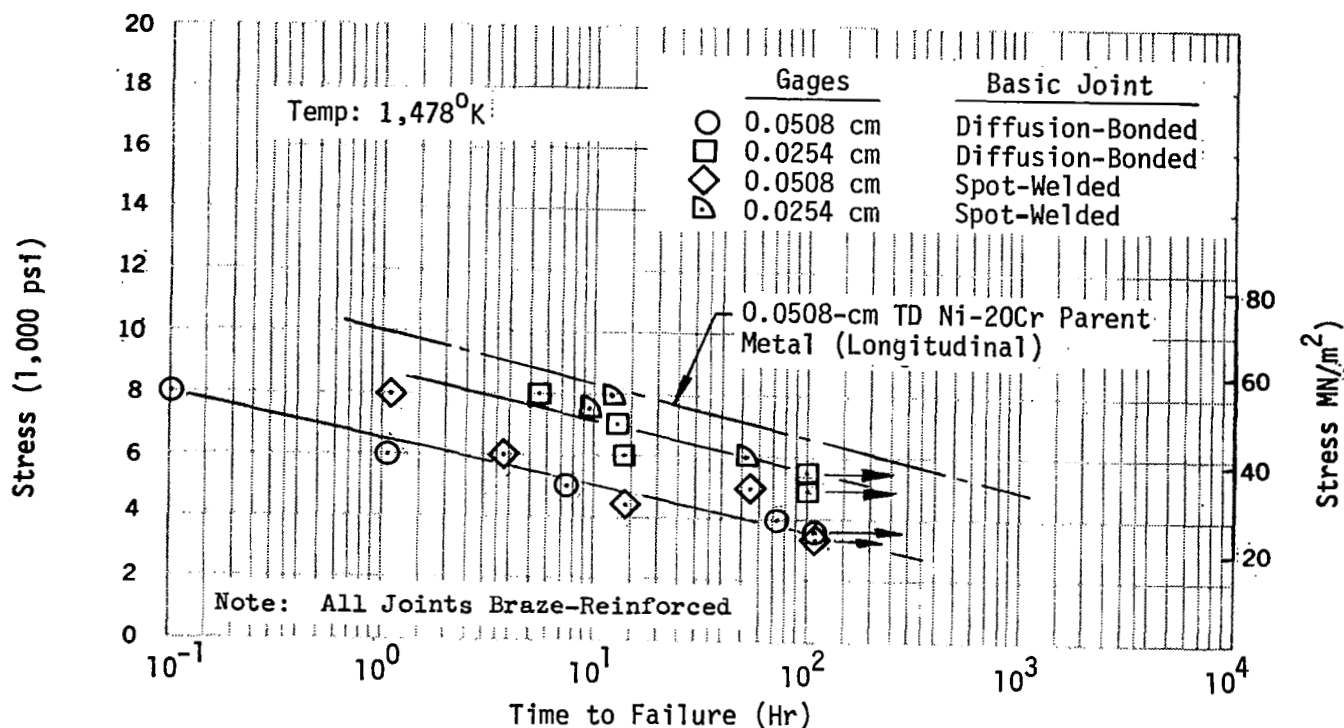


Figure 3-12. Stress Rupture Tests of Braze-Reinforced Joints at 1,478°K

### 3.2.4 Residual Strength Tests

Residual strength tests were conducted to determine degradation effects on braze-reinforced joints caused by exposure to elevated-temperature, low-pressure environments. Residual strengths were determined at room temperature, at 1,368°K (2,000°F), and at 1,477°K (2,200°F). The joint samples were exposed in a vacuum furnace to a temperature environment of 1,477°K (2,200°F) for 25 hours at a partial pressure of  $5 \times 10^{-2}$  torr prior to testing. This environment approximates the cumulative temperature and pressure combination experienced by a metallic heat shield in 100 Shuttle entry flights.

As in the case of the stress rupture samples, the residual strength specimens failed in the parent metal area instead of the joint overlap region. Failure in the parent metal occurred in the same manner as previously noted in the tensile specimens, and thus data obtained from the braze-reinforced joints

were compared with the residual strength results obtained from cyclic creep specimens tested in the Astrofurnace chamber. Data from the residual strength tests of braze-reinforced joints are included in Figure 3-8.

### 3.2.5 Summary of Braze-Reinforced Joint Tests

Results from braze-reinforced joint tests are summarized as follows:

- Fatigue life at room temperature is improved considerably when compared to unreinforced spot-welded joints. Life improvement by a factor of 10 is indicated from room temperature fatigue tests. Fatigue strength was approximately doubled for a given life.
- Efficiency in fatigue for braze-reinforced joints approaches that of TD Ni-20Cr parent metal at 1,368°K (2,200°F).
- Stress-rupture strengths at 1,368°K and 1,477°K (2,000°F and 2,200°F) were reduced from parent metal values. Reductions in joint efficiencies generally ranged from 6.89 MN/m<sup>2</sup> to 20.6 MN/m<sup>2</sup> (1,000 psi to 3,000 psi), with the reduction being dependent on gages used in the samples. Such reductions in joint efficiencies were judged to result from eccentricity of the joint configuration or from braze cycle effects.
- The braze-reinforced joints showed no significant degradation from exposure to 1,477°K (2,200°F) for 25 hours in a partial pressure of  $5 \times 10^{-2}$  torr.
- Joint efficiencies approaching 100 percent can be achieved with overlap configurations similar to that found in actual structure.

## Section 4

### DESIGN CONCEPT SELECTION

Parametric studies of candidate TPS designs were conducted to serve as a basis for selecting two promising panel designs for Phase I tests. Initial efforts were devoted to layout drawings of candidate panel designs, attachment systems, support structure, and insulation systems. TPS studies included panel designs of the types shown in Table 4-4, with a basic panel size having a 50.8-cm (20-in.) length and 91.2-cm (36-in.) width. The panel cross sections were sized initially using material properties reduced to account for degradation effects of 100 missions as outlined in Reference 2, Appendix C. Subsequently, cumulative creep data from cyclic multiple-parameter tests were used in creep analyses to check the selected designs for expected maximum permanent deflections. A maximum panel deflection criterion of  $\delta \leq 0.025L + 0.25\text{-cm}$  ( $\delta \leq 0.01L + 0.10\text{-in.}$ ) was used in the initial studies. Panel designs were also checked for resistance to flutter and fatigue, and evaluations of the designs were made with regard to thermal performance, fabricability, cost, reliability, and ease of installation or refurbishment.

The TPS parametric study utilized a summation of weighted values for each design concept, each concept being evaluated in the areas of weight, cost, fabricability, refurbishability, reliability, and efficiency. In cases where two support systems for the heat shield panels appeared feasible, both systems were evaluated. Also, variations in joining methods were studied; the three joining approaches evaluated were spot-welding, braze-reinforced spot-welds, and brazing (honeycomb concept).

While detailed discussions of the parametric studies are contained in Reference 2, Appendix D, a summary of the TPS evaluation parameters is presented at this point.

Weight. Weight evaluations were based on layout drawings for the various panel and support concepts, the required insulation and insulation retaining material, fasteners, closeouts, panel edge members, and doublers. Packaged insulation weights were based on thermal studies that defined insulation thickness required to maintain a substructure temperature of 364°K (200°F)

throughout the entry flight until landing. Panel weights were based on differential pressure loads, acoustic sound pressure levels, and stiffness requirements to prevent panel flutter.

Cost. Production costs were evaluated by outlining detailed fabrication requirements based on heat shield configuration and scrappage rates; assessing tooling requirements; determining material costs; and estimating manhours associated with all tooling, planning, manufacturing, and quality assurance operations.

Fabricability. The detailed fabrication procedures used in cost evaluations also formed the basis for evaluating the fabricability of each concept. Industrial engineering and manufacturing engineering personnel used past fabrication experience to evaluate development time, tooling complexity, and projected rejection rates associated with the various concepts.




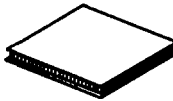

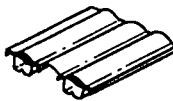
Refurbishability. Refurbishability studies utilized data from Reference 9 and combined such data with evaluations of the attachment systems developed in layout drawings of the various designs to assess ease of replacement for each concept. Frequency of replacement for each concept was also estimated and combined with ease of replacement to evaluate the refurbishability of each design approach.

Reliability. Evaluations of reliability were based upon the experience and judgement of key personnel in areas of design, manufacturing engineering, and quality assurance.

Efficiency. Overall efficiency of each TPS concept was evaluated as to (1) flexibility in mating with various substructure geometries and arrangements, (2) potential service life, (3) minimal heat paths to substructure, and (4) potential for design modifications with minimum cost.



**Table 4-1**  
**SUMMARY OF HEAT SHIELD PARAMETRIC STUDY**

TPS Configuration Summary			TPS Study Parameters and Weighting												Rating Summary	
Heat Shield Configuration	Support System	Panel Joining Method	TPS Weight (0.20)		Cost (0.20)		Fabricability (0.15)		Refurbishability (0.15)		Reliability (0.15)		Efficiency (0.15)		Sum of Weighted Rating	Order of Rating
	Transverse Beams at Panel Ends	Spotwelded	6	1.20	8	1.60	7	1.05	8	1.20	7	1.05	7	1.05	7.15	2
		Spotwelded and Braze Reinforced	4	0.80	5	1.00	5	0.75	8	1.20	8	1.20	8	1.20	6.15	6
	Multiple Post	Spotwelded <sup>(1)</sup>	3	0.60	10	2.00	7	1.05	7	1.05	4	0.60	2	0.30	5.60	7
	Transverse Beams at Panel Ends	Spotwelded <sup>(1)</sup>	9	1.80	9	1.80	6	0.90	9	1.35	3	0.45	1	0.15	6.45	4
	Transverse Beams at Panel Ends	Spotwelded	8	1.60	9	1.80	7	1.05	7	1.05	7	1.05	7	1.05	7.60	1
		Spotwelded and Braze Reinforced	5	1.00	6	1.20	5	0.75	7	1.05	8	1.20	8	1.20	6.40	5
	Multiple Post	Brazed	3	0.60	2	0.40	2	0.30	6	0.90	6	0.90	9	1.35	4.45	8
	Transverse Beams at Panel Ends	Spotwelded	2	0.40	6	1.20	4	0.60	5	0.75	5	0.75	3	0.45	4.15	9
	Transverse Beams at Panel Ends	Spotwelded	8	1.60	7	1.40	6	0.90	7	1.05	7	1.05	5	0.75	6.75	3

<sup>(1)</sup> Edge members and clips spotwelded to panel.

The TPS parametric studies are summarized in Table 4-1. As a result of the parametric studies, the two panel configurations selected for tests in Phase I were the single-faced corrugation-stiffened panel and the zee-stiffened panel. Spot-welding was selected for the joining technique to be used in fabrication of both panel designs.

The weight and cost penalties associated with braze reinforcement may be noted in the rankings of Table 4-1, where the zee-stiffened panel dropped from first to fifth ranking when braze reinforcement of the spot-welded panels was added to the fabrication cycle. Similarly, the corrugation-stiffened heat shield dropped from second to sixth in overall ranking when braze reinforcement was considered.

The single-corrugated-sheet configuration supported by transverse beams at its ends was rated high for its low weight. However, it was reduced in the overall rankings because of sensitivity to flutter (Reference 2, Appendix D). This sensitivity was reflected in lowered ratings in reliability and efficiency.

The two approaches with the highest rankings, the single-face zee-stiffened panel and the single-face corrugation-stiffened configuration, were selected for Phase I full-scale, subsize panel tests. The support system selected used transverse beams at the panel ends, the support beam spacing being approximately 50.8-cm (20-in.). Metallic-foil-packaged, low-density insulation was placed on the interior side of the heat shields.

## Section 5

### SUBSIZE HEAT SHIELD PANEL DESIGN AND TESTING

Evaluation tests were conducted with full-scale, subsize panels using the two design approaches selected at the conclusion of the parametric studies. The objective of Phase I testing was to determine the better-performing design for use in Phase II evaluations where full-size TPS designs were tested. The evaluation tests conducted in Phase I were of three types: (1) cyclic tests of full-scale, subsize TPS designs with programmed temperature, load, and static pressure conditions interspersed with acoustic tests; (2) flowing gas tests of two different panel edge joint designs; and (3) meteoroid impact tests followed by simulated entry in a flowing gas (plasma-arc) environment on sample panels of the two selected heat shield designs. The panel designs, fabrication of the panels, instrumentation and test results are described in this section for each of the three types of test panels.

All panel designs had full-scale cross sections, but were subsize in planform area. Panels to be tested in the Plasma Arc Tunnel (PAT) facility were restricted to a planform size of 10.16-cm by 10.16-cm (4-in. by 4-in.) to fit within the uniform core area of the plasma stream. Thus, the simulated joint components and the meteoroid impact panels were both limited to a 10.16-cm by 10.16-cm (4-in. by 4-in.) planform. The smaller panels also were designed with scarfed corners, again for the purpose of remaining within the uniform stream area. Stiffener depths on both the corrugation-stiffened and zee-stiffened designs were 2.54-cm (1.0-in.) for all test panels, including those tested in the space simulation chamber. The latter panels were 45.7-cm (18-in.) long and approximately 17.3-cm (6.8-in.) wide. The larger panels simulated full-span beam-supported heat shields, but were somewhat smaller in width than projected for full-size Orbiter heat shields. A sheet thickness of 0.0254-cm (0.010-in.) was used for both face sheet and stiffening elements in both panel designs.

The design approach used in Phase I involved sizing of initial panel cross sections based on static loads. The initially sized panels were then evaluated for suitability in areas of fatigue and panel flutter (Reference 2,

Appendix D). Also, meteoroid penetration of the panel designs was considered, as discussed subsequently in Section 5.1. In both zee-stiffened and corrugation-stiffened designs, the panel cross sections developed from static loadings were sufficient to meet fatigue and flutter criteria. The meteoroid penetration criterion (Reference 2, Appendix E) was relaxed to allow a 0.95 probability of one or less penetration in a seven-day mission. Thermal protection system criteria, test panel configurations, and testing of the heat shield designs are discussed in the remainder of this section.

## 5.1 DESIGN CRITERIA

Basic design criteria for the heat shields are presented in detail in Reference 2, Appendix A and were discussed briefly in Section 2. The criteria used in design of the full-scale subsize test panels and TPS components are summarized in Table 2-1, those criteria also being used in designing the full-scale, full-size heat shields discussed in Section 6.

The meteoroid criteria for the Shuttle were applied to the TD Ni-20Cr heat shield designs to evaluate their effects on the required thickness of material. Detailed calculations are presented in Reference 2, Appendix E while the results of the evaluations are summarized at this point.

The meteoroid flux-mass model of Figure 2-8 was used in the evaluation, and a criterion specifying a 0.95 probability of no puncture was assessed initially. A mission duration of 7 days was selected and an exposed surface area of approximately  $123 \text{ m}^2$  ( $1,320 \text{ ft}^2$ ) was projected for the TD Ni-20Cr heat shield area on the lower surface of the Orbiter. With the above criterion and assumptions, a heat shield thickness of 0.106-cm (0.0417-in.) is required to provide a 0.95 probability of no puncture. A relaxation of puncture criterion to allow one or less puncture [ $P(0, 1) = 0.95$ ] would reduce the thickness required to 0.0605-cm (0.0238-in.). The latter criterion of  $P(0, 1) = 0.95$  was selected as an initial meteoroid penetration design criterion for the combined sheet thicknesses of test heat shield panels.

This criterion was assessed in simulated meteoroid impact tests followed by exposure to simulated entry heating in the Plasma Arc Tunnel facility. As shown by test results presented later in this section, the relaxed meteoroid puncture criterion is expected to be satisfactory for TD Ni-20Cr radiative heat shields because of their ability to withstand entry flow conditions after puncture without serious hot gas ingestion or material degradation.

## 5.2 METEOROID IMPACT PANEL TESTS

The tests conducted in this portion of the program were designed to evaluate the damage incurred by TD Ni-20Cr heat shields when subjected to simulated meteoroid impacts, and to further evaluate the survivability of the selected designs when exposed to simulated entry airflow conditions after impact.

Testing was accomplished in two steps, a first set of tests being conducted at the McDonnell Douglas Aerophysics Laboratory at El Segundo, California. This facility possesses good simulation capabilities through the use of a light-gas gun. The MDAC light-gas gun is a two-stage, heavy-piston type specifically designed for high-speed impact studies with a high firing rate. Since the light-gas gun cannot match the actual average meteoroid velocity of 20 km/s, the mass of each sphere used in the impact tests was scaled to equal the kinetic energy of an actual meteoroid. The borosilicate glass spheres used in the tests were sized for equal kinetic energy at a velocity of approximately 7.62 km/s (25,000 ft/sec). Using this velocity, the borosilicate spheres were scaled to a mass of approximately  $48.0 \times 10^{-6}$  grams. That mass compares to a computed mass for an actual meteoroid of  $6.99 \times 10^{-6}$  grams, a mass that was derived by using the criterion of a 0.95 probability of one or less penetrations in a seven-day mission (Reference 2, Appendix E). The borosilicate spheres used in the tests had a diameter of 0.033-cm (0.013-in.).

The zee-stiffened panel was tested first with the aiming point on the panel being in an area having a single-skin thickness of 0.0254-cm (0.010-in.). The glass sphere used in the first shot weighed  $50.2 \times 10^{-6}$  grams and the velocity attained by the sphere was 7,170 m/s (23,500 ft/sec). The shot

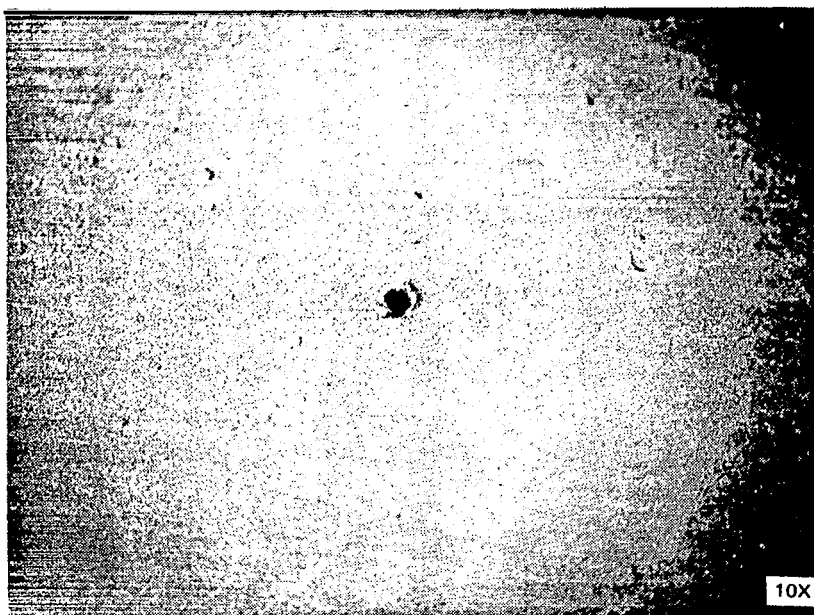
penetrated the front face, and examination under a light microscope showed a hole shape that indicated the penetration was in the ballistic limit range. The stabilizing flange on the outstanding leg of the zee stiffener was located approximately 2.54 cm (1 in.) behind the point of penetration, and an examination of the stiffener showed no damage from the sphere. The point of penetration on the panel face is shown in Figure 5-1a. The hole shown in Figure 5-1a was 0.033 cm (0.013 in.) in diameter.

The second panel was tested using an aiming point where the corrugation stiffener was attached to the face sheet, thus forming a double thickness of TD Ni-20Cr sheet material. Both the face sheet and the corrugation-stiffening member were 0.0254-cm (0.010-in.) thick sheet, providing a total thickness of 0.0508-cm (0.020-in.) at the aiming point. The borosilicate sphere used in this test weighed  $47.8 \times 10^{-6}$  grams and attained a velocity of 7,010 m/s (23,000 ft/sec). No penetration occurred in this test, the double thickness being sufficient to sustain impact without penetration. A magnified view of the impact area is shown in Figure 5-1b. Particles from the disintegrated sabot also impacted the second test panel, and a portion of the plastic carrier was deposited on the panel as a thin layer of char material. This area may be seen in the middle left portion of Figure 5-1b. The two impacted panels were then shipped to St. Louis for the second set of tests in the plasma Arc Tunnel.

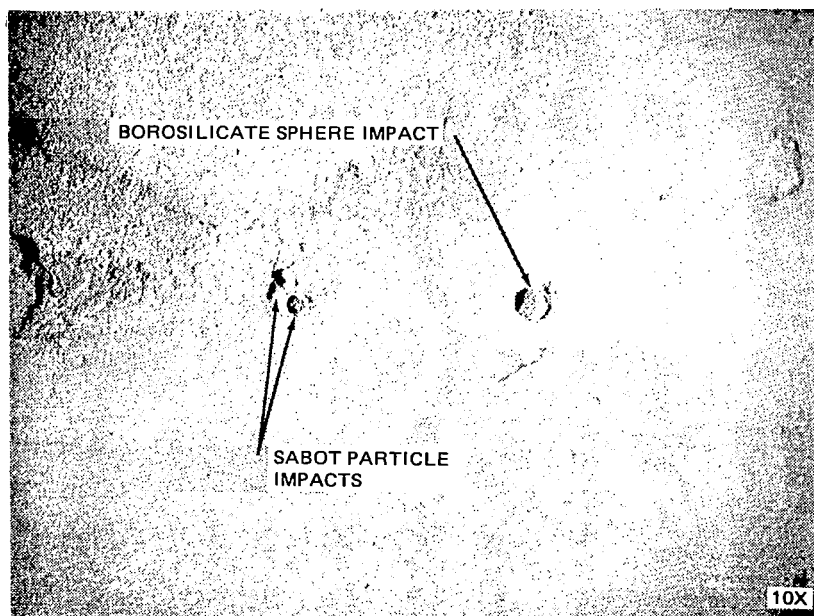
### 5.3 PLASMA-ARC TESTS

The impacted panels were each subjected to one simulated entry cycle in the Plasma Arc Tunnel to determine whether entry airflow conditions caused further damage to the impact areas on the panels. The arc heater configuration for tests in this program utilized a nozzle with a 2.54-cm (1.0-in.) throat diameter and a 20.3-cm (8.0-in.) exit diameter.

The operating envelope of the Plasma Arc Tunnel is shown in Figure 5-2; the point at which stream conditions were set is noted in the envelope. The noted condition was used in both the meteoroid impact panel tests and the simulated panel joint tests.



a. PENETRATION POINT IN FACE SHEET OF ZEE-STIFFENED PANEL



b. IMPACT AREAS ON FACE SHEET OF CORRUGATION-STIFFENED PANEL

Figure 5-1. Magnified Views of Panel Faces After Simulated Meteoroid Impact Tests

Test stream conditions were checked with a calibration module and, after the stream was stabilized at the desired test conditions, each of the test panels was rotated into the stream and held for the desired time. Each of the meteoroid test panels was tested at a nominal surface temperature of 1,477°K (2,200°F) for 30 minutes (1,800 sec.).

All of the test panels were instrumented with Pt/Pt-10 percent Rh thermocouples tack welded to the rear surface of the face sheet and to the stiffening members. In addition, front surface temperatures were measured with a pyrometer. Thermocouple and pyrometer sighting locations are shown in Figure 5-3.

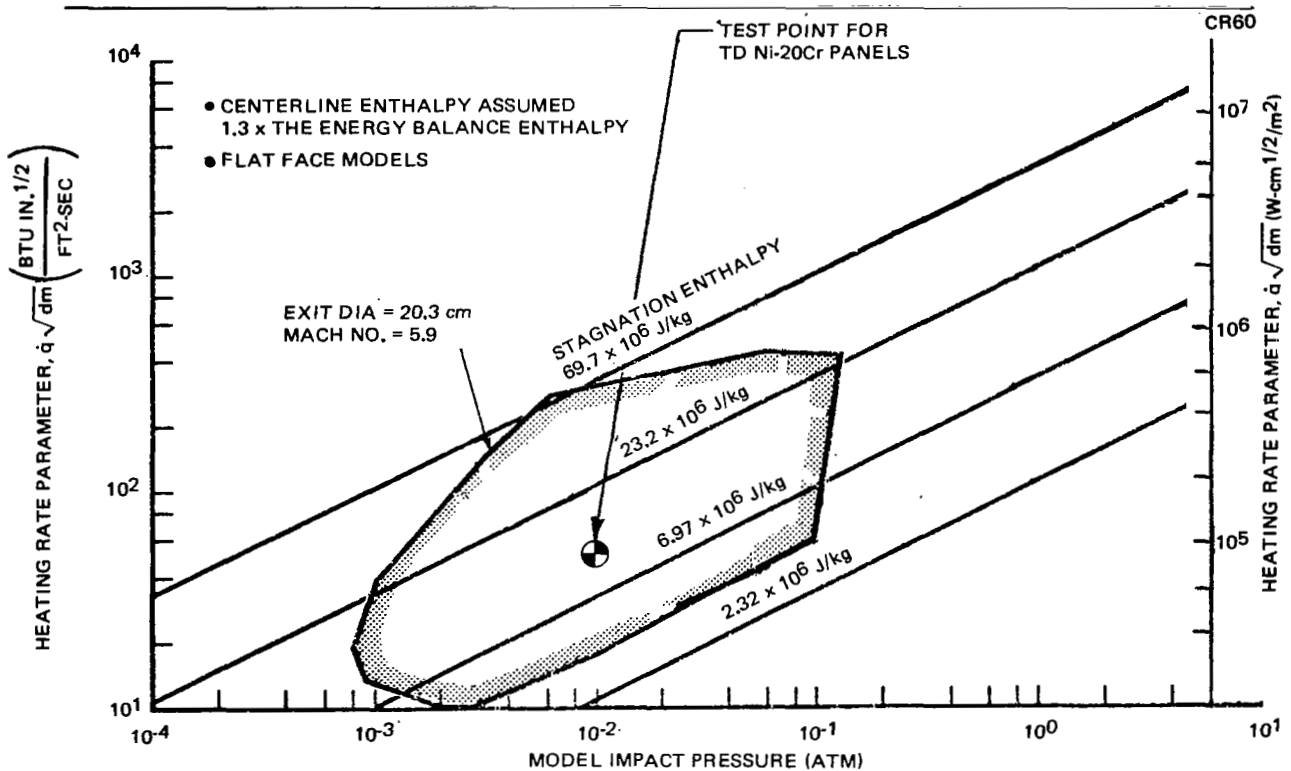


Figure 5-2. PAT Facility Testing Capability (Flat Face Model)



The optically measured meteoroid panel surface temperatures are presented in Table 5-1 for the pyrometer sighting locations shown in Figure 5-3. Temperature variations across the surface of the corrugation-stiffened panel ranged from 1,378°K (2,020°F) to 1,485°K (2,210°F). Similarly, temperatures on the zee-stiffened panel ranged from 1,361°K (1,990°F) to 1,489°K (2,220°F). Where comparisons between pyrometer readings and thermocouple recordings were possible, good agreement was noted between the two techniques.

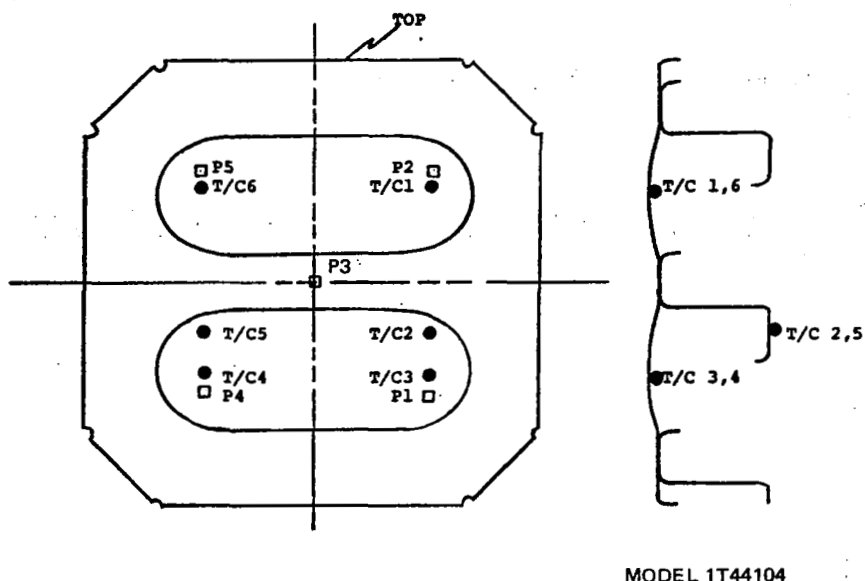
Table 5-1  
OPTICALLY MEASURED PANEL SURFACE TEMPERATURES,  
METEOROID IMPACT PANELS

Panel Configuration	Run No.	Temperature at Pyrometer Sighting Position					Run Time (sec)
		P1	P2	P3	P4	P5	
Corrugation-Stiffened	3659	1,400 (2,060)	1,400 (2,060)	1,378 (2,020)	1,482 (2,210)	1,378 (2,020)	1,810
Zee-Stiffened	3659	1,432 (2,120)	1,361 (1,990)	1,372 (2,010)	1,489 (2,220)	1,368 (2,000)	1,795

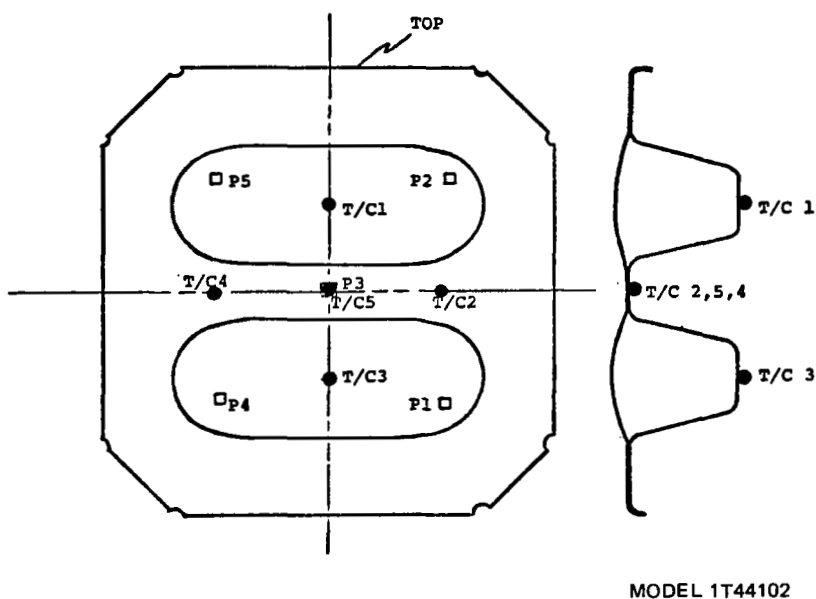
Note: Temperatures shown as °K primary units and (°F) secondary units.

Temperature time histories of thermocouples on the corrugation-stiffened meteoroid impact panel are shown in Figure 5-4, while similar data for the zee-stiffened panel are presented in Figure 5-5. Maximum temperature difference on the corrugation-stiffened panel during the steady-state portion of the test was approximately 67°K (120°F). This difference occurred between Thermocouple 4, located on the face sheet, and Thermocouple 3, located on the corrugation at its maximum-depth position (Figure 5-3). This difference was less between Thermocouples 5 and 3, Thermocouple 5 being located at the center of the panel in a position closer to Thermocouple 3.

Temperature differences between face-sheet positions and stiffener flanges on the zee-stiffened panel were greater than similar readings on the corrugation-stiffened panel. During steady-state portions of the test, a temperature difference of approximately 200°K (360°F) existed between Thermocouples 2 and 3 (Figure 5-5). Also, a difference of approximately 189°K (340°F) was noted between Thermocouples 4 and 5 on the zee-stiffened panel.

**Notes:**

- \*P1 through P5 - Pyrometer sighting locations.
- \*T/C 1 through T/C 6 - Tack-welded thermocouple locations.

**a. ZEE-STIFFENED PANEL****Notes:**

- \*P1 through P5 - Pyrometer sighting locations.
- \*T/C 1 through T/C 5 - Tack-welded thermocouple locations.

**b. CORRUGATION-STIFFENED PANEL**

**Figure 5-3. Thermocouple and Pyrometer Sighting Locations on Meteoroid Impact Panels**

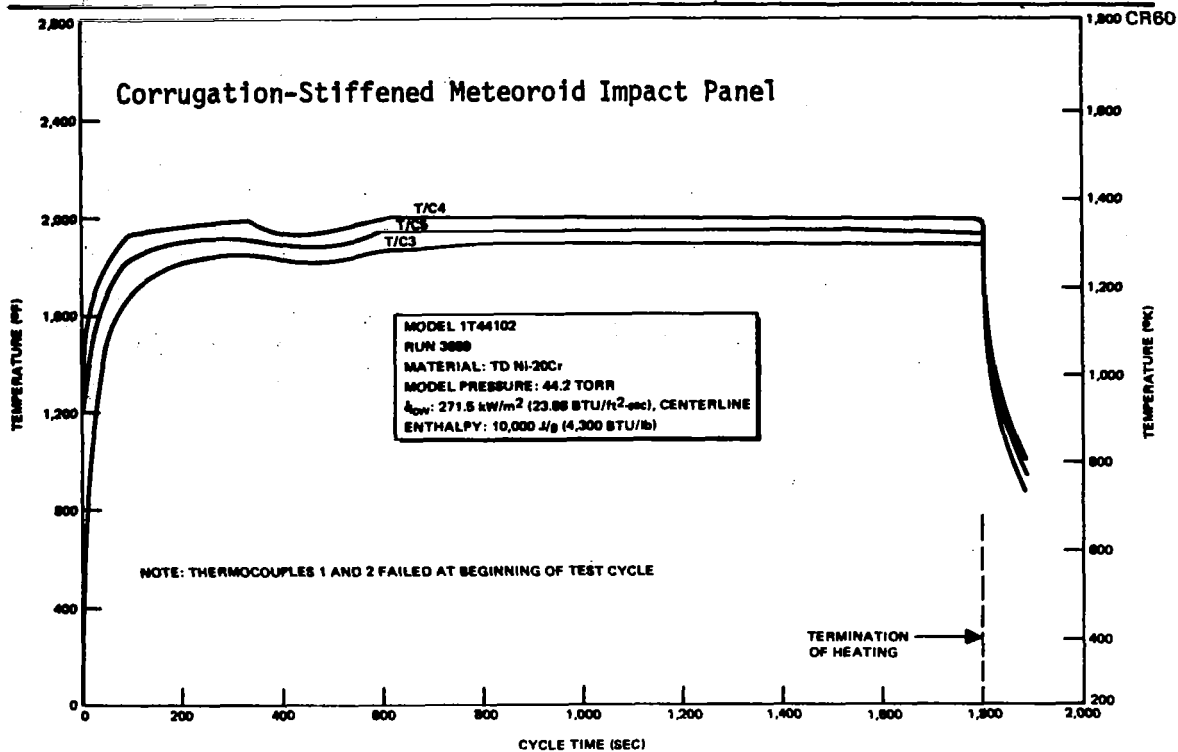


Figure 5-4. Panel Thermocouple Temperature Histories

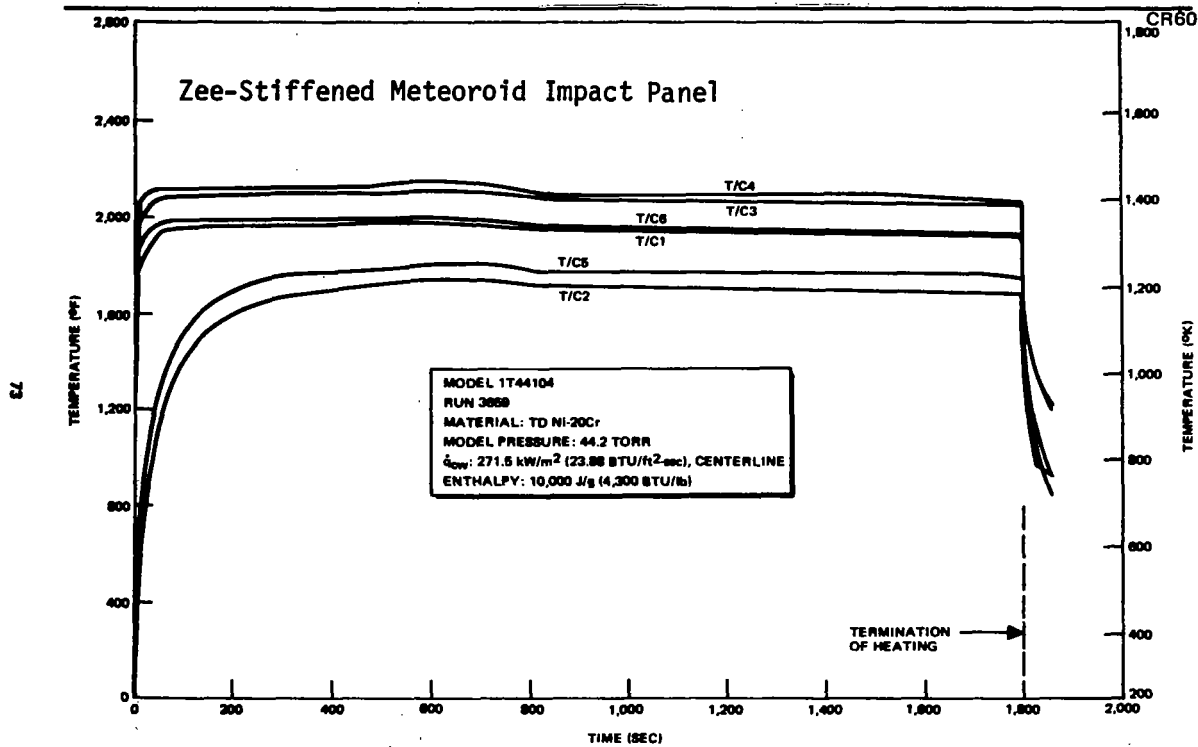


Figure 5-5. Panel Thermocouple Temperature Histories

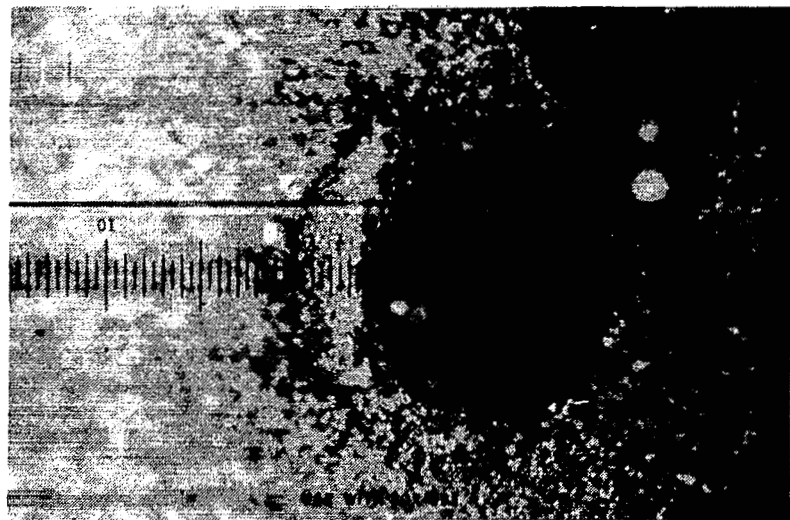
Pretest and posttest photographs were made of the penetration point on the zee-stiffened panel to determine if any enlargement or change occurred as a result of exposure to the 1,477°K (2,200°F) simulated entry airflow conditions in the PAT tests. Comparison of the pretest and posttest photographs (Figure 5-6) showed no change in the hole size or appearance. In a similar manner no change of the cratered area on the corrugation-stiffened panel was apparent after the PAT tests. Results from these tests on the meteoroid impingement panels indicated a high survivability capability for TD Ni-20Cr heat shields during entry following meteoroid impact. Based on temperature readings from thermocouples located on the interior side of the panel, no apparent localized temperature excursions which might be expected from hot gas ingestion were observed.

Posttest examination of the meteoroid impact test panels showed that several spot welds failed during Plasma Arc Tunnel tests. Since the failures were local and did not precipitate additional spot weld failures, the panels continued to sustain the test conditions until completion of the runs.

#### 5.4 SIMULATED JOINT TESTS

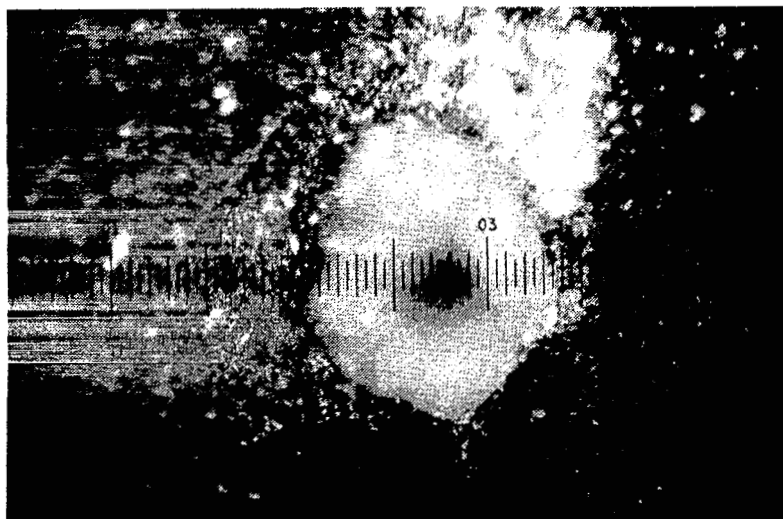
Tests were also conducted in the Plasma Arc Tunnel to evaluate the effectiveness of two panel joint design concepts. One design simulated a panel closeout design employing a closure strip to cover the gap between panel edges. The second design simulated an overlapping edge joint concept in which one panel edge overlaps the adjacent panel edge. Size was again restricted to a 10.16 by 10.16-cm (4 by 4-in.) planform to fit within the plasma stream core. All sheet metal parts and the threaded fasteners were made from TD Ni-20Cr.

Tests of the joint panels were conducted with the objective of providing comparative evaluations of the two designs under high-velocity, elevated-temperature flow conditions simulating entry airflow over heat shield panel edges. Thermocouples were installed on the joint designs as shown in Figure 5-7 to determine if local heating inside the joint occurred from flow penetration. Qualitative evaluations were also made by observing posttest flatness of the edges and the general condition of the panels and fasteners.



100X

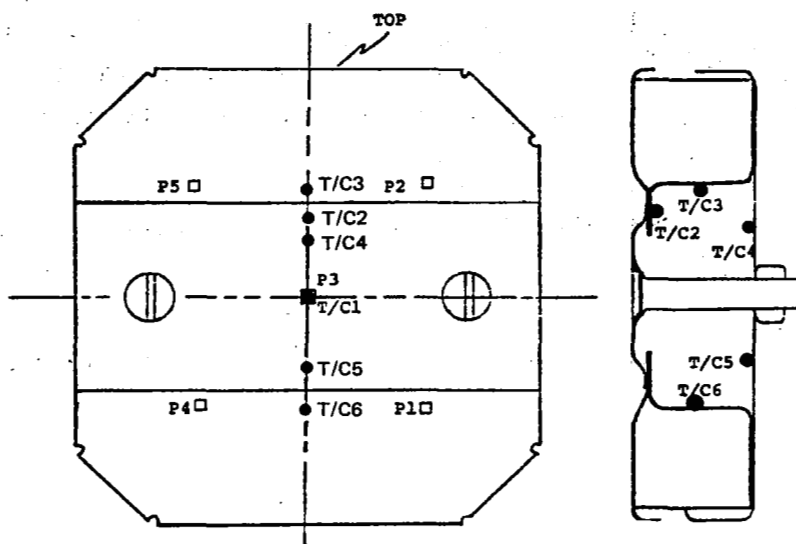
a. PRIOR TO PLASMA ARC TUNNEL TESTS



100X

b. AFTER PLASMA ARC TUNNEL EXPOSURE

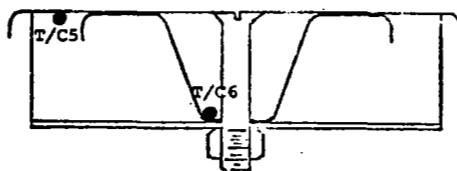
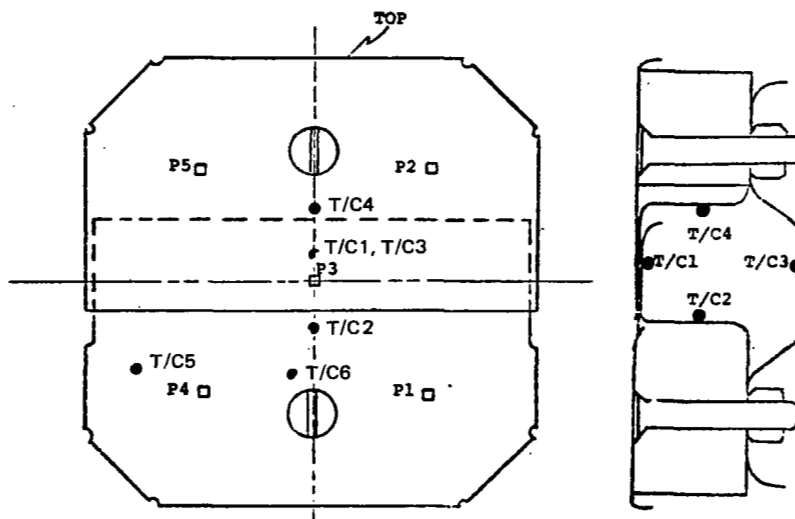
Figure 5-6 . Magnified Views of the Zee-Stiffened Panel Face Sheet Penetration Point



**Notes:**

- \*P1 through P5 - Pyrometer sighting locations.
- \*T/C 1 through T/C 6 - Tack-welded thermocouple locations.

**a. CLOSURE STRIP JOINT DESIGN**



**Notes:**

- \*P1 through P5 - Pyrometer sighting locations.
- \*T/C 1 through T/C 6 - tack-welded thermocouple locations.

**b. OVERLAPPING EDGE DESIGN**

Figure 5-7. Thermocouple and Pyrometer Sighting Locations for Panel Joint Samples

Each of the joint designs was subjected to 10 plasma stream exposures with the front face of the sample being held at 1,477°K (2,200°F) for 20 minutes in each exposure. The samples were tested alternately so that each design experienced a 20-minute cooling cycle between immersions in the plasma stream.

Temperature time histories taken from thermocouple recordings during the tenth test cycle are shown in Figures 5-8 and 5-9. Such data show the temperature histories of interior portions of each joint design as well as the surface temperature histories. In both designs, the interior temperatures remained nearly constant after achieving equilibrium heating, a condition that indicates no significant ingestion of hot gases into the interior portions of the joints. Because the data of Figure 5-8 and 5-9 were obtained on the tenth test cycle, it was concluded that repeated cycles would not degrade the joint designs significantly, even though slight waviness from thermal stresses occurred on the outer surface of the overlapping edge design. The data of Figure 5-8 show a steady-state temperature difference of approximately 111°K (200°F) from the outer surface at Thermocouple 1 to the interior support rail, where Thermocouple 3 was located. The overlapping edge test sample is shown in Figure 5-10 after completion of cyclic exposure in the Plasma Arc Tunnel. This joint design developed a crack at one corner as shown in Figure 5-11.

In the closure strip design (Figure 5-9), the difference between the outer surface at Thermocouple 1 and the internal support position (Thermocouples 4 and 5) was approximately 122°K (220°F). Thus, both joint designs showed similar temperature decreases at the centerline of the joint between the outer surface and the simulated structure to which the panels were attached. The closure strip design was judged to have the better performance, based on the fact that it exhibited no distortion, whereas the overlapping edge design suffered permanent set in the form of sine-wave-shaped distortions along the lip of the outer panel edge. Temperature recordings showed no increased transient heating due to hot gas ingestion in either joint design.

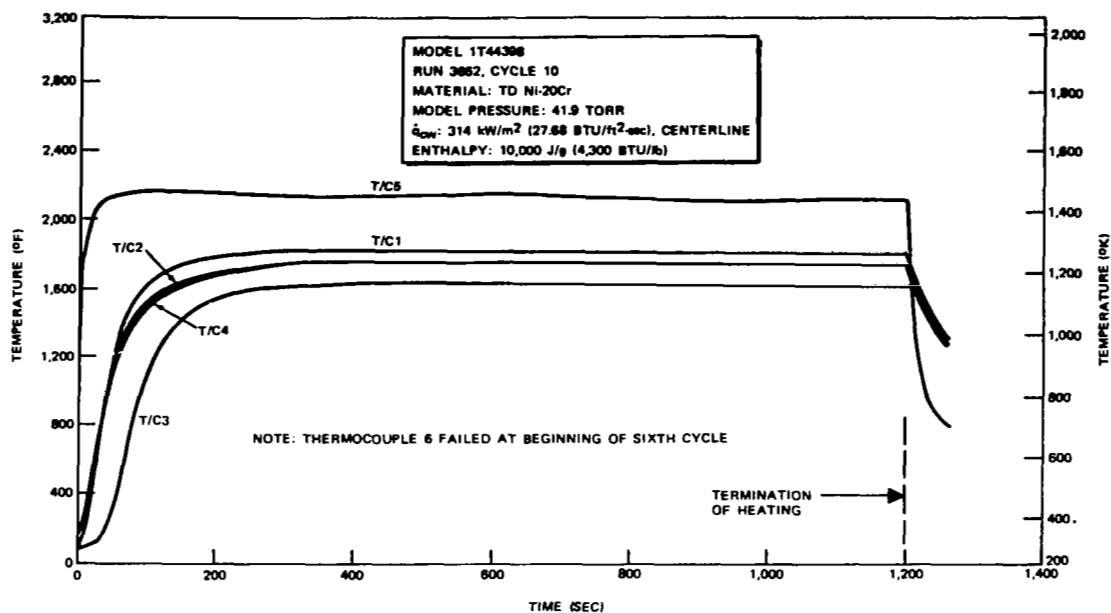


Figure 5-8. Panel Edge Joint Temperature Histories; Overlapping Edge Design

CR60

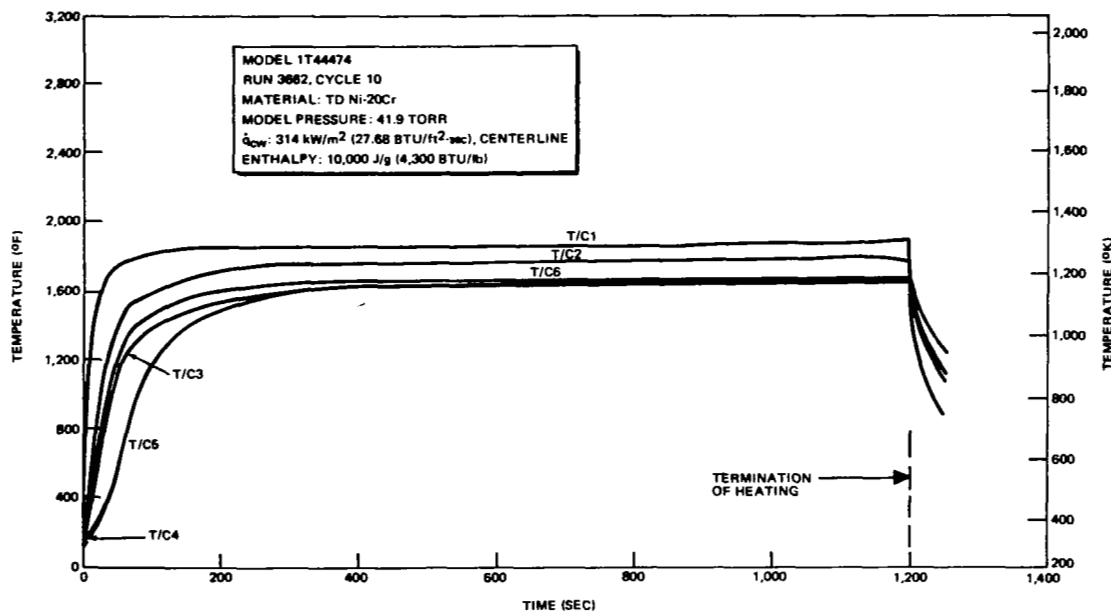


Figure 5-9. Panel Edge Joint Temperature Histories; Closure Strip Design





**Figure 5-10. Overlapping Panel Edge Joint After Cyclic Exposures in the Plasma Arc Tunnel**



**Figure 5-11. Corner of Overlapping Panel Joint Showing Crack at Relief Radius**

## 5.5 FULL-SCALE SUBSIZE PANEL TESTS

The full-scale subsize panels were designed to simulate full-length beam-supported panels with simulated attachments and packaged low-density insulation underneath the TD Ni-20Cr heat shields. Programmed cycles of differential pressure, temperature, and static pressure were applied to simulate boost, entry, and cruise flight conditions experienced at the selected TPS area on the lower surface of the Orbiter (Figure 2-5). Simulated boost flight acoustic loads were interspersed with the cyclic pressure and temperature conditions.

The test system used for the Phase I subsize specimens is shown schematically in Figure 5-12, which also shows the sequence of testing. So that both competing panel designs would experience identical histories of loads, temperatures, pressures, and acoustic levels, they were mounted for testing in the same basic test fixture, a stainless steel pressure box with TD Ni-20Cr end supports that held the test panels. The test fixture was designed to permit its use in both the Space Simulation Chamber and the Acoustic Facility so that the test panels could remain in place except for necessary inspections.

The programmed cycles of differential pressure, chamber pressure, and temperature are shown in Figure 5-13, and Figure 5-14 presents the spectrum selected for acoustic tests. The chamber pressure desired for the test profile was lower than that shown in Figure 5-13. However, to maintain the desired panel differential pressure profile, it was necessary to use a higher chamber pressure during portions of the test cycle. During the simulated entry portion of the test cycle, the chamber pressure ranged between approximately 1 and 15 torr. This pressure range, while higher than the computed ambient pressure during the Orbiter entry flight, was sufficiently low to simulate the low-pressure effects that could cause degradation from chromium depletion under elevated-temperature, low-pressure environments (see Reference 2, Appendix C).

The panel designs and their instrumentation points are shown in Figures 5-15 and 5-16. Detail parts of the corrugation-stiffened panel are shown in Figure 5-17, and Figure 5-18 shows the assembled test panels after being

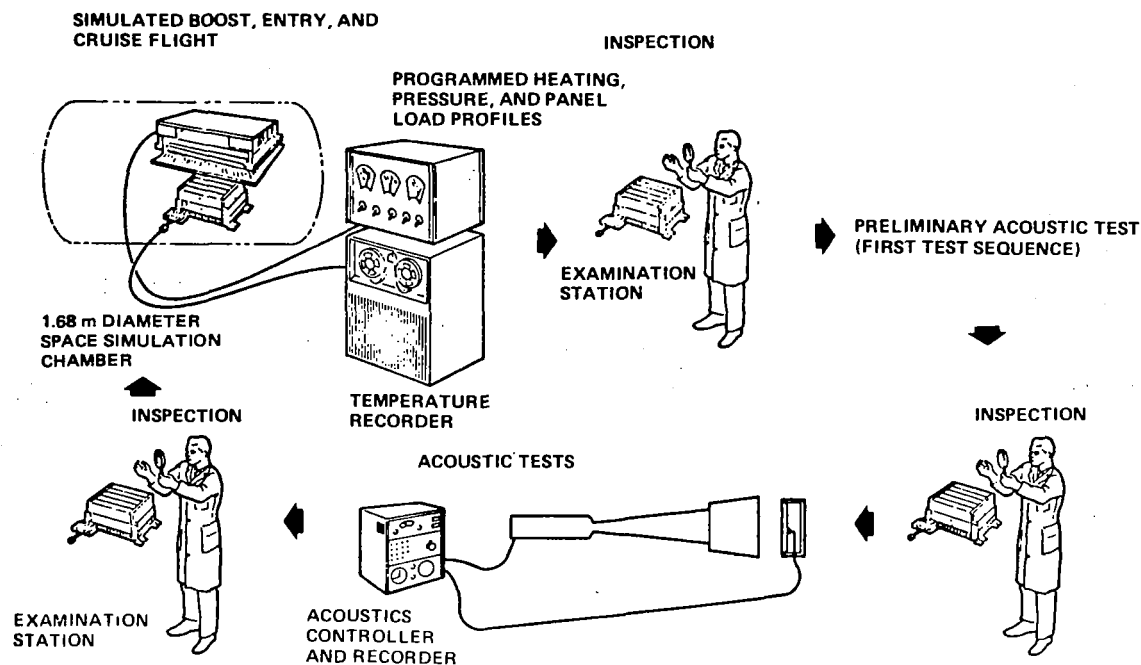


Figure 5-12. Full-Scale Subsize Panel Test Sequence

CR60

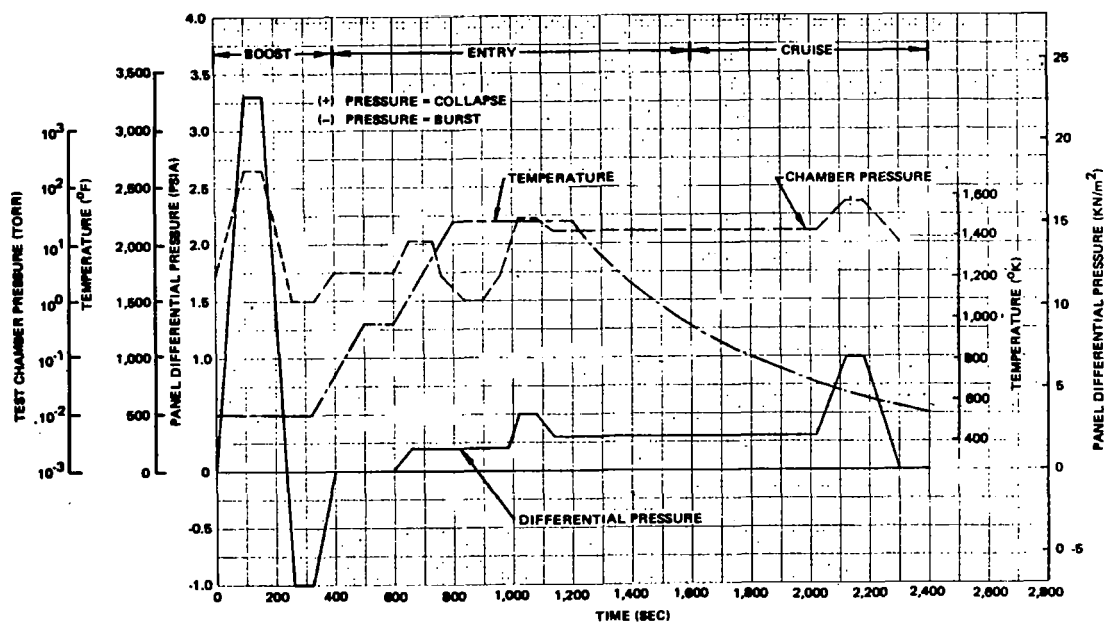


Figure 5-13. Full-Scale Subsize Panel Test Profiles

NOTE: DIMENSIONS IN cm

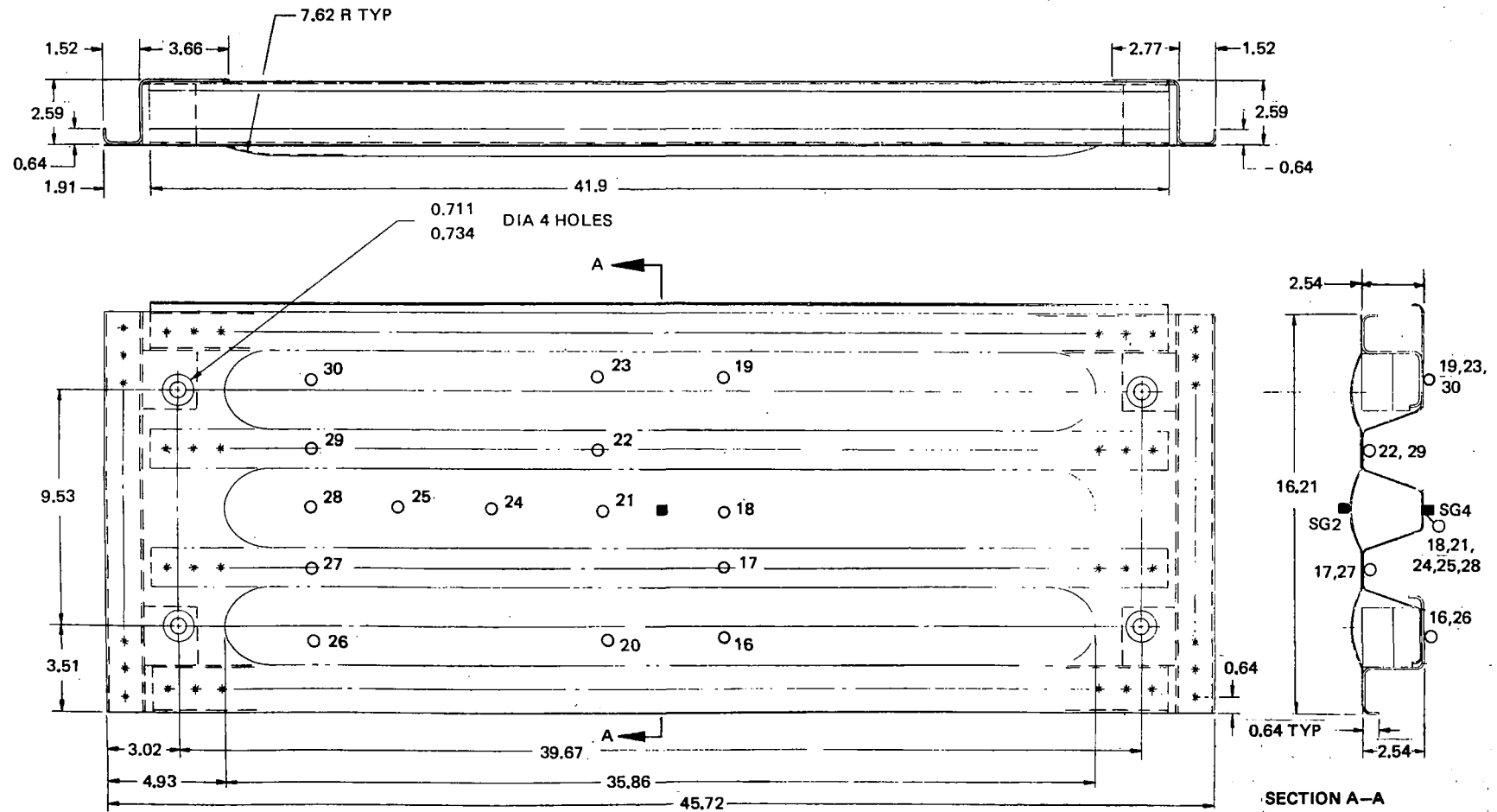


Figure 5-16. Instrumentation Points on Corrugation-Stiffened Test Panel

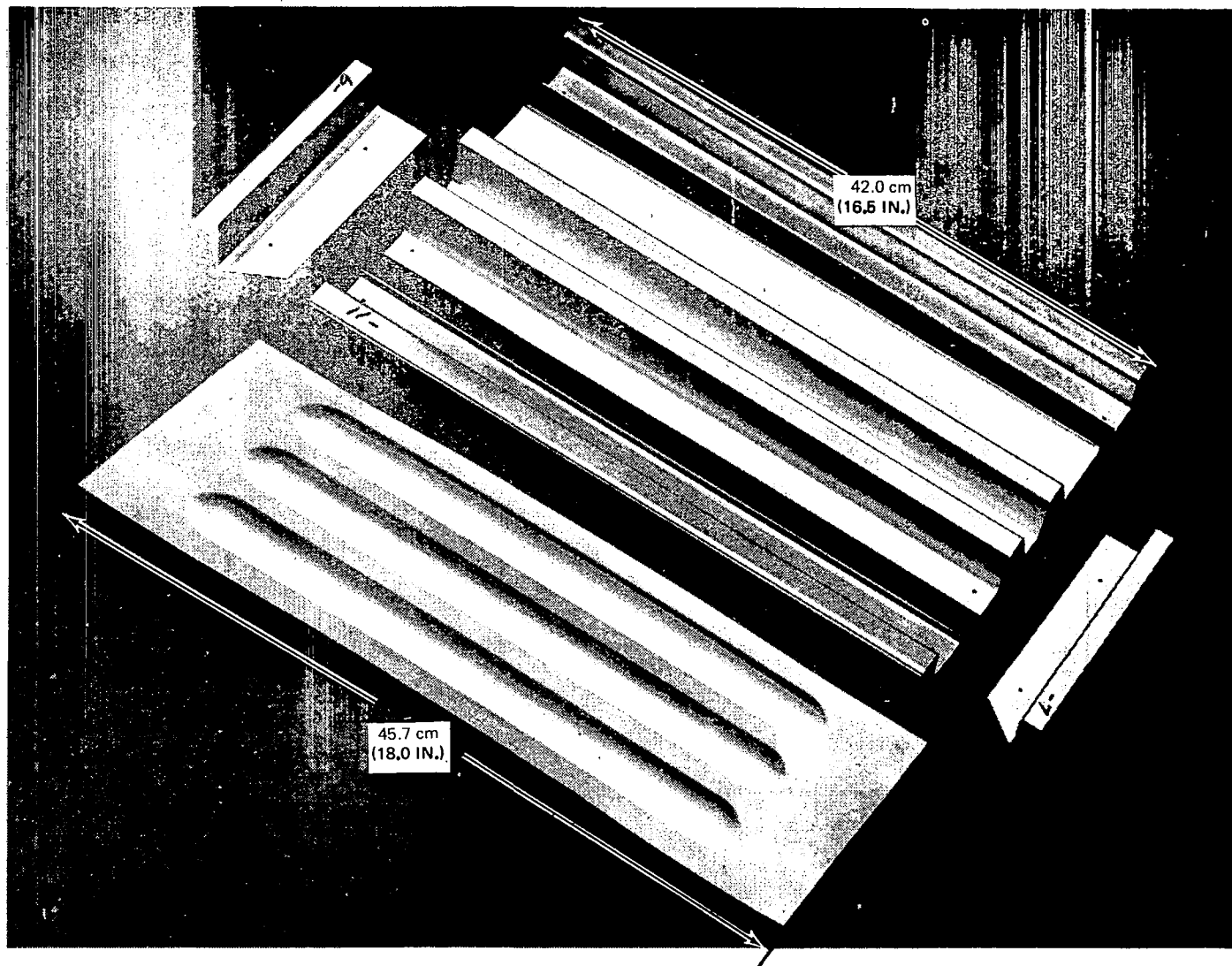


Figure 5-17 Detail Parts for Corrugation-Stiffened Test Panel

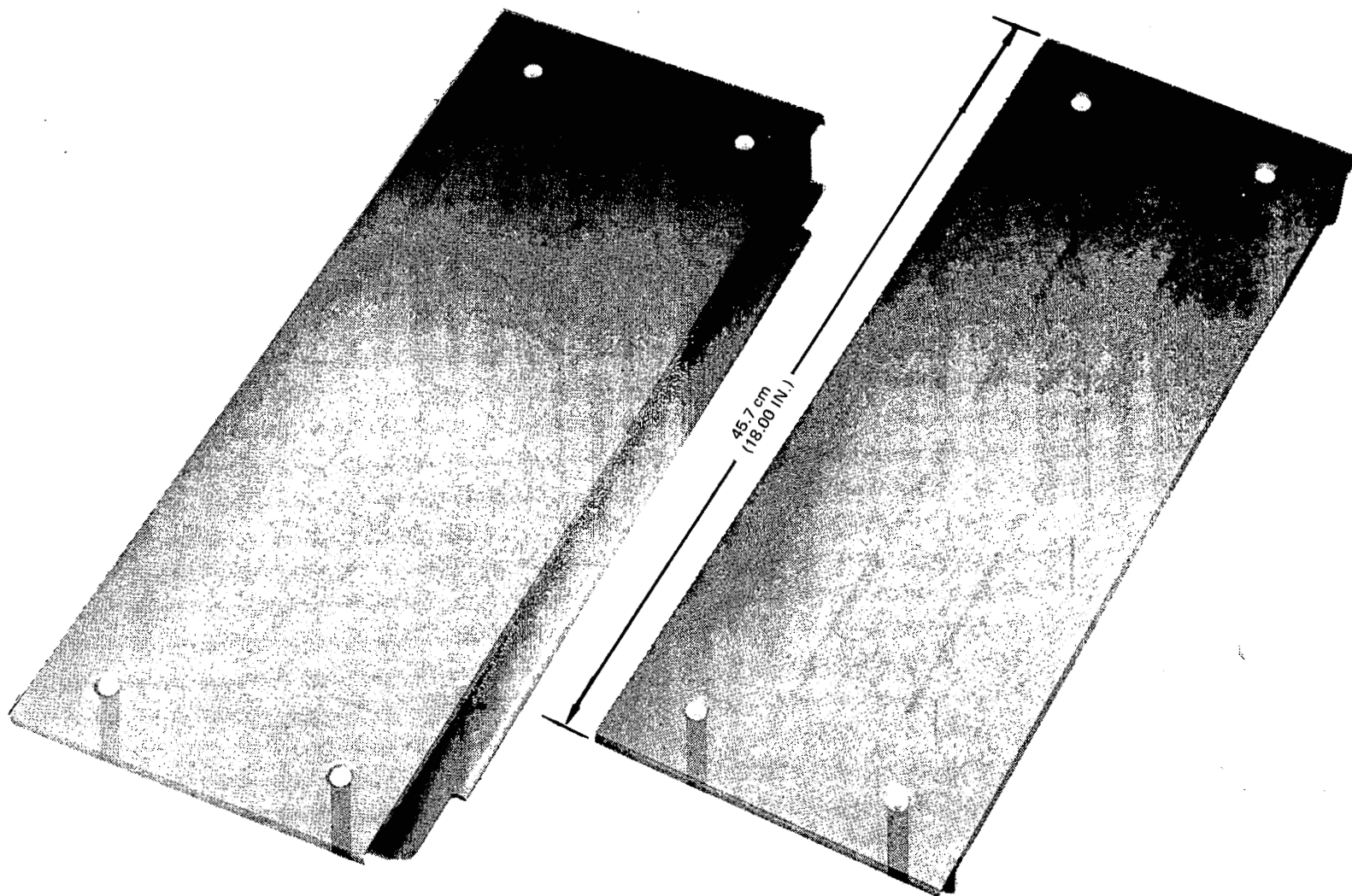


Figure 5-18. Full-Scale Subsize Test Panels

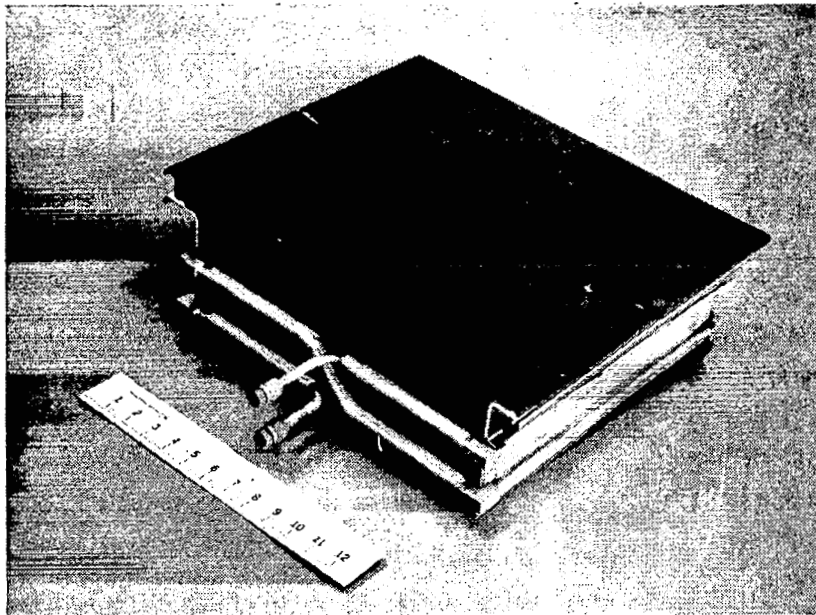


Figure 5-19. Assembled Test Unit

nearest the panels, and three thermocouples were located in similar positions on the cool side of the package away from the test panels. The insulation package thermocouple locations are shown in Figure 5-20.

After delivery of the TD Ni-20Cr test panels and associated components to the Space Simulation Facility, strain gages were installed at the center of each full-scale subsize test panel (Figures 5-15 and 5-16) to monitor stresses in preliminary differential-pressure trials and in preliminary acoustic tests.

Uniaxial gages were mounted on the external surface of the face sheet of each panel and on the stiffening elements on the internal side of the panel. For the zee-stiffened panel, the interior strain gage was mounted on the cap of the stiffener (Figure 5-15); for the corrugation-stiffened panel, a gage was mounted at the center of the panel on the corrugation (Figure 5-16).

Trial runs were conducted at room temperature to determine stresses that occurred at various levels of differential pressure. The trial runs were conducted in simple steps up to the maximum collapse and burst differential

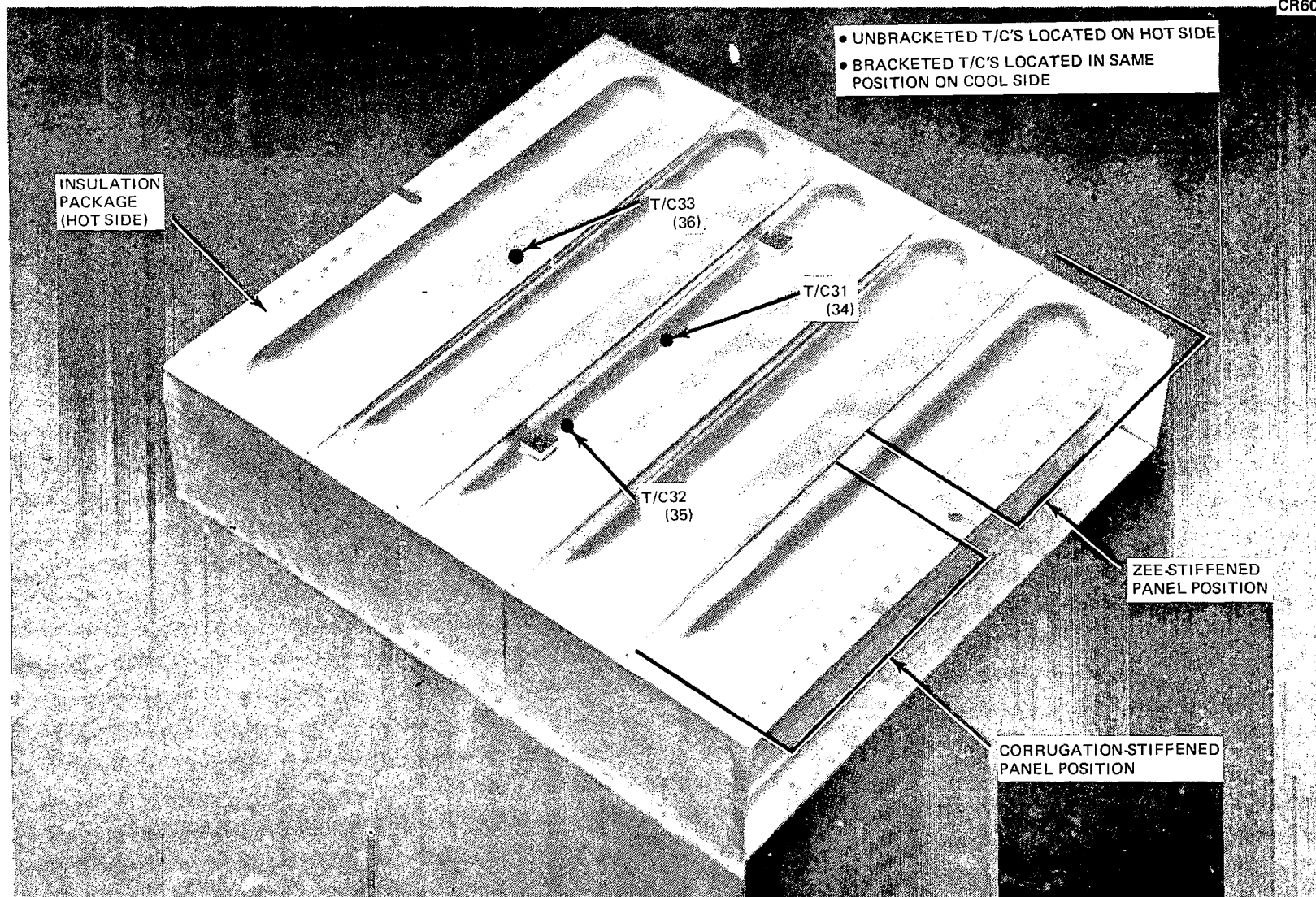


Figure 5-20. Insulation Package Thermocouple Locations



pressure levels programmed for the boost flight portion of the cyclic tests. As shown in Figure 5-13, a maximum collapse differential pressure of  $22.8 \text{ kN/m}^2$  (3.3 psi) and a maximum burst differential pressure of  $-6.89 \text{ kN/m}^2$  (-1.0 psi) were programmed for the boost portion of the test cycle.

Stress levels recorded in the zee-stiffened panel during preliminary trials at the peak pressure of  $22.8 \text{ kN/m}^2$  (3.3 psi) were  $47.1 \text{ MN/m}^2$  (6,830 psi) compression in the face sheet and  $85.8 \text{ MN/m}^2$  (12,440 psi) tension in the zee stiffener. Similar stresses in the corrugation-stiffened panel were  $53.8 \text{ MN/m}^2$  (7,800 psi) compression in the face sheet and  $52.3 \text{ MN/m}^2$  (7,560 psi) tension in the corrugation. The trial burst-pressure test stresses were lower, ranging from  $15.1 \text{ MN/m}^2$  (2,190 psi) tension to  $16.8 \text{ MN/m}^2$  (2,440 psi) compression.

Preliminary acoustic tests were conducted next to determine stress responses at the center of each panel. An overall sound pressure level (OASPL) of 150 db was used initially, and progressively higher acoustic levels were applied until an OASPL of 165 db was reached. Maximum stress levels recorded were less than  $20.7 \text{ MN/m}^2$  (3,000 psi). The overall rms stress level at each strain gage position varied with OASPL as indicated in Figure 5-21.

Thermocouples were installed on the panels after the preliminary differential pressure and acoustic tests were conducted. Modifications were also made to the pressure box to permit instrumentation leadouts, to provide mounting positions for the deflection transducers, and to install instrumentation connectors on the box surface opposite the panels.

After modifications to the pressure box were completed, the panels were installed and instrumentation checks were made. The box and panel edges were then sealed to prevent leakage and preliminary differential pressure checks were conducted.

In addition to the deflection transducers installed to measure normal deflection at the centers of the panels, two transducers were installed at the ends of the panels to measure panel expansion at elevated temperatures.

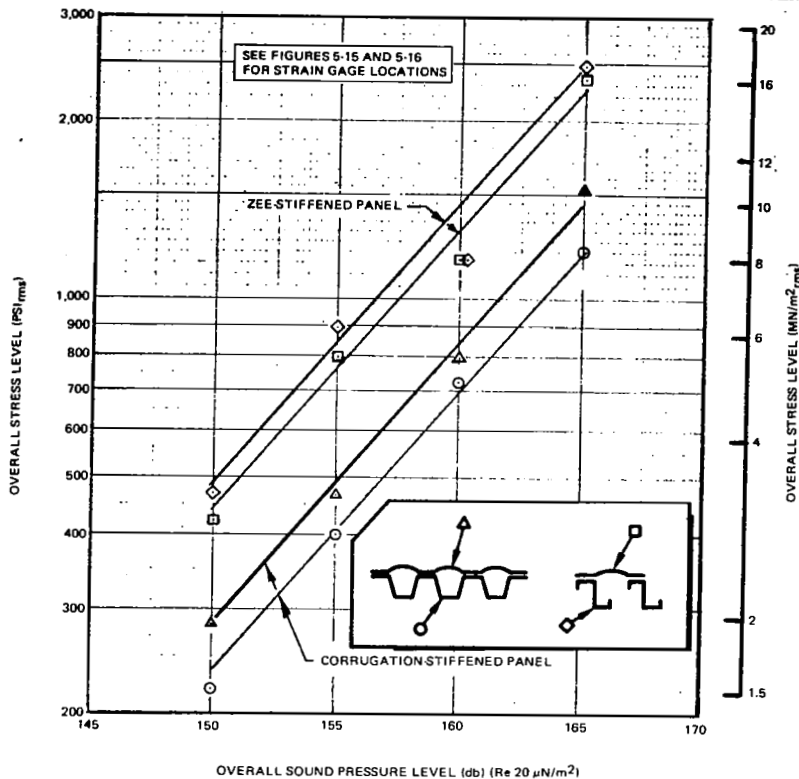
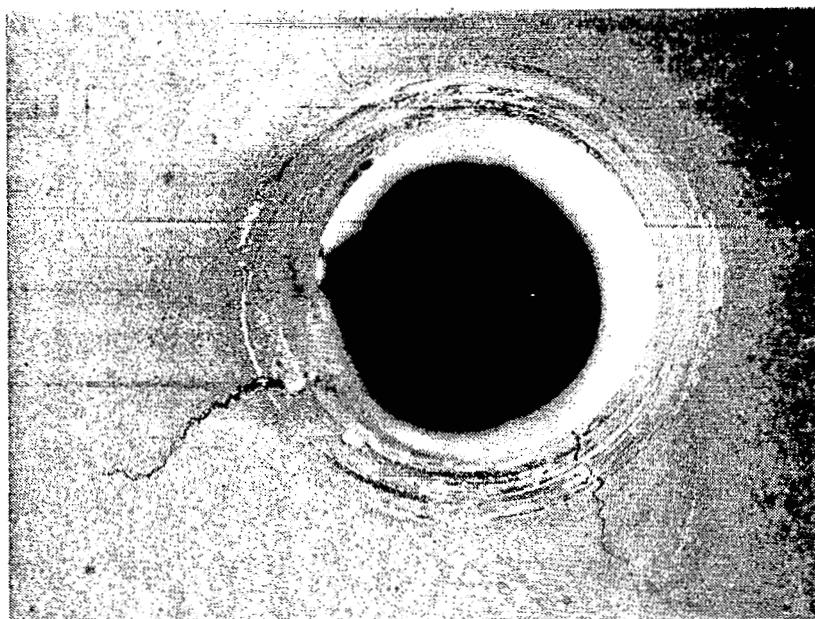


Figure 5-21. RMS Stress as a Function of Overall Sound Pressure Level

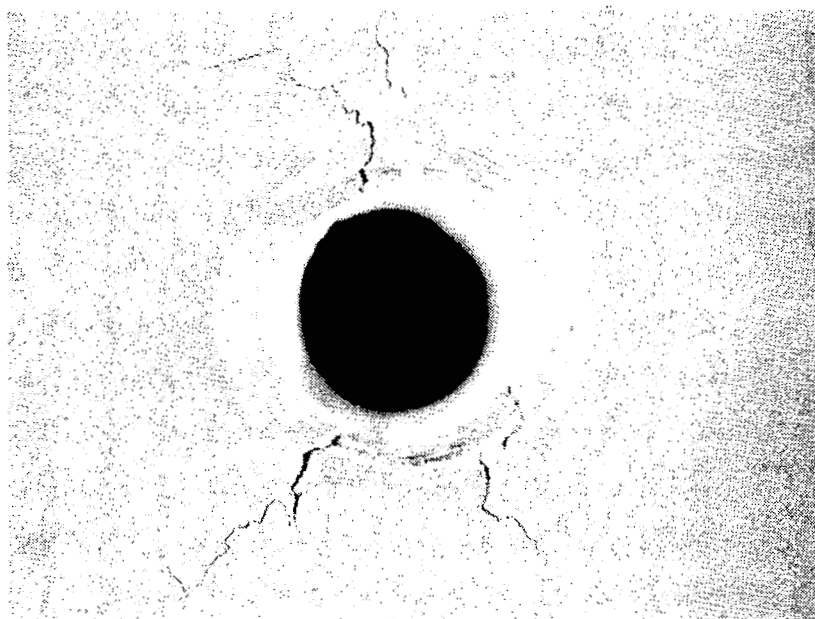
Preliminary thermal cycles were run at several temperature levels up to 1,368°K (2,000°F). Panel expansions appeared normal in the check runs, and testing then proceeded to full load and thermal cycles using the profiles of Figure 5-13.

Twelve cycles were applied to the two panels in the initial set of runs using the Space Simulation Chamber. The panels were then removed and given a detailed visual inspection. As a result of this inspection, a number of hairline cracks were detected. A majority of the cracks were observed around the dimpled holes in the panel face sheets, the cracks progressing radially outward from the edges of the holes. Typical cracks observed at the end of the first twelve runs are shown in Figure 5-22. Two other hairline cracks were observed along spotweld rows in the zee-stiffened panel, and a slight buckle was observed in one of the face sheet beads on the zee-stiffened panel. An inspection of the internal insulation package showed no deterioration of that portion of the TPS test components.



a. ATTACH POINT NO. 1

5X



b. ATTACH POINT NO. 3

5X

Figure 5-22 Typical Cracks Observed at End of Twelfth Thermal/Load Cycle

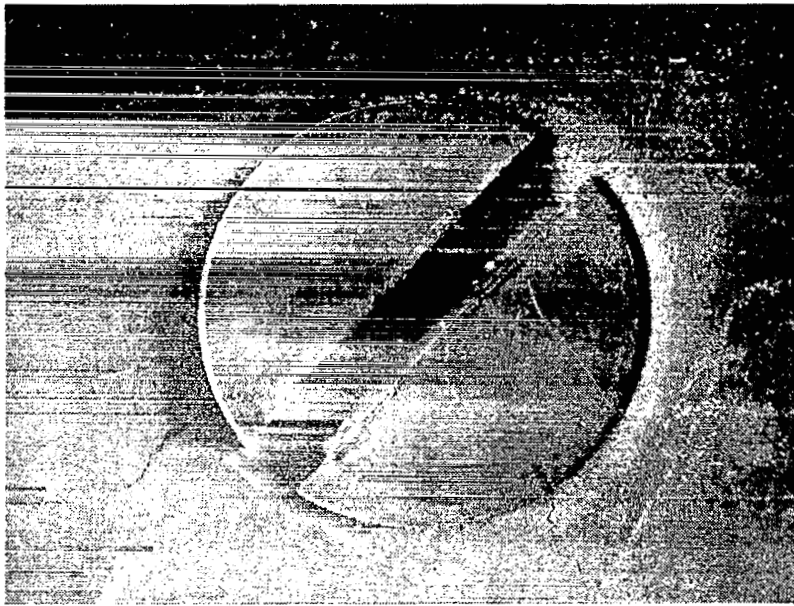
The cracks appeared to be small enough to permit continuation of programmed test cycles. Consequently, the first acoustic load test was started with a 1-minute exposure of the panels to an overall sound pressure level of 165 db. The programmed level was 160 db, but 165 db was inadvertently used since the maximum level applied in preliminary tests was 165 db. Examination of the panels after 1 minute at 165 db showed substantial extension of the radial cracks at the attach points. Details of several attach points are shown in Figure 5-23, and extension of the cracks is evident when compared to those shown in Figure 5-22. A detailed inspection showed similar extensions of existing cracks at other panel attach positions.

Reinforcement of the holes was necessary to continue through the test series. Despite the cracks in the attach positions, the panels were judged to be capable of sustaining additional testing if the holes in the face sheets were reinforced. Reinforcing washers made from 0.0457-cm (0.018-in.) thick TD Ni-20Cr sheet were added under the head of each screw, the size of each washer being approximately 2.54 by 2.54-cm (1.0 by 1.0-in.). With the reinforcing washers in place, the instrumentation was replaced where necessary and cyclic load and thermal testing was resumed.

During removal of the panels after the twelfth cycle, seizing of two of the fasteners occurred. One fastener was subsequently freed without damage to threads on either the nut or bolt, but the second fastener was damaged beyond use and required replacement before proceeding with additional tests.

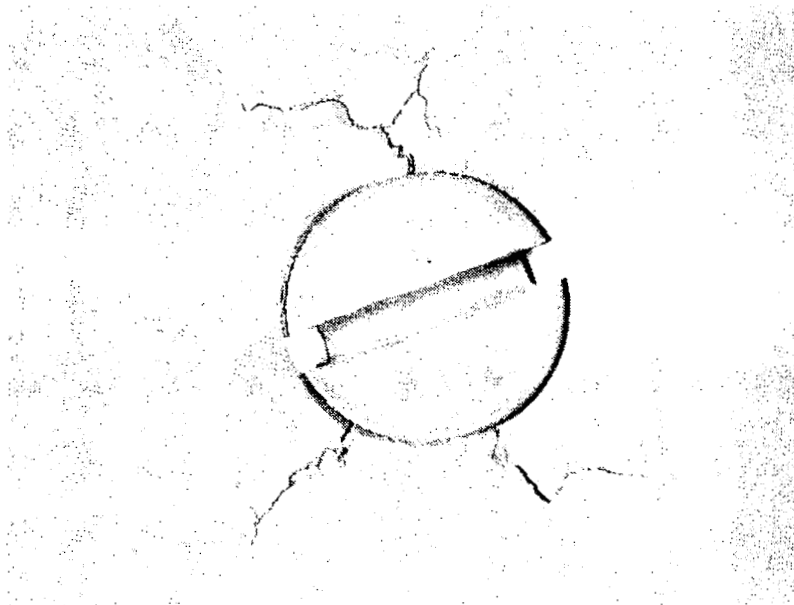
Inspection of the screws and nuts showed that fine particles of the fibrous insulation material used for a pressure seal had fallen into the thread engagement area. The insulation particles, combined with some oxide particles from the fasteners, caused the fasteners to seize during the first 12 test cycles. In subsequent tests, care was taken to ensure that all threads were cleaned prior to attaching the panels and that the threads were properly coated with a high temperature lubricant.

An additional 63 load and thermal cycles were applied before the panels were again removed for inspection. Thus, with a total of 75 cycles, the panels were inspected before applying acoustic loads equivalent to 75 simulated



a. ATTACH POINT NO. 1

5X



b. ATTACH POINT NO. 3

4X

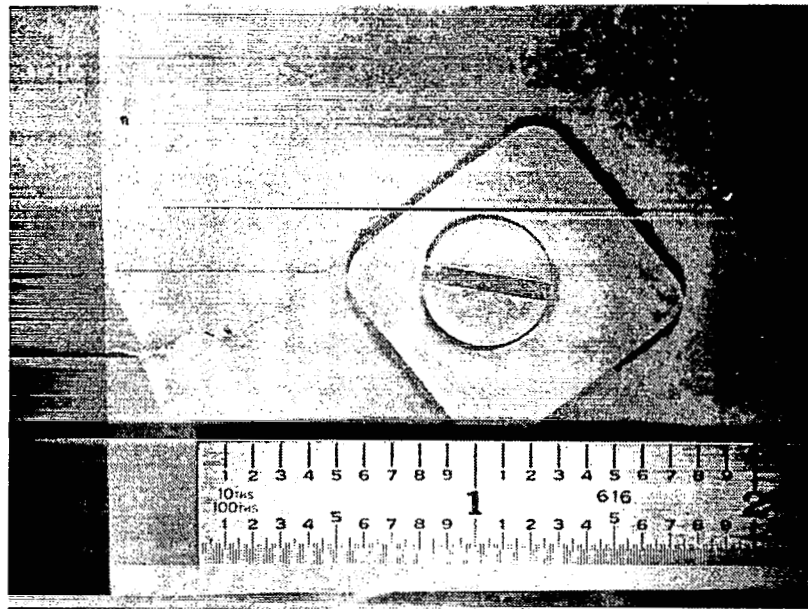
Figure 5-23. Panel Face Sheet Cracks After Initial Acoustic Exposure at 165 db

boost flights. Crack extensions did not appear beyond the edge of the reinforcing washers except at attach point one. The growth at attach point one, shown in Figure 5-24, extended to the edge of the panel. Despite this extension, the panel was judged to be capable of sustaining additional tests, and acoustic tests at 160 db OASPL were conducted. The acoustic exposure at this point consisted of 36.5 minutes at 160 db, bringing the total acoustic exposure time to 37.5 minutes. With 30 seconds being equivalent to one lift-off exposure, 75 cycles of acoustic exposures had been applied at that point.

The acoustic exposures were followed by another 14 load and thermal cycles and an additional 7 minutes of acoustic exposure to bring the total simulated cycles to 89. The panels were removed from the pressure box at that time to permit inspection and to allow replacement and repair of thermocouples where necessary. The appearance of the panels was similar to that seen at the inspection after the 12th cycle. Slight additional growth of the cracks in the panel edge members was noted, but the general condition of the panels was the same as noted after 12 thermal cycles plus the initial 1-minute acoustic exposure at 165 db.

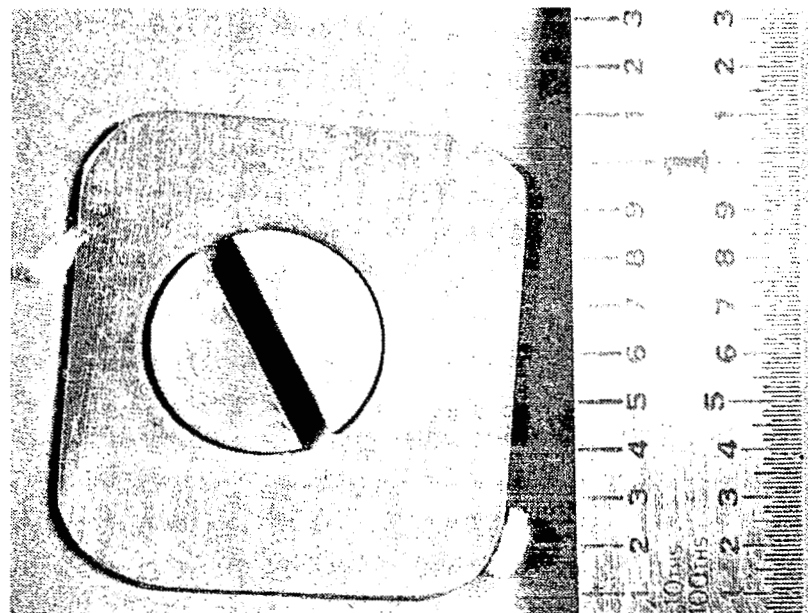
After repair of the instrumentation, the panels were reinstalled on the test fixture and subjected to the final 11 thermal and load cycles plus the additional 5.5 minutes of acoustic loading required to simulate 100 mission cycles.

At the end of the full 100 cycles, a visual inspection was made at the Space Simulation Laboratory before shipment of the components to the Huntington Beach facility. This inspection showed the panels to be in the same condition as noted at the previous inspection after 89 cycles. Posttest photographs of the heat shields and insulation are shown in Figures 5-25 through 5-27 after completion of the full 100 test cycles. Figure 5-25 shows the heat shields after removal of the fasteners and reinforcing washers. The increased cracking and damage at the attach points is evident, particularly at attach point 5 on the zee-stiffened panel. An edge view of the corrugation-stiffened panel is shown in Figure 5-26 while the panels were still attached to the fixture. This view shows the relative overall flatness maintained by the panels even though the 0.0254-cm (0.010-in.) face sheet exhibited a small



a. ATTACH POINT NO. 1

1.5X



b. ATTACH POINT NO. 3

2.5X

**Figure 5-24. Panel Face Sheet Cracks After 75th Thermal/Load Cycle**

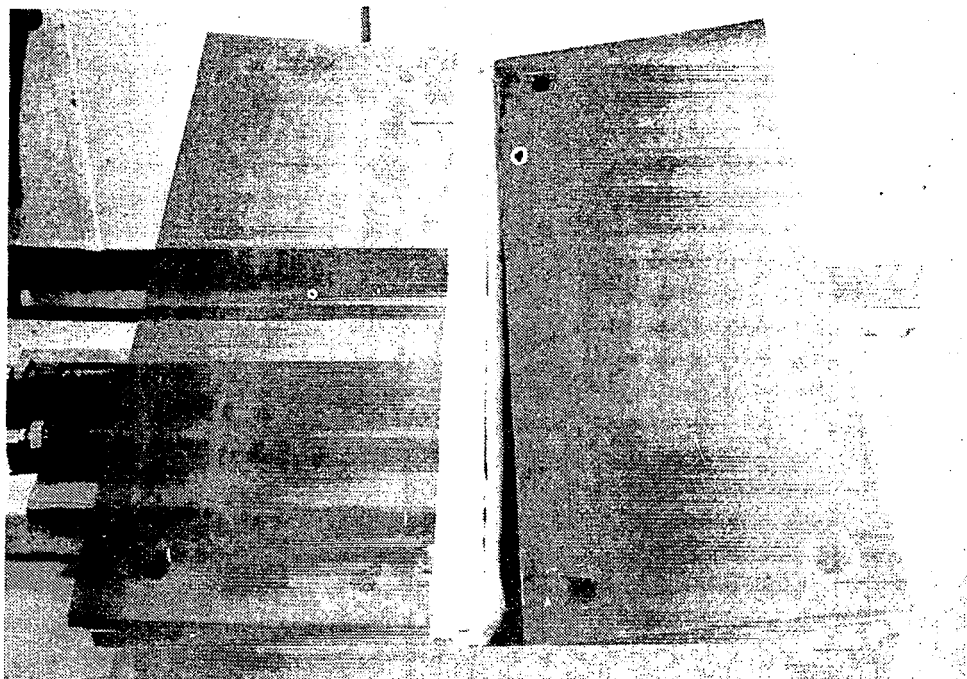


Figure 5-25. Full Scale Subsize Heat Shield After 100 Test Cycles

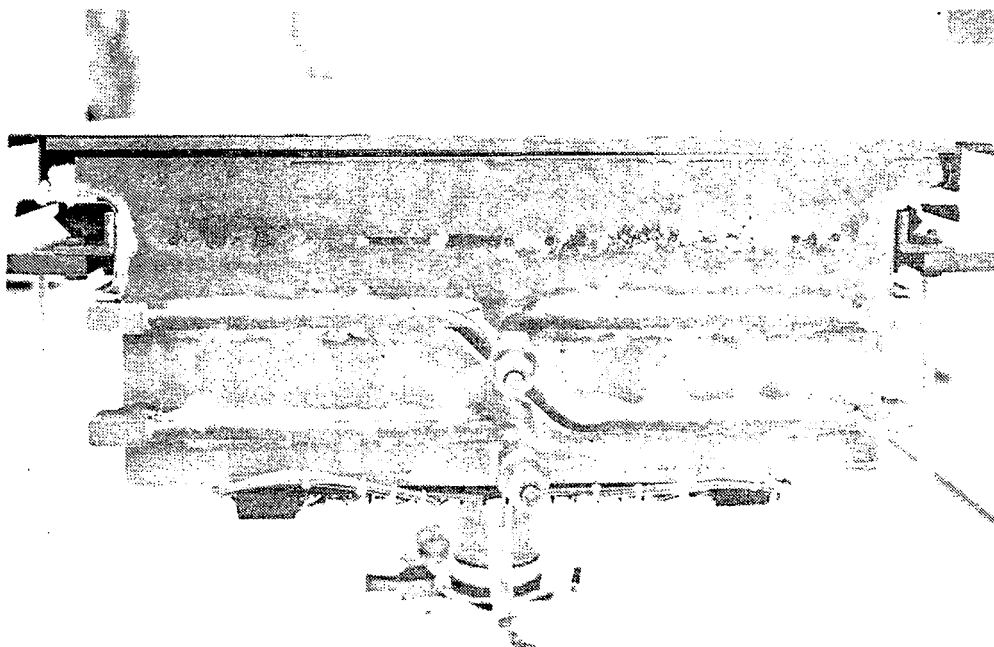


Figure 5-26. Edge View of Panels After 100 Test Cycles



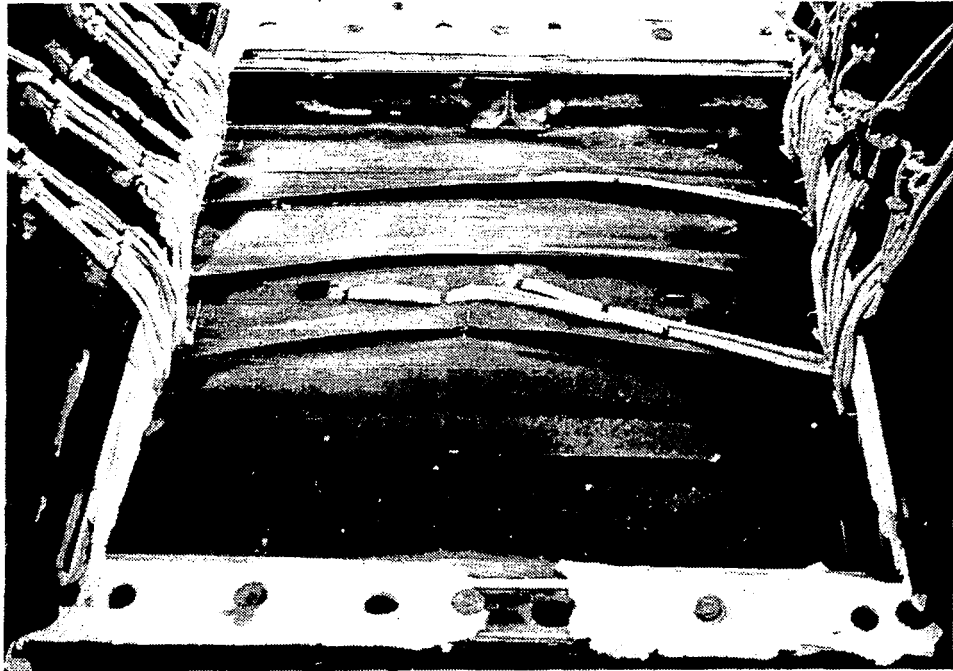


Figure 5-27. Insulation Package at Completion of 100 Test Cycles

amount of waviness along its edge. Figure 5-27 shows the insulation package at the termination of 100 test cycles. Permanent set of the outer face of the 0.0127-cm (0.005-in.) foil used for packaging the low-density insulation occurred as shown in Figure 5-27.

Data recorded in each thermal and load cycle included time-histories of the differential pressure applied to the panels; chamber pressure, temperature at each thermocouple location, and deflections at the four deflection transducers. Typical data are shown in Figures 5-28 through 5-30 for test run 41. Panel differential pressure and chamber pressure are shown in Figure 5-28, while typical temperatures recorded on the panels are shown in Figure 5-29. Figure 5-30 presents deflection measurements.

The insulation package temperatures presented in Figure 5-29 show the lower temperature registered by Thermocouple 34 on the cool side of the package when compared to the temperatures at Thermocouples 35 and 36. The higher temperatures at the latter two positions were judged to have resulted from

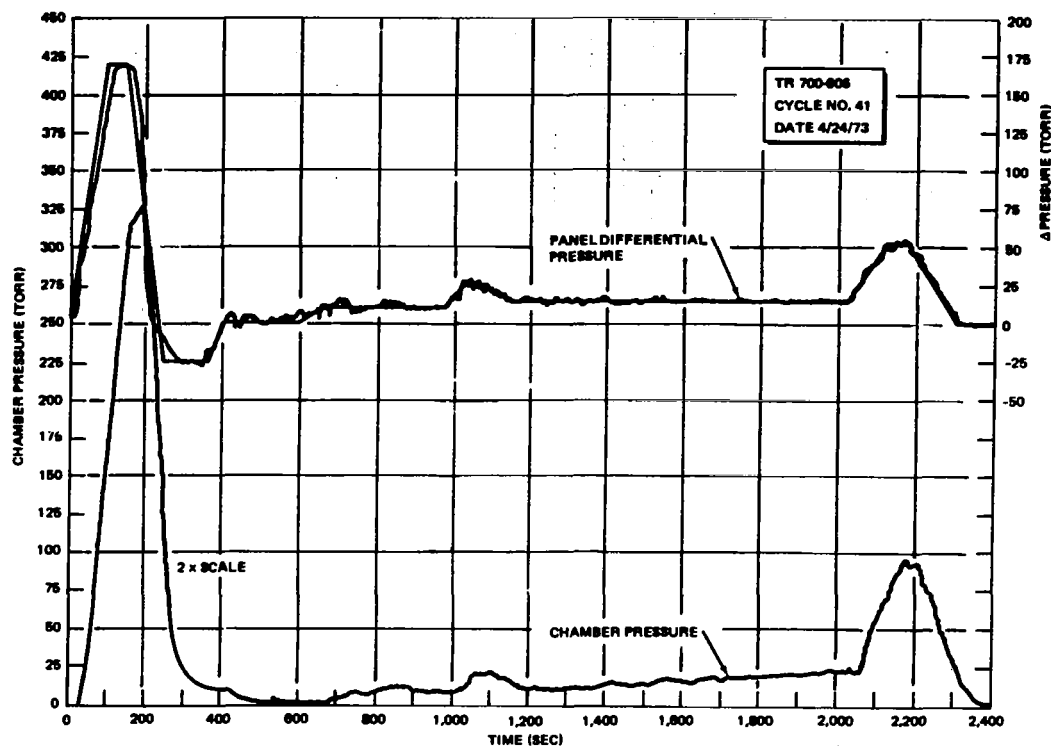


Figure 5-28. Panel Differential Pressure and Chamber Pressure, Run 41

convection effects caused by some flow of heated air through the passages used for deflection rods and through the gap between the test fixture and the edge of the insulation package. At maximum-temperature conditions ( $t = 1,100$  sec), the temperature differential between Thermocouples 31 and 34 was approximately  $973^{\circ}\text{K}$  ( $1,750^{\circ}\text{F}$ ). The temperature time history computed in thermal analyses for the cool side of the insulation package is shown in Figure 5-29 for an assumed static pressure of 10 torr. Comparison of Thermocouple 34 and the computed temperature time history indicates the lower efficiency of the actual test package in the initial portion of the test. However, the maximum temperature at Thermocouple 34 did not exceed  $445^{\circ}\text{K}$  ( $340^{\circ}\text{F}$ ), while the computed temperature near the end of the test was  $550^{\circ}\text{K}$  ( $530^{\circ}\text{F}$ ). Thus, the test insulation package, in areas not affected by convective heating, maintained cool-side temperatures lower than those predicted by analysis.

The deflections, shown in Figure 5-30, indicate maximum normal deflections at panel midspan positions of approximately  $\pm 0.33\text{-cm}$  ( $0.13\text{-in.}$ ). The normal deflection during the simulated entry portion of the test ( $t = 800$  to  $1,600$

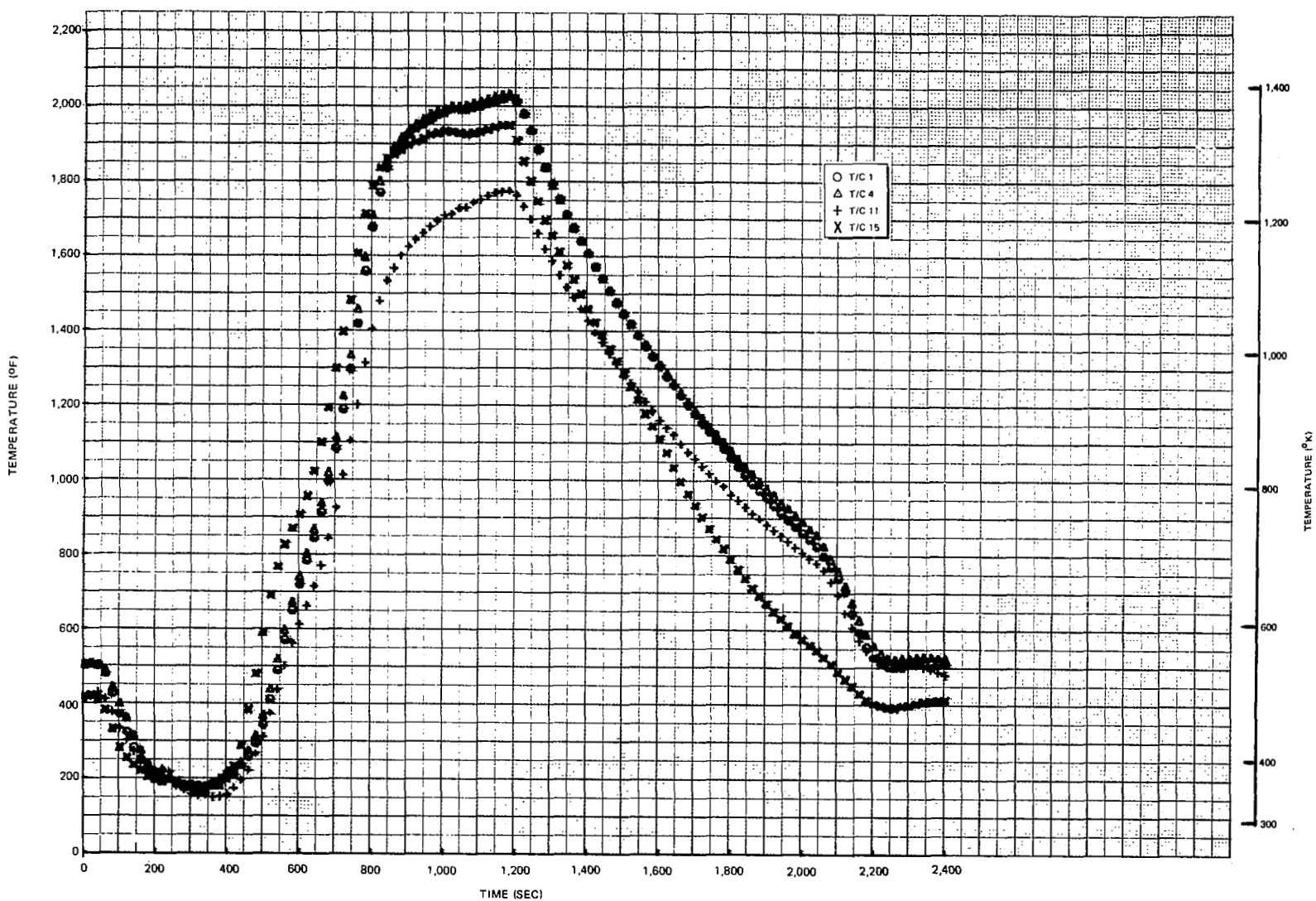


Figure 5-29. Thermocouple Recordings, Run 41 (Page 1 of 2)

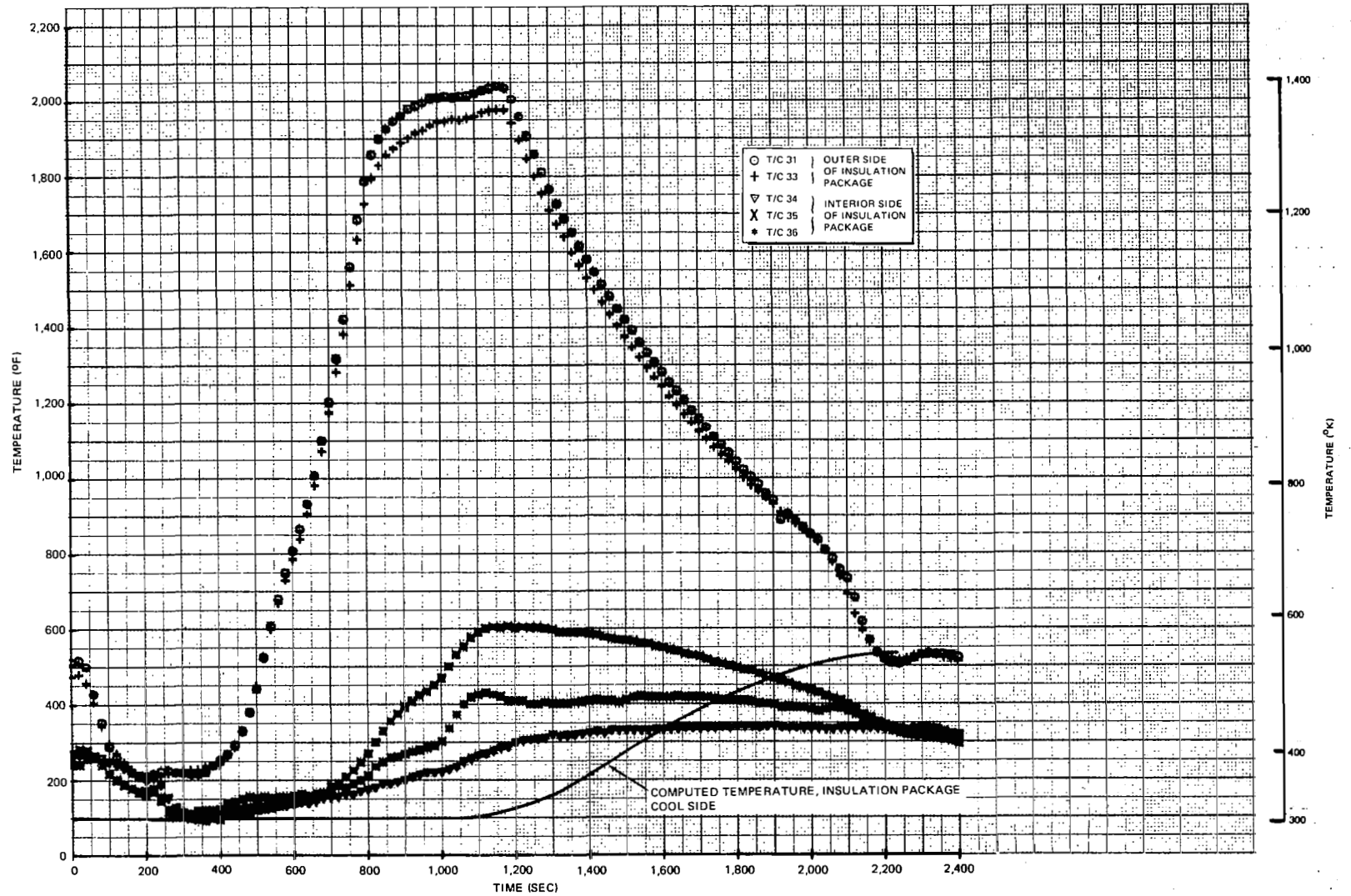


Figure 5-29. Thermocouple Recordings, Run 41 (Page 2 of 2)

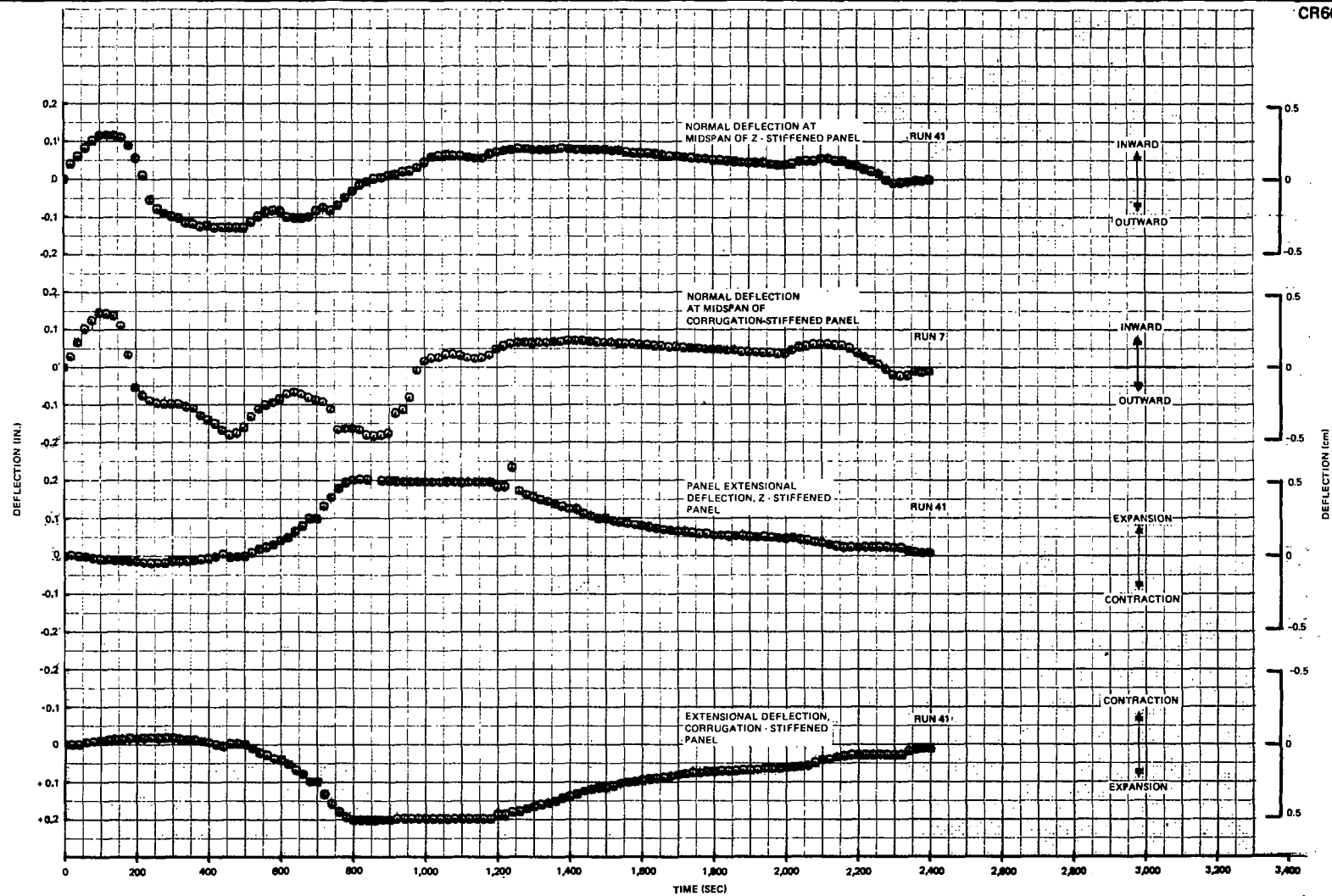


Figure 5-30. Panel Deflections

sec) was 70 percent of the maximum inward deflection during the boost portion of the test cycle, even though the differential pressure (collapse) during entry was only 15 percent of the boost flight pressure loads. The significantly lower modulus of elasticity at elevated temperature conditions accounts for the relatively high deflections during the simulated entry tests. Expansions and contractions caused by heating and cooling portions of the test cycle are also shown in Figure 5-30. Maximum expansion recorded was 0.508-cm (0.20-in.), which occurred during the maximum-temperature portion of the entry ( $t = 800$  to 1,200 sec). The initial contraction between  $t = 0$  and  $t = 400$  sec. resulted from a continuation of cooldown from the prior test cycle. Figure 5-29 shows the initial temperature drop in the panel during the early portion of the test cycle. Cooldown of that type occurred in the early portion of each test in a series except the first run. The temperature drop was primarily due to introduction of air to bring the chamber pressure back to that required for boost flight simulation.

Results of the full-scale, subsize panel tests under programmed load, temperature, and acoustic level profiles showed the TD Ni-20Cr heat shields to be capable of sustaining 100 simulated missions without incurring significant permanent set. With the exception of cracks at attach hole positions in the face sheet and in the 0.0254-cm (0.010-in.) edge members, the overall appearance of the panels was good. The surface condition of both panels appeared to be unchanged, which indicated the panel surface emittance suffered little or no deterioration. The corrugation-stiffened panel was judged to have performed better during the full-scale subsize panel tests based on (1) lower stress levels in the corrugation-stiffened design in preliminary acoustic tests (Figure 5-21), (2) lower tension stresses in the corrugation-stiffened panel during preliminary static load tests, (3) the more severe cracking at the zee-stiffened panel attach points, (4) the appearance of small cracks along spotweld rows in the zee-stiffened panel, and (5) the occurrence of a slight buckle in one of the face sheet beads on the zee-stiffened panel. Because of its better performance, the corrugation-stiffened heat shield design was selected for use in tests of full-scale, full-size heat shield test arrays.

The cracks at the panel attach points were judged to have resulted from an overload in the dimpled area of the 0.0254-cm (0.010-in.) face sheets. Both heat shield designs employed slightly oversize, predimpled holes of approximately 0.710-cm (0.280-in.) diameter. This practice was based upon dimpling tests which showed that an oversize predimpled hole was required to produce satisfactory crack-free dimples in thin sheets of TD Ni-20Cr. Use of the larger-diameter holes provided a relatively small bearing surface for the flush-head fasteners. The resultant high stresses at the periphery of the hole caused by burst pressure loads and by thermal gradients initiated the radial cracks, and subsequent exposure to acoustic loads caused further growth of the cracks. Despite the severity of the cracks, reinforcements of the dimpled holes permitted completion of a full 100 test cycles.





## Section 6

### FULL-SIZE HEAT SHIELD TEST ARRAY DESIGNS

The three Phase II heat shield arrays were all designed to meet requirements of the Shuttle Orbiter TPS environment defined in Phase I of the program. The defined environment (see Sections 2 and 5) included typical acoustic levels and duration during each mission, temperature profiles for a full mission, and differential pressure loads on the specific TPS area shown in Figure 2-5 where TD Ni-20Cr heat shields are applicable.

While designed to the same basic Orbiter requirements, the three test arrays were to be tested in three different facilities, and each was therefore to sustain a different test environment. The McDonnell Douglas Space Simulation Laboratory was used to evaluate heat shield performance under programmed differential pressure and thermal loads. Acoustic load effects were also evaluated in a separate test chamber at the McDonnell Douglas test laboratories in St. Louis. Two TD Ni-20Cr heat shield arrays were also designed and fabricated for aerodynamic testing in Langley test facilities, one for the 8-foot High Temperature Structures Tunnel (HTST) and the second for the Langley Thermal Protection System Test Facility (TPSTF). Tests in the Langley HTST and TPSTF were not completed during Phase II and performance evaluations of TD Ni-20Cr heat shields presented herein were thus based on mission simulation tests conducted in contractor test facilities.

Each heat shield array designed for Phase II tests employed the same basic design for the main surface panels and the smaller close-out panels. The basic design, selected from Phase I evaluations, consisted of a corrugation-stiffened, single-face configuration with stiffening members at each edge. The heat shield panels were designed as wide beams supported at each end by transverse beams formed from TD Ni-20Cr sheet. A sheet thickness of 0.0254-cm (0.010-in.) was used for both face sheets and corrugations in each panel design. Reinforcing members on the panel sides were made from 0.0254-cm (0.010-in.) thick sheet for the MDAC test array; however, initial thermal and differential pressure tests indicated a requirement to increase the edge

stiffness. Consequently, the lateral edge members for the HTST and TPSTF main test panels were made from 0.0508-cm (0.020-in.) thick TD Ni-20Cr sheet. Other changes from the Phase I panel designs are discussed in greater detail subsequently in this section.

#### 6.1 HEAT SHIELD ARRAY FOR CONTRACTOR TESTS

The contractor TPS tests were conducted in the Space Simulation Laboratory and the Acoustic and Vibration Laboratory at the McDonnell Douglas Test Laboratory complex at St. Louis. The Space Simulation Laboratory was used to apply programmed differential pressure load and temperature profiles in a reduced pressure test chamber. As in tests of the subsize panels, the test profiles were applied in cycles to simulate repeated missions that would be experienced by the TPS on the selected lower surface area of the Orbiter. Acoustic loadings were applied separately in the Acoustic Laboratory. To eliminate disassembly and reassembly of the heat shield array when it was moved from one laboratory to the other, the test fixture was designed to be mounted in either laboratory.

The heat shield array tested at the McDonnell Douglas laboratories was designed to fit a test fixture with a 78.5-cm by 128.2-cm (30.9-in. by 50.5-in.) opening. The complete test fixture consisted of two halves, the upper half forming a holding frame in which the TPS components were mounted and the lower half forming a mating closed cavity that contained the quartz lamp heating units. The test fixture upper half is seen in Figure 6-1, which shows the low-density fibrous insulation packages that were mounted in the upper portion of the fixture between the heat shield panels and the simulated substructure. Although not shown in Figure 6-1, an aluminum simulated substructure was also mounted on the upper half of the test fixture. The lower half of the fixture formed a closed cavity with three groups of quartz lamps. The three groups of quartz lamps, each covering approximately one-third of the heat shield array surface area, were controlled separately to provide relatively uniform temperatures over the test array. The lower half of the test fixture is shown in Figure 6-2. The heat shield, cover strips, and edge seals formed a continuous surface at the intersection of the two

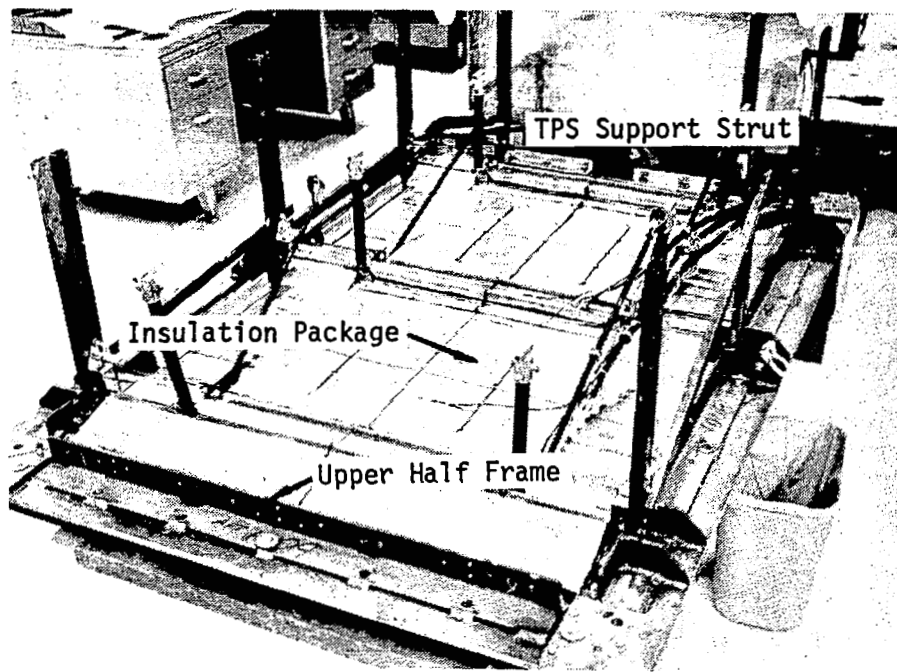


Figure 6-1. Upper Half of Contractor TPS Test Fixture

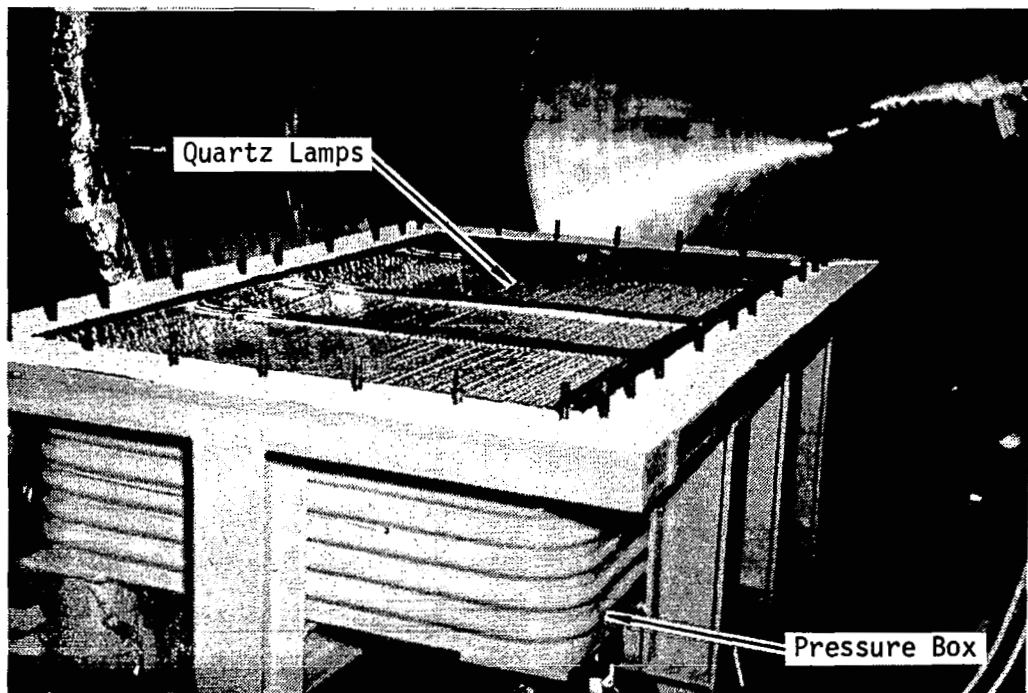


Figure 6-2. Lower Half of Contractor TPS Test Fixture

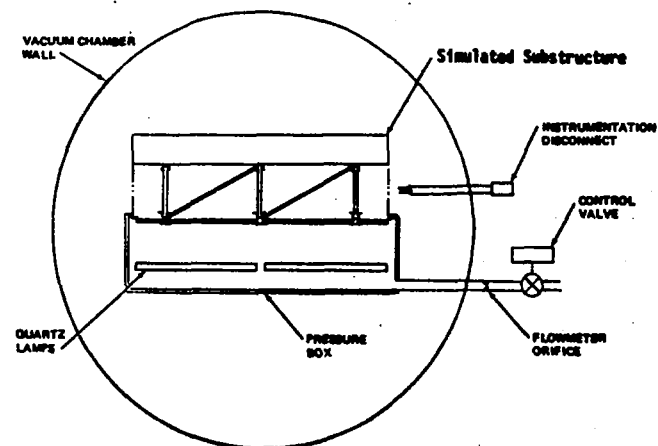
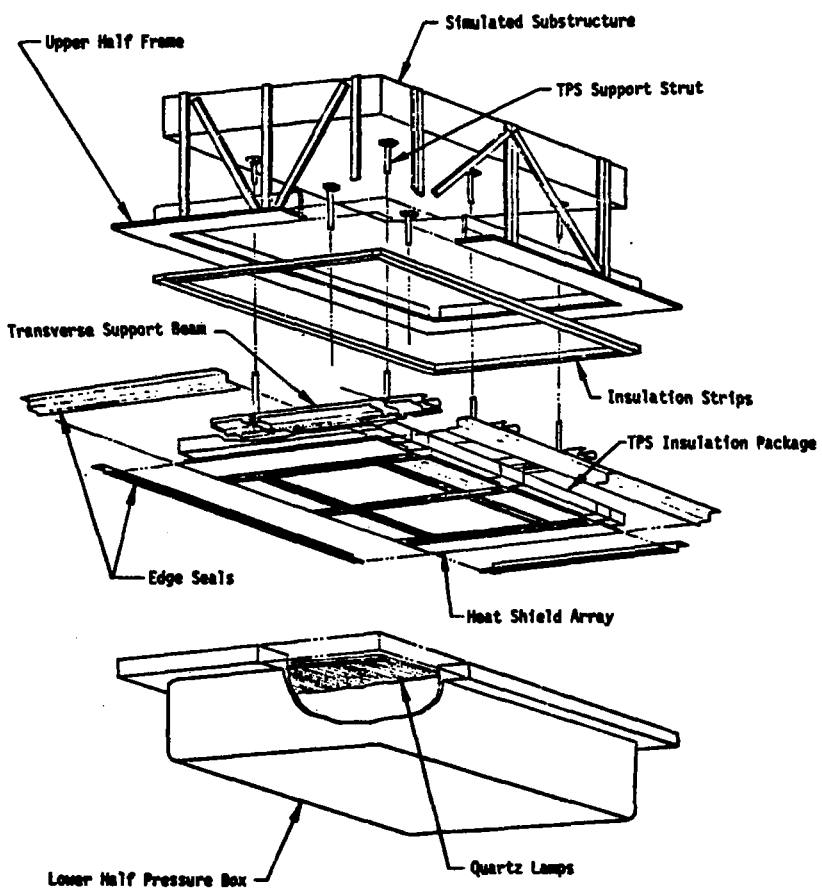
halves of the test fixture, and in this manner allowed programmed differential pressure loads to be applied to the heat shields by adjusting the pressures in the main test chamber and in the closed half of the test fixture. The test fixture halves, TD Ni-20Cr heat shield array, and simulated aluminum substructure are shown schematically in Figure 6-3.

#### 6.1.1 TPS Design Configuration

The basic TPS concept, derived in Phase I and developed to a full-scale, full-size array in Phase II, consisted of discrete panels attached to a TD Ni-20Cr support structure in a manner to permit expansion between panels at elevated temperatures and thus to minimize the effects of thermal stresses. Floating nutplates were used to provide the required expansion for each panel. For contractor tests, the TD Ni-20Cr heat shield panel array consisted of two main test panels, four side close-out panels, two end close-out panels, and cover strips to span the gaps between panel edges. Support beams and fasteners were also made from TD Ni-20Cr material, as were the seal strips used at the edges of the holding fixture.

The complete TPS array was composed of the external heat shields and cover strips, the support beams, standoff struts, foil-enclosed insulation packages, and a simulated aluminum substructure. As shown in Figure 6-3, the substructure was mounted to the test fixture frame by a series of struts at the frame periphery. The TD Ni-20Cr support beams were in turn mounted to the substructure by a series of struts that penetrated the insulation packages at discrete points. Attachment of the panels, cover strips, and insulation packages completed the upper half of the test assembly except for installation of the TD Ni-20Cr edge seals. The latter members were used to provide an overlapping set of seals to close the gap between the close-out panels and the internal edges of the test fixture frame.

The nominal thickness of all panels was 2.54-cm (1.0-in.). Formed beads were incorporated in the face sheets of all main test panels and in a majority of the closeout panels with the design objective of permitting controlled deformation in the panel surfaces at elevated temperature conditions. The



Test Array and Fixture in Space Simulation Chamber

Figure 6-3. Schematic of Contractor TPS and Test Fixture

outward projecting beads added approximately 0.25-cm (0.10-in.) to the panel thickness at their maximum height. A continuous corrugation was spot-welded to the inner surface of the face sheet to provide bending and torsional strength in the panels. The ends of the panels were closed off with zee-shaped stiffening members made from 0.0508-cm (0.020-in.) thick TD Ni-20Cr sheet, while the panel lateral edges were reinforced by the corrugation terminations which mated with the face sheet edges. The face sheet and corrugation edges were spot-welded together, and a formed lip at the panel edge provided additional stiffness.

Transverse beams made of 0.102-cm (0.040-in.) thick TD Ni-20Cr formed sheet were located at the panel ends and provided the basic support members to which the panels were attached. Pan head TD Ni-20Cr bolts of 0.635-cm (0.25-in.) diameter were used to attach the panels to floating nuts that were also made from TD Ni-20Cr and were mounted on the transverse beams. Support struts made from L605 cobalt alloy were used to attach the support beams to the simulated aluminum substructure.

Packages of low-density insulation with a nominal thickness of 6.35-cm (2.50-in.) were located between the heat shield panels and the substructure. The insulation was enclosed in a metallic foil package made of 0.0102-cm (0.004-in.) thick Hastelloy X. Five 1.27-cm (0.50-in.) thick layers of insulation made up the total insulation thickness, the outer (hottest) layer being  $192.2 \text{ kg/m}^3$  ( $12 \text{ lb/ft}^3$ ) Dynaflex and the inner four layers being  $56.0 \text{ kg/m}^3$  ( $3.5 \text{ lb/ft}^3$ ) Microquartz.

Closure strips were mounted independently from the heat shield panels at all four edges so that the strips overlapped the edges of adjacent panels and closed off the expansion space provided between panels. The closure strips were formed from 0.0508-cm (0.020-in.) thick TD Ni-20Cr sheet, and, like the heat shield panels, were attached to floating nuts mounted on the support beam so that expansion of the closure strips could occur without restraint along the length of the strips when they were at elevated temperatures.

The heat shield array is shown in Figure 6-4 after preoxidation, a process used to produce a dark, high-emittance surface on the panels and cover strips. Figure 6-4 shows the preoxidized panels and cover strips in position on the heat shield support beams before the fasteners were installed.

Unit weights for the contractor test array were derived from actual weights of the TD Ni-20Cr components combined with computed weights of the insulation packages. Actual component weights and weight per unit area are presented in Table 6-1. Heat shield supports were redesigned for the HTST and TPSTF arrays to reduce the TPS weight. Also, the low-density insulation was packaged in high temperature quartz cloth for the HTST and TPSTF arrays to reduce weight and costs associated with the metallic foil packaging system. Since the support system and insulation depths for the HTST and TPSTF arrays differed from those of the contractor test array, the unit weights were slightly different for each of the remaining TPS arrays. Such differences are discussed subsequently in this section.

**Table 6-1**  
TPS WEIGHTS OF CONTRACTOR TEST ARRAY

COMPONENT	WEIGHT kg (lb)	UNIT WEIGHT kg/m <sup>2</sup> (lb/ft <sup>2</sup> )
MAIN PANEL	1.420 (3.13)	5.78 (1.185)
LATERAL COVER STRIP	0.236 (0.52)	0.96 (0.197)
LONGITUDINAL COVER STRIP	0.095 (0.21)	0.39 (0.080)
SUPPORT BEAM	1.175 (2.59)	4.79 (0.981)
EDGE CHANNEL	0.377 (0.83)	1.53 (0.314)
PANEL ATTACH BOLTS	0.095 (0.21)	0.39 (0.079)
COVER STRIP BOLTS	0.196 (0.43)	0.79 (0.163)
INSULATION PACKAGE <sup>(1)</sup>	2.330 (5.14)	9.49 (1.945)
INSULATION ATTACH	0.091 (0.20)	0.37 (0.076)
TOTAL		24.49 (5.020)

(1) Insulation Thickness: 6.35 cm (2.50 in).

Dimensions Shown in cm (in.)

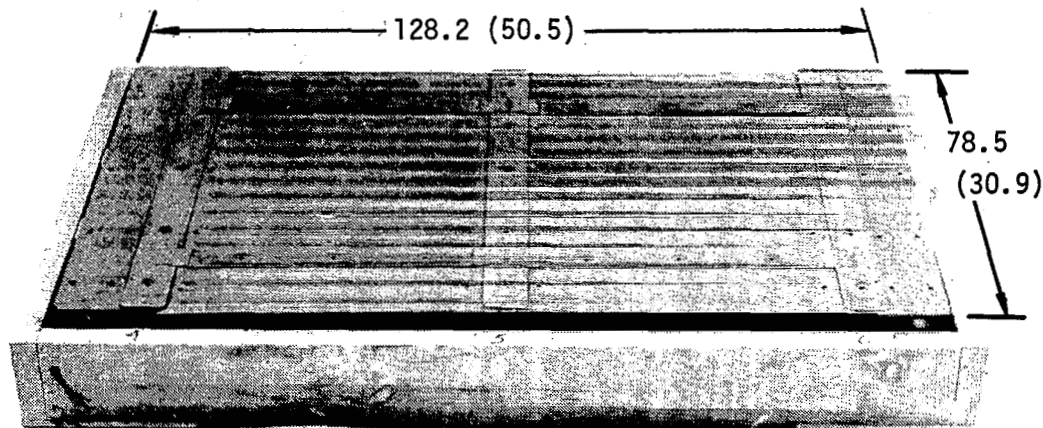


Figure 6-4. Pre-Oxidized Panels in Place on Support Beam

As a result of Phase I evaluations a braze-reinforced panel was included in the Phase II contractor test array. Evaluations of braze-reinforced spotwelded samples conducted in Phase I showed improved fatigue life for braze-reinforced joints when compared to simple spotwelded joints. Such evaluations led to the decision to test one of the side close-out panels as a braze-reinforced panel in the contractor TPS tests. A spare side close-out panel was therefore fabricated to the same configuration as the basic design with the exception that its spotwelded areas were braze-reinforced and the panel fasteners were recessed in a full-depth pocket. The latter feature, shown in Figure 6-5, was incorporated in the braze-reinforced panel to assess the thermal effects of an attachment system with a smaller mass and with a fastener that did not act as a conductive path from the outer surface to the interior of the heat shield panel.

The braze-reinforced panel was fabricated at MDAC facilities up to the point of actual brazing. Initial fabrication at MDAC included manufacture of detail



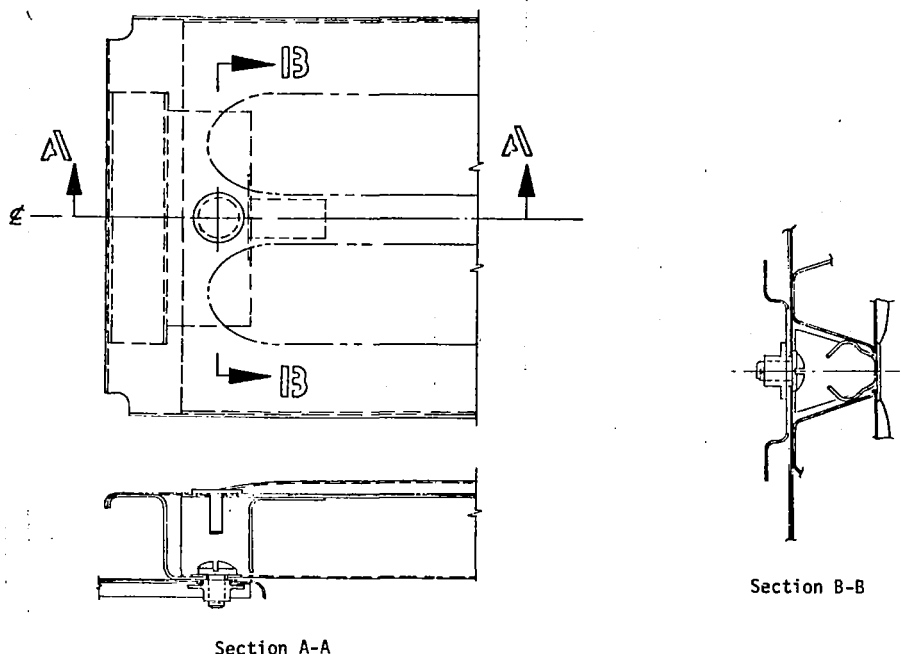


Figure 6-5. Fastening Design for Braze-Reinforced Panel

parts, cleaning, emplacement of braze alloy, and assembly by spotwelding. The panel was then shipped to the Langley Research Center where the brazing and preoxidation processes were accomplished. The panel was shipped subsequently from Langley Research Center to MDAC facilities at St. Louis. It was then installed in the test array as a replacement component for a spotwelded panel.

The braze-reinforced panel is shown in Figure 6-6 before being subjected to the brazing cycle. Figure 6-7 shows the panel's appearance after completion of the brazing pre-oxidation processes. The light areas seen in Figure 6-7 indicate the extent of the brazed areas in the faying surfaces of the panel. The lighter areas seen in Figure 6-7 were not as clearly discernible by visual inspection alone and the different shadings seen in the photographs of the panel are believed to be the result of slightly different oxide formations that occurred in the brazed regions during pre-oxidation of the panel. Such differences in the oxide were judged to be caused by lower temperatures locally in the brazed areas due to the larger thermal mass of the braze alloy. No thermocouples were attached to the panel during preoxidation and thus temperature variations that are judged to have existed were not verified. However, oxide

where

$K_1, K_2$  = Ultimate to limit ratios for external and thermal loads respectively.

$L_{ext}$  = Mechanical externally applied loads; e.g., inertial loads.

$L_{ther}$  = Thermally induced loads.

$K_1$  = 1.4 for boost conditions when the term is additive to the algebraic sum,  $\Sigma L$ .

$K_1$  = 1.5 for entry, atmospheric cruise, and landing when the term is additive to the algebraic sum,  $\Sigma L$ .

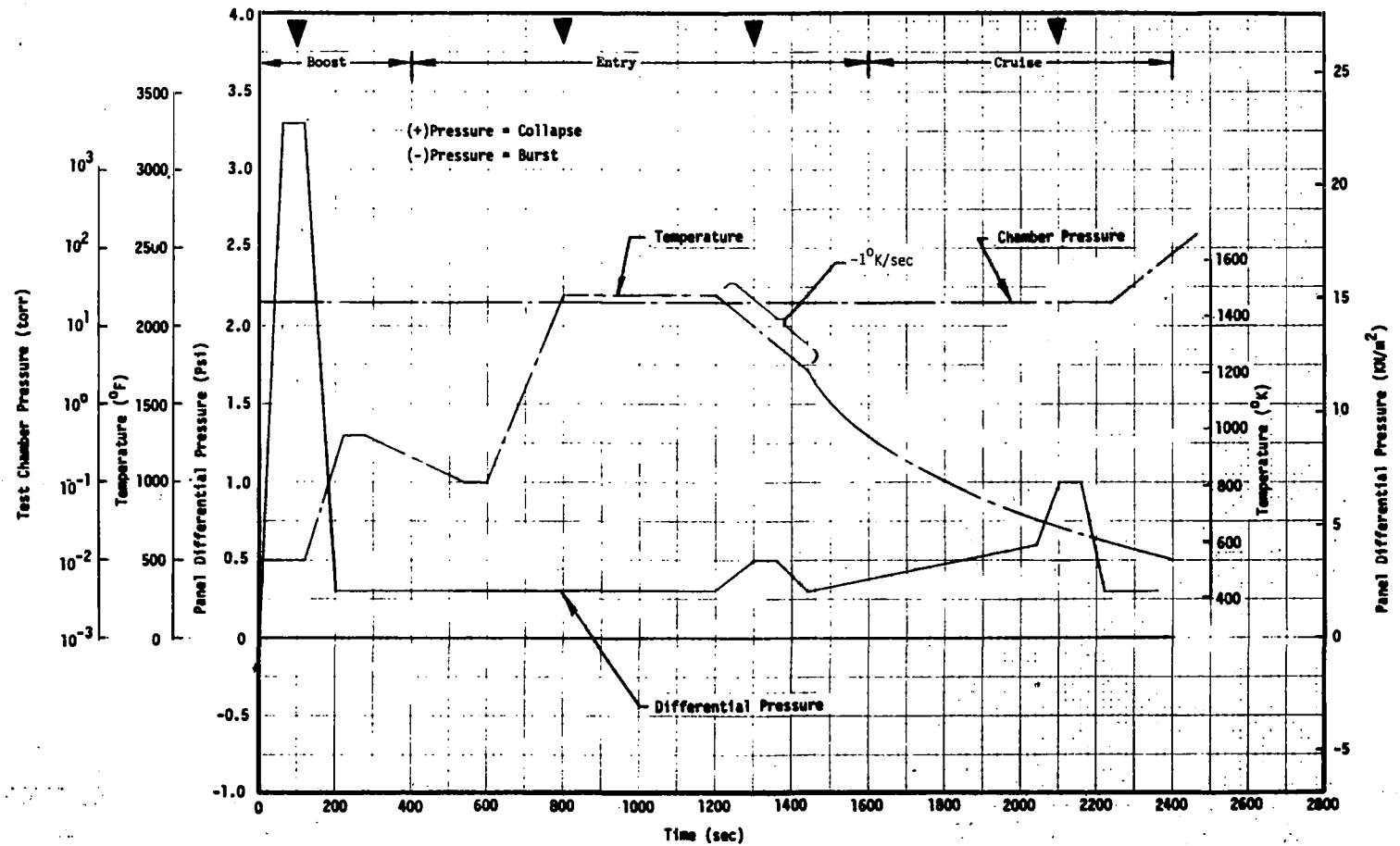
$K_2$  = 1.5 when the term is additive to the algebraic sum,  $\Sigma L$ .

$K_1, K_2$  = 1.0 when the term is subtractive to the algebraic sum,  $\Sigma L$ .

Using Equation (3), critical heat shield stresses were determined for the contractor TPS array in several different locations.

The programmed differential pressure loads and external surface temperatures for contractor tests, presented in Figure 6-8, were used to develop panel temperature time-histories and to evaluate the combined effects of thermal and mechanical stress levels at three places on a typical full-size panel. The programmed test temperature profile was also used to develop internal temperature time-histories for the test array insulation package and substructure. Temperature time-histories at points through the TPS and substructure are shown in Figure 6-9. In the temperatures of Figure 6-9, an initial run in a series of test cycles was assumed so that external surface temperatures were at room temperature at the start of the test run.

Panel temperature distributions were evaluated in three areas, one area being at the center of a main panel, a second being at the panel edge at midspan, and a third at the panel edge near the support struts. Such areas corresponded closely to thermocouple locations of the instrumented contractor TPS array (see Section 7). Typical temperatures at two locations are shown in Figures 6-10 and 6-11. Four time points were selected in the simulated mission test profile as being critical for thermal and aerodynamic load conditions. The selected times, shown in Figure 6-8, included a point in the boost flight where maximum aerodynamic loads are experienced, a point in the entry flight where surface temperatures have reached a maximum, a point shortly after the start of external surface cooldown from maximum temperature conditions, and a



▼ Analysis Time Points

Figure 6-8. Programmed Temperatures and Differential Pressures for Contractor Test Array

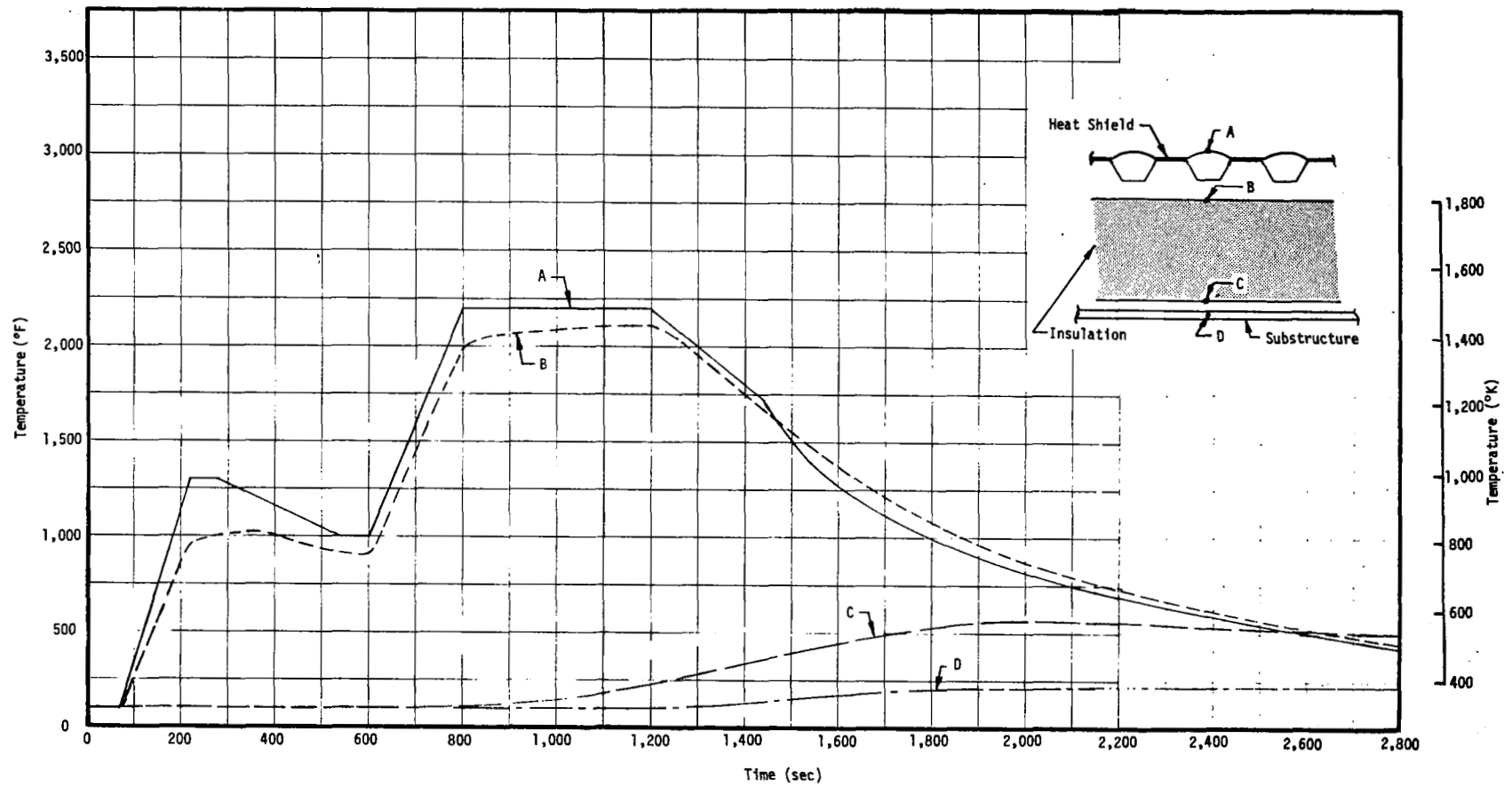


Figure 6-9. Projected Temperature Time-Histories; Contractor Test Array

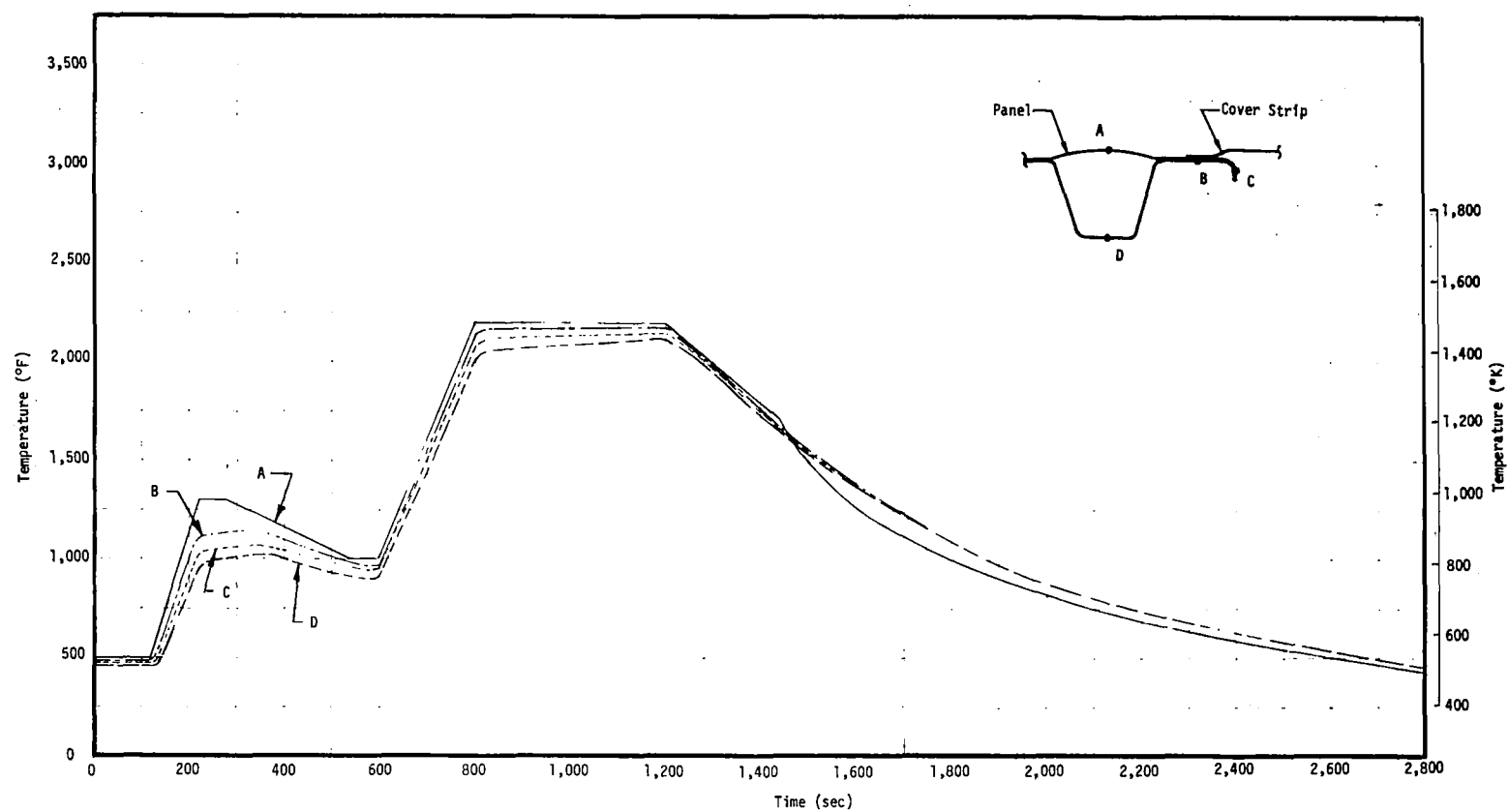


Figure 6-10. Projected Temperature Time-Histories at Panel Edge; Midspan Location

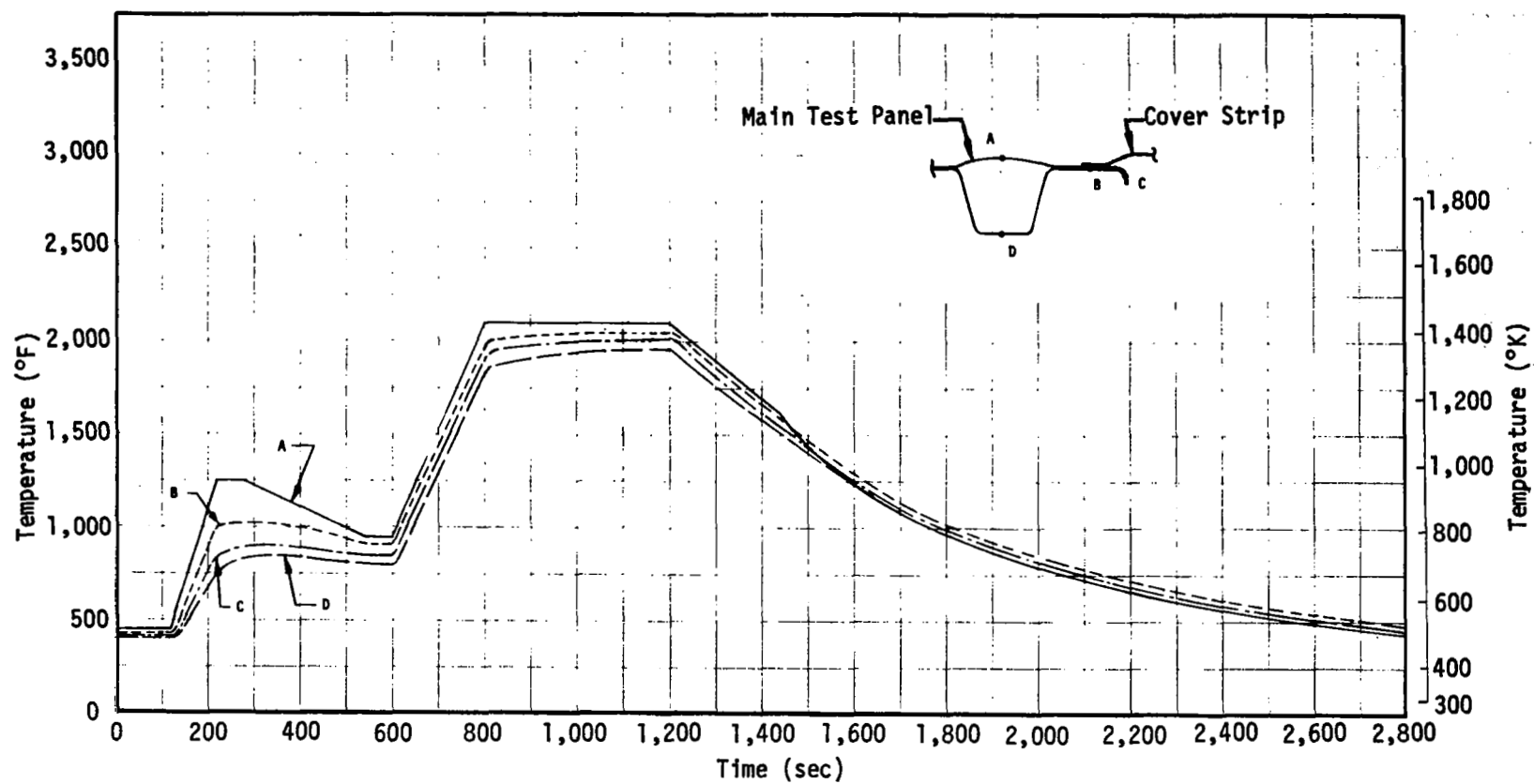


Figure 6-11. Projected Temperature Time-Histories at Panel Edge Near Support Strut

point in the cruise portion of the entry flight where external surface temperatures have decreased at the same time that internal temperatures are still near a maximum. The latter time point also coincided with the period in the cruise flight when aerodynamic loads were at a maximum in the simulated mission profile.

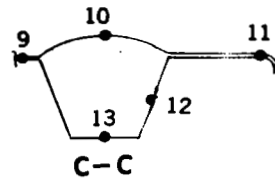
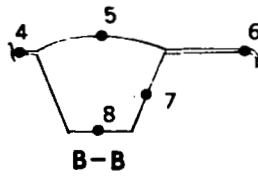
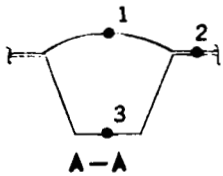
Panel stresses were analyzed in the selected panel areas at the four time points and combined according to the previously described criteria. The resultant stresses and margins of safety are summarized in Table 6-2. Critical stresses occurred at two of the four selected time points, the first critical condition occurring at  $t = 100$  seconds during the simulated boost portion of the test profile and the second at the point during the simulated entry portion of the test where the heat shield temperature first reaches  $1,477^{\circ}\text{K}$  ( $2,200^{\circ}\text{F}$ ). Test results are discussed subsequently in Section 7, and comparisons with panel analyses are made at that point.

## 6.2 TEST ARRAY FOR THE HIGH TEMPERATURE STRUCTURES TUNNEL

The 8-ft. HTST test array was the largest of the three TPS arrays constructed during Phase II. A detailed description of the 8-ft. HTST may be found in Reference 9. Details of the constraints of the tunnel and the special design conditions of the HTST panels are given in Reference 3.

The HTST TD Ni-20Cr test array included two main panels, four side closeout panels, two end closeout panels, cover strips, support structures, insulation packages, and a simulated substructure. The planform dimensions of the array were 108-cm by 152.4-cm (42.5-in. by 60-in.). The simulated substructure was designed for attachment to the set of steel mounting channels located within the cavity of the panel holder in the tunnel. The location of the mounting channels in the holder limited the total thickness of the TPS and substructure to 12.7-cm (5.0-in.), a thickness that in turn limited the insulation package thickness to approximately 7.6-cm (3.0-in.). Such thickness limitations led to the selection of titanium for the simulated substructure since substructure temperatures in the range of  $477^{\circ}\text{K}$  to  $588^{\circ}\text{K}$  ( $400^{\circ}\text{F}$  to  $600^{\circ}\text{F}$ ) were projected for the HTST tests.

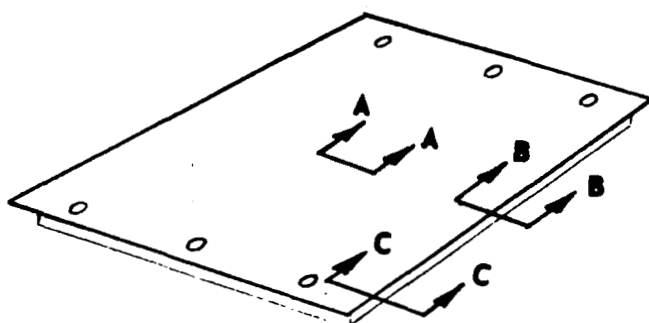
Table 6-2  
Contractor Test Array Panel Stresses



		t = 100 sec			t = 800 sec		
	Panel Ref. Point	Stress MN/m <sup>2</sup> (psi)	Temperature °K (°F)	Margin of Safety	Stress MN/m <sup>2</sup> (psi)	Temperature °K (°F)	Margin of Safety
Panel Center	1	-162.0 (-23,500)	533 (500)	.06	36.2 (5,245)	1,477 (2,200)	.98
	2	-80.6 (-11,700)	528 (490)	4.21	31.1 (4,510)	1,468 (2,180)	1.30
	3	269.0 (39,000)	486 (415)	1.54	-76.8 (-11,150)	1,368 (2,000)	.03
Panel Edge, Midspan	4	-77.5 (-11,250)	528 (490)	5.42	32.2 (4,660)	1,468 (2,180)	1.04
	5	-111.3 (-16,140)	533 (500)	.55	41.4 (5,995)	1,477 (2,200)	.52
	6	-61.7 (-8,950)	525 (485)	6.48	16.6 (2,410)	1,416 (2,090)	3.06
	7	59.0 (8,550)	519 (475)	HIGH	-21.9 (-3,170)	1,410 (2,080)	1.72
	8	193.1 (28,000)	511 (460)	2.50	-66.5 (-9,650)	1,373 (2,015)	.06
Panel Edge, Near Attach Point	9	-11.38 (-1,650)	494 (430)	HIGH	29.0 (4,200)	1,382 (2,030)	1.45
	10	-50.7 (-7,350)	505 (450)	2.61	63.1 (9,150)	1,427 (2,105)	.09
	11	-1.04 (-150)	491 (425)	HIGH	-18.6 (-2,700)	1,351 (1,975)	7.52
	12	33.1 (4,800)	486 (415)		-27.9 (-4,050)	1,318 (1,910)	1.96
	13	40.4 (5,850)	477 (400)	↓	-55.9 (-8,100)	1,281 (1,845)	1.94



Table 6-2 (Cont)  
Contractor Test Array Panel Stresses



t = 1300 sec			t = 2100 sec		
Stress MN/m <sup>2</sup> (psi)	Temperature °K (°F)	Margin of Safety	Stress MN/m <sup>2</sup> (psi)	Temperature °K (°F)	Margin of Safety
20.5 (2,945)	1,368 (2,000)	2.90	-12.7 (-1,840)	672 (750)	HIGH
-10.2 (-1,480)	1,358 (1,980)	HIGH	-16.3 (-2,360)	675 (755)	↓
-9.23 (-1,340)	1,349 (1,965)	8.31	27.2 (3,940)	697 (795)	↓
-8.1 (-1,175)	1,358 (1,980)	HIGH	27.8 (4,030)	661 (730)	HIGH
22.4 (3,245)	1,368 (2,000)	2.54	-8.93 (-1,295)	672 (750)	↓
-20.5 (-2,980)	1,349 (1,965)	7.06	-10.02 (-1,455)	680 (765)	↓
-5.45 (-790)	1,351 (1,970)	HIGH	-27.4 (-3,980)	703 (805)	5.28
9.03 (1,310)	1,333 (1,940)	9.00	25.0 (3,630)	709 (815)	HIGH
31.0 (4,500)	1,304 (1,885)	2.13	-5.17 (-750)	678 (760)	↓
2.07 (300)	1,316 (1,905)	HIGH	-1.03 (-150)	672 (750)	↓
10.35 (1,500)	1,245 (1,780)	↓	35.2 (5,100)	675 (755)	↓
-13.45 (-1,950)	1,238 (1,765)	↓	-13.45 (-1,950)	686 (775)	↓
-36.2 (-5,250)	1,139 (1,690)	2.08	-15.51 (-2,250)	689 (780)	↓

The panel design of the HTST test array was basically the same as the design used for the MDAC test array with minor modifications at the attach positions to provide recessed fasteners. Additional stiffness was incorporated at the HTST main panel sides by using 0.0508-cm (0.020-in.) thick separate reinforcing edge members instead of the 0.0254-cm (0.010-in.) thick corrugation that was used to reinforce the lateral edges of the contractor test array panels. The thickness of all panels in the HTST array was 2.54-cm (1.0-in.) and the basic panel cross-section was the same as that used in the test array panels for contractor tests.

The support structure was changed in the HTST array to reduce the TPS weight and to curtail heat transfer to the substructure. Panel supports in the HTST design consisted of pylon configurations made from 0.0254-cm (0.010-in.) thick TD Ni-20Cr sheet material. Floating attach nuts machined from TD Ni-20Cr bar were mounted in each pylon support.

Figure 6-12 shows the HTST test array substructure and edge frames. The latter members contain the insulation packages and provide mounting supports for the end closeout panels as well as edge seals along the lateral edges of the test array. In Figure 6-13 the heat shield panel array is shown in place on the substructure and supports.

Unit weights of the HTST test array are presented in Table 6-3. Comparison of the HTST weights with those of the contractor test array weights (Table 5-1) shows a reduction in the HTST unit weight of  $6.53 \text{ kg/m}^2$  ( $1.34 \text{ lb/ft}^2$ ). The weight reduction resulted primarily from a redesign of the heat shield support system and a revision of the insulation packaging system. The support system was changed from beam supports to pylon-type supports, this change permitting a reduction in TD Ni-20Cr sheet thickness of the support system from 0.102-cm (0.040-in.) in the beams to 0.025-cm (0.010-in.) for the pylon supports. To effect further weight reductions the insulation packaging was changed from a metallic foil container to a high temperature quartz cloth for packaging the fibrous insulation.

**Table 6-3**  
**WEIGHTS OF HTST TEST ARRAY**

COMPONENT	WEIGHT kg (lb)		UNIT WEIGHT kg/m <sup>2</sup> (lb/ft <sup>2</sup> )	
Main Panel	1.81	(3.99)	7.39	(1.51)
Closure Strips	0.31	(0.69)	1.27	(0.26)
Panel Supports	0.27	(0.59)	1.10	(0.22)
Ceramic Pads	0.07	(0.15)	0.29	(0.06)
Insulation Package	1.66	(3.66)	6.77	(1.39)
Bolts	0.28	(0.61)	1.14	(0.23)
			17.96	(3.68)

### 6.3 TEST ARRAY FOR THE THERMAL PROTECTION SYSTEM TEST FACILITY

Details of the Thermal Protection System Test Facility test conditions and the constraints which controlled the design of the test array for the TPSTF are given in Reference 3. The TPSTF test array was the smallest of the three TPS arrays constructed, its planform dimensions being 61-cm by 91.4-cm (24-in. by 36-in.). Design of the TPSTF array was similar to that used for the other two arrays with the exception that only one full-size test panel could be included in the array because of the smaller planform size available in the TPSTF holder. Also, the small transverse dimension of 61-cm (24-in.) left a relatively small gap between the sides of the main panel and the edge of the holder cavity. As a consequence, side closeout panels were eliminated in the TPSTF array and wider edge seals were used as side closeout members.

The TPSTF test array holder, shown in Figure 6-14, has a water-cooled welded steel picture frame as its outer member which is bolted to a larger welded steel inner frame. Slotted holes around the periphery of the inner frame provide attachment positions for mounting the test array in the holder. Ports are also located in the edge members of the inner frame for passage of instrumentation leads.

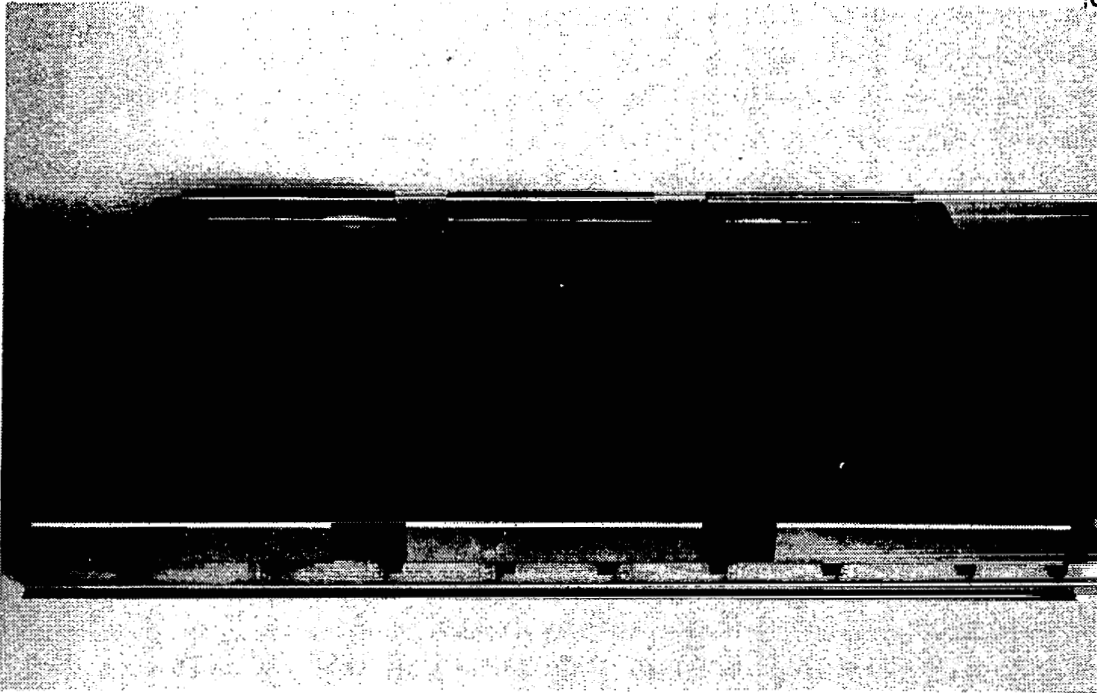


Figure 6-12. Substructure and Side Frames of HTST Test Array

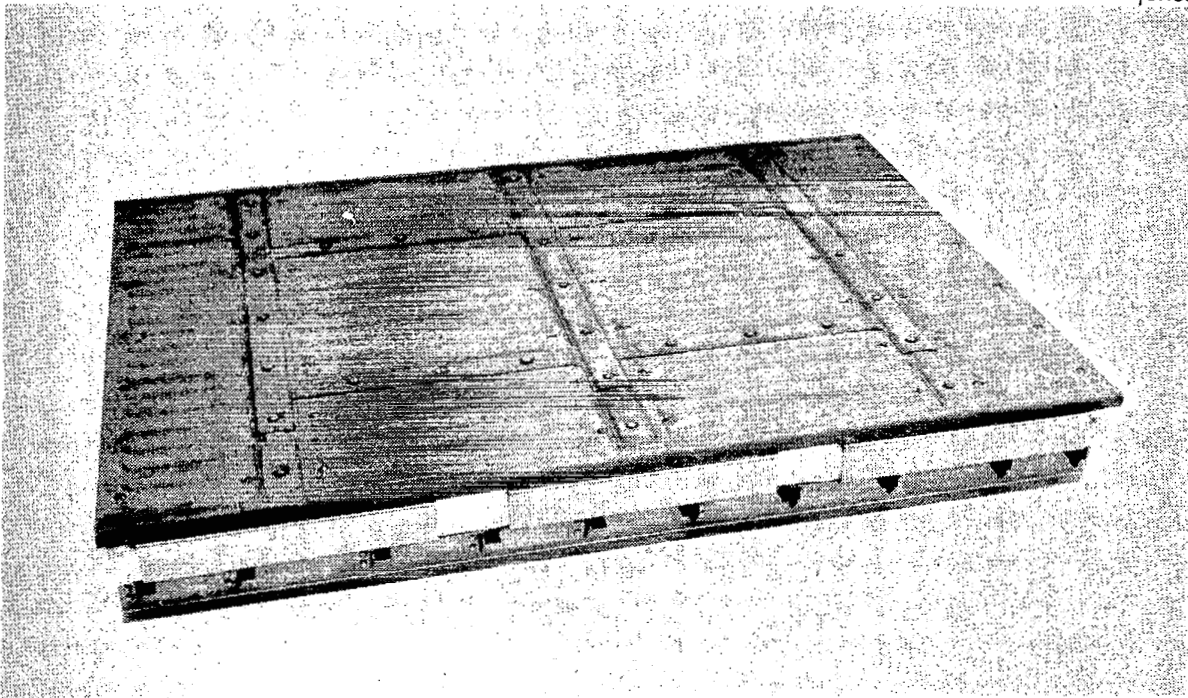


Figure 6-13. Completed HTST Test Array

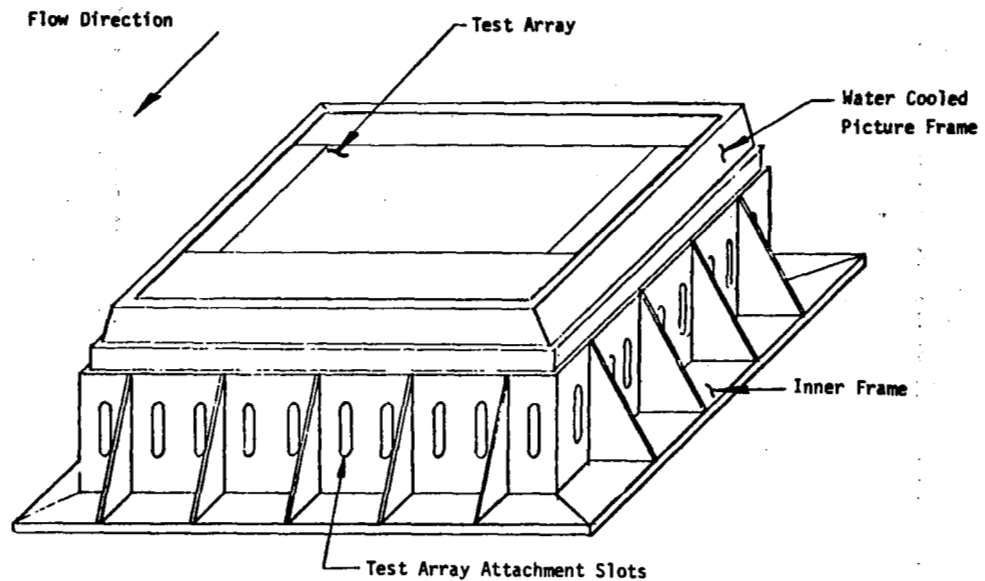


Figure 6-14. Test Array Holder for the TPSTF

As in the other two test arrays, the nominal panel thickness in the TPSTF test array was 2.54-cm (1.0-in.). A test fixture cavity depth of 17.6-cm (6.93-in.) permitted a slightly thicker insulation package of 8.88-cm (3.50-in.) to be used in the TPSTF test array. Seven insulation layers were used, each layer being 1.27-cm (0.50-in.) thick. The four outer layers were made of  $128\text{-kg/m}^3$  ( $8\text{-lb/ft}^3$ ) Fiberfrax Hi-Fi fibrous insulation and the three inner layers were made of  $96\text{-kg/m}^3$  ( $6\text{-lb/ft}^3$ ) microquartz. The insulation was again packaged in high temperature quartz cloth using the same basic approach as employed with the HTST TPS array.

TD Ni-20Cr pylon panel supports provided attach points for the panels, and alumina insulating pads were located at points where the pylons were attached to the simulated titanium substructure. The substructure formed the floor of an open rectangular box, and the TD Ni-20Cr sides of the box were designed to

mate with the interior surfaces of the test fixture cavity. "Z"-shaped clips were located at eight points around the periphery of the test array frame to provide attachment to the inner steel frame of the test fixture. TD Ni-20Cr edge members were mounted on top of the test array side frames to provide closeout members along the lateral edges of the test array.

The TPSTF test array components are shown in Figures 6-15 through 6-18. The substructure and side frames are shown in Figure 6-15, the substructure being a spotwelded titanium structure simulating a skin-stringer-frame segment of the Shuttle primary structure. The TD Ni-20Cr side frames provided containment for the insulation packages and also served as supports for the test array close-out members. The attach clips on the frame members are also visible in Figure 6-15. The heat shield supports and a portion of the insulation packages are shown in Figure 6-16 prior to installation of the surface panels and cover strips. Figure 6-17 shows the heat shields and a cover strip positioned on the heat shield supports before installation of the fasteners and side close-out members. The completely assembled test array is shown in Figure 6-18.

Unit weights of the TPSTF test array components that comprise the full-size, full-scale TPS were very similar to those of the HTST. Weight differences between the HTST test array and the TPSTF array were due primarily to differences in insulation thickness and in the sizes of the closeout panels.

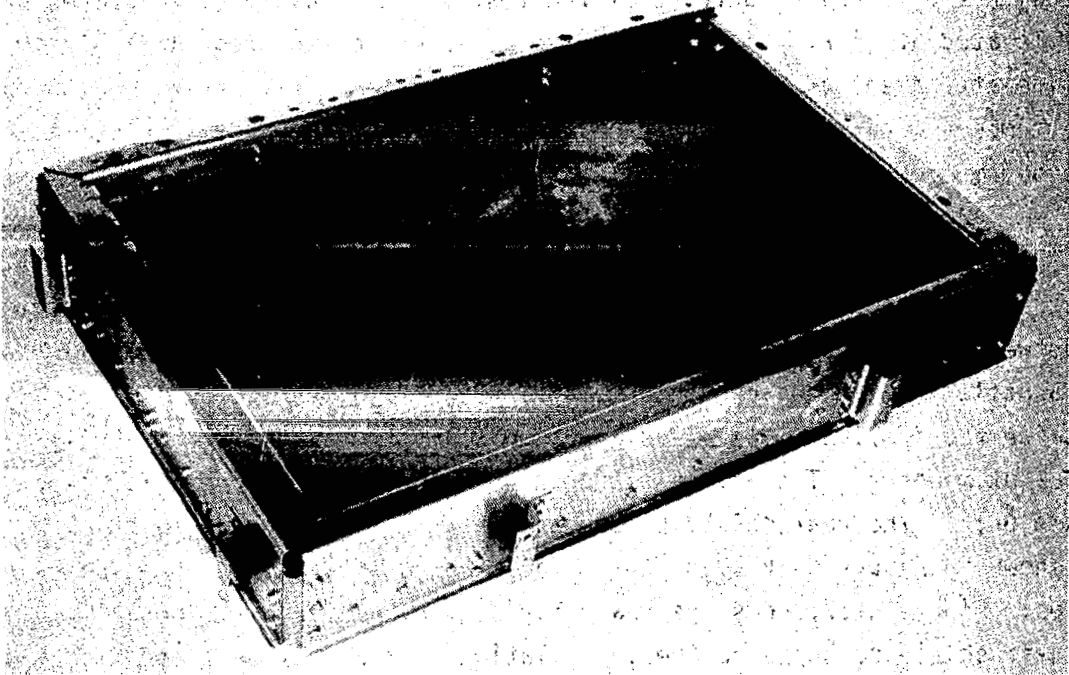


Figure 6-15. Substructure and Side Frames; TPSTF Test Array

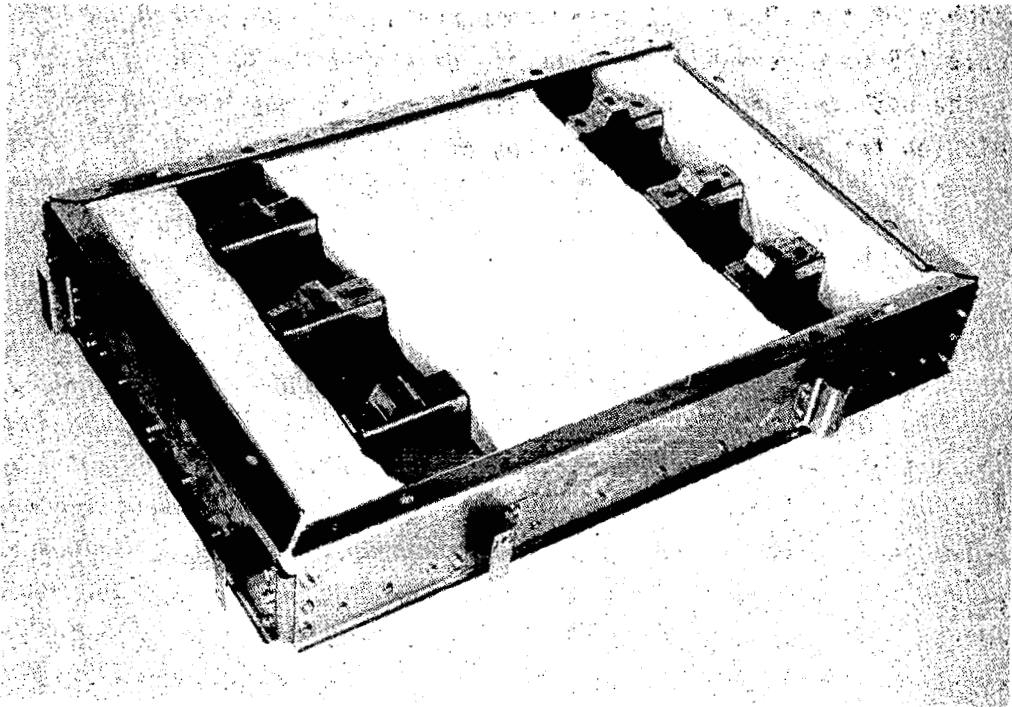


Figure 6-16. Installed Insulation and Heat Shield Supports

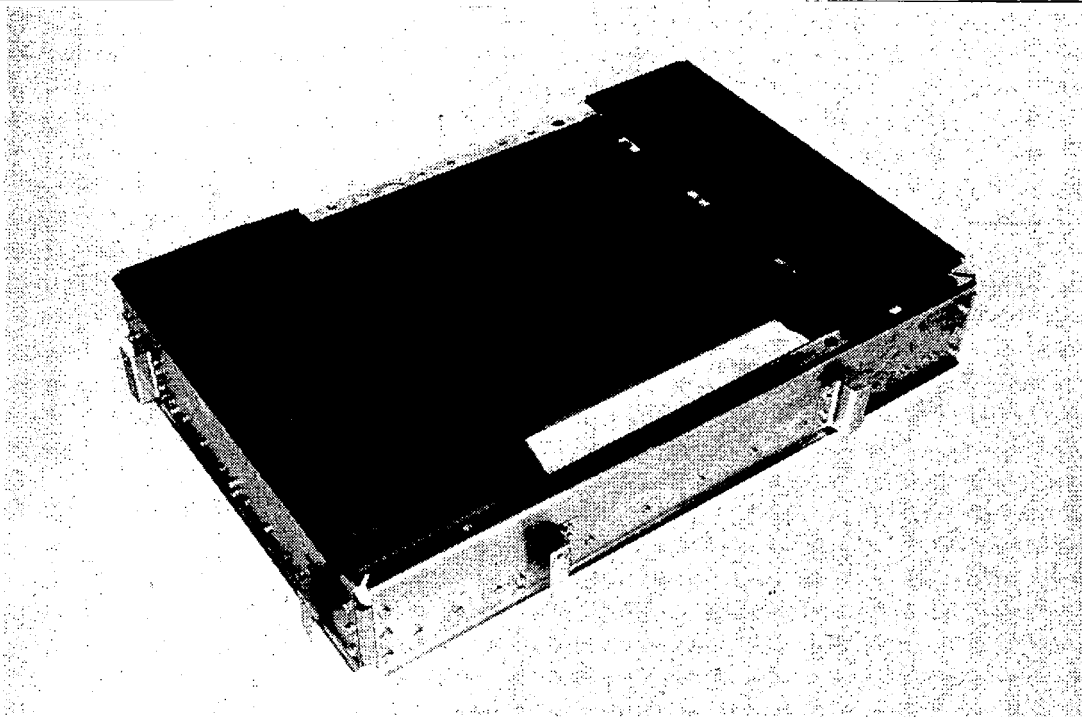


Figure 6-17. Partially Assembled Heat Shield Array

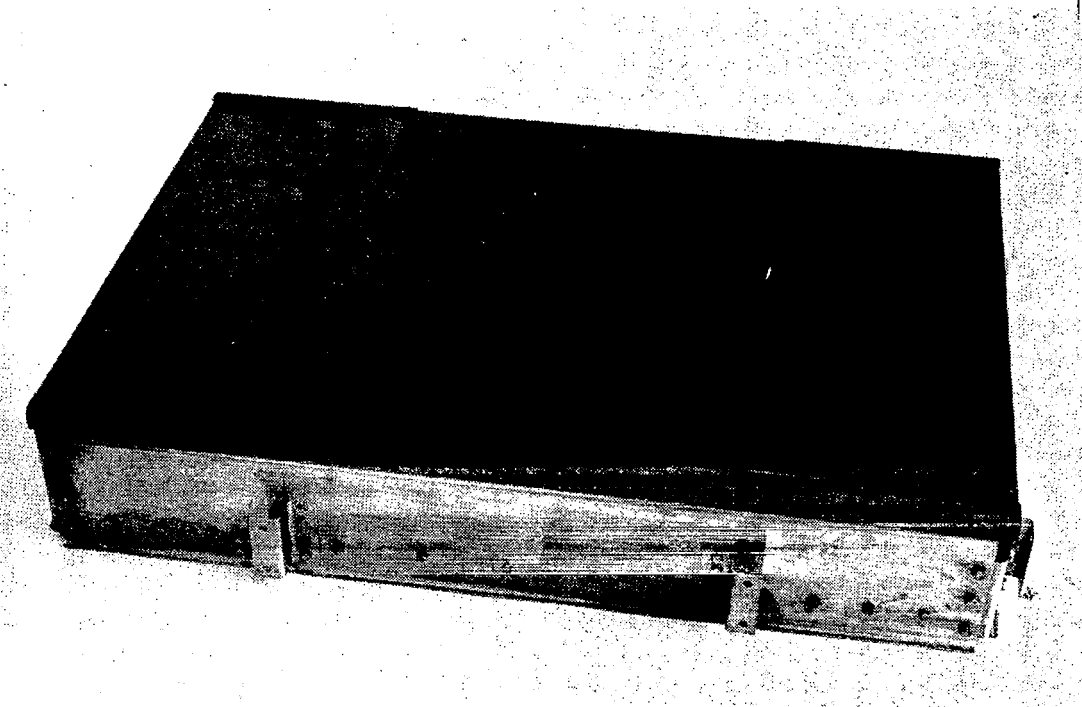


Figure 6-18. Completed TPSTF Test Array



## Section 7

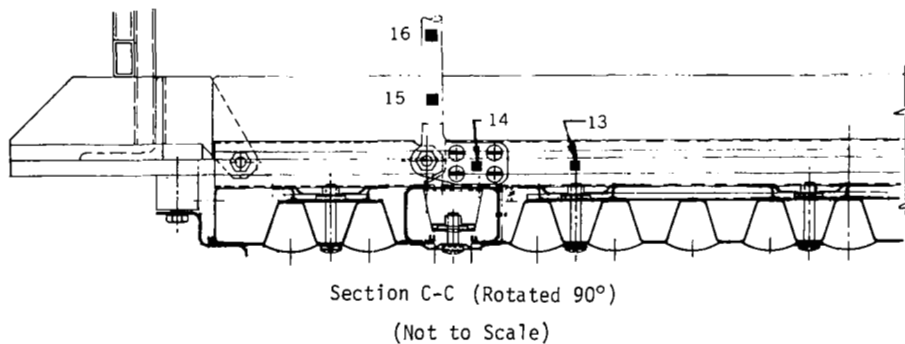
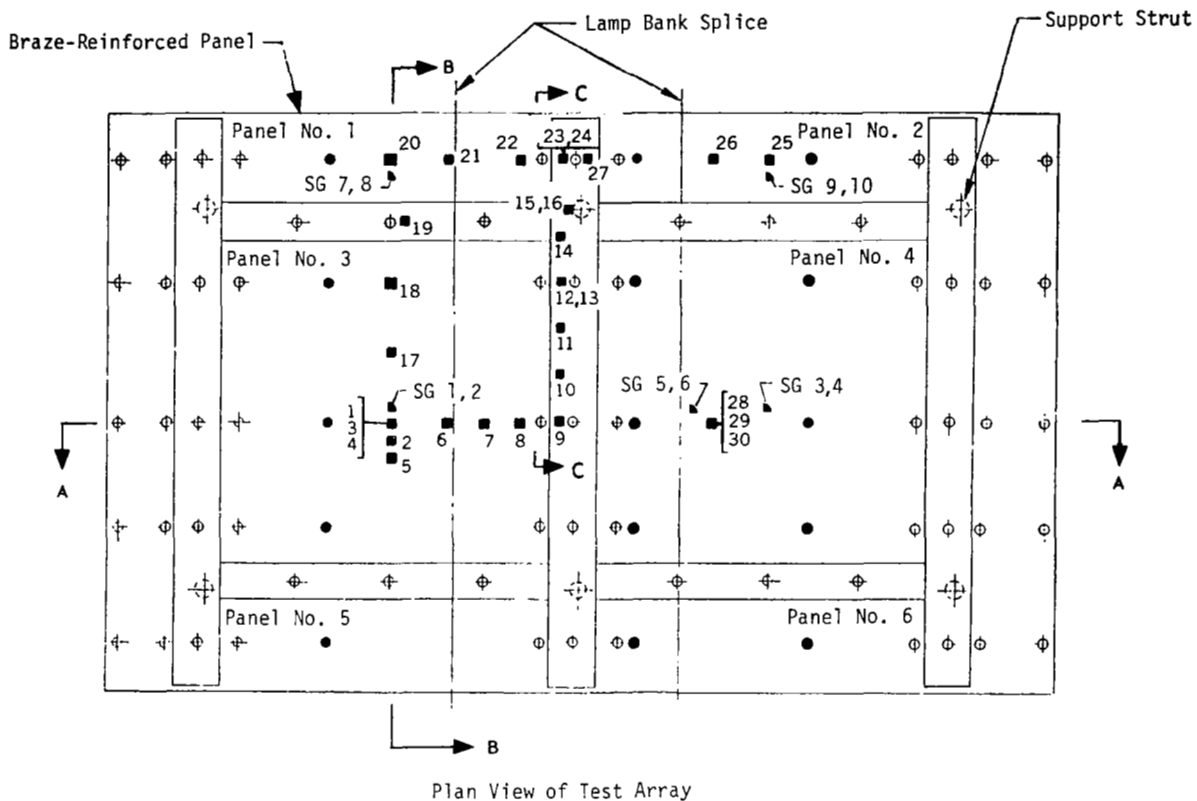
### FULL-SIZE THERMAL PROTECTION SYSTEM TESTS

The full-scale, full-size contractor TPS array was designed to simulate a segment of a complete TD Ni-20Cr metallic radiative thermal protection system including heat shields, heat shield supports, insulations, and the primary structure. The test system for the full-size contractor TPS array was the same as that used for the subsize panel tests. The overall system is shown schematically in Figure 4-14, which also shows the sequence of testing. As in subsize panel tests, the test fixture was designed to permit its use in both the Space Simulation Chamber and the Acoustic Facility so that the test array could remain in place except for necessary inspections and instrumentation replacement.

The programmed cycles of differential pressure, main chamber pressure, and temperature were shown previously in Figure 5-10, and Figure 4-16 shows the sound pressure level spectra used in full-scale panel tests as well as subsize panel tests. The main chamber pressure used for the test profile (Figure 5-10) was greater than that predicted for the Orbiter entry flight because (1) the pumping capacity for the main chamber was limited and (2) excessively low pressures caused arcing of the quartz lamps. As shown in Figure 5-10; the main chamber pressure was held at 20 torr (0.4 psi) throughout a majority of the test cycle. This test pressure, while higher than the computed ambient pressure during the Orbiter entry flight, was sufficiently low to simulate the low-pressure effects that could cause degradation from chromium depletion under elevated temperatures combined with low-pressure environments.

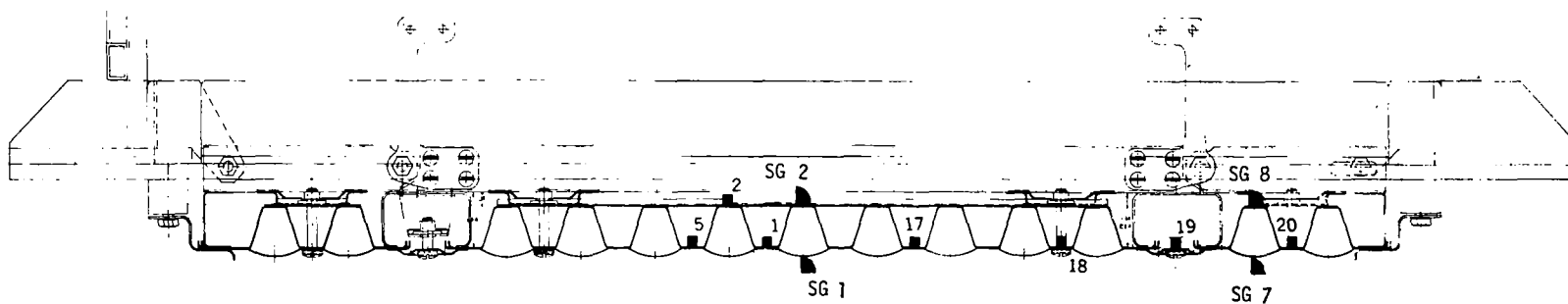
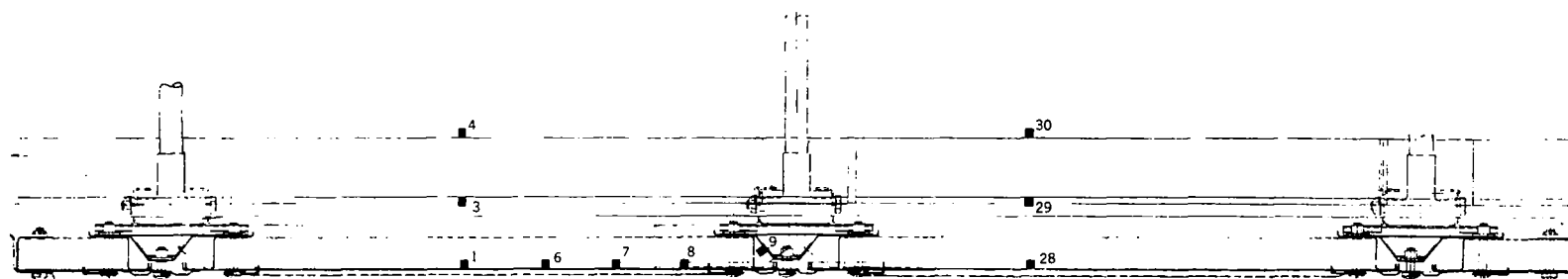
#### 7.1 TPS ARRAY INSTRUMENTATION

The TPS array was instrumented with 10 strain gages, 30 data thermocouples, and 15 control thermocouples as shown in Figure 7-1. Strain gages were employed to evaluate maximum stresses when differential pressure loads were applied to the panels in the initial tests. All panel stress tests were conducted as preliminary tests at room temperature since the simulated cyclic



- Control Thermocouple
- Data Thermocouple
- ▲ Strain Gage

Figure 7-1. Thermocouple and Strain Gage Locations on Contractor Test Array



Section B-B (Rotated 90°)  
(Not to Scale)

- Control Thermocouple
- Data Thermocouple
- ▲ Strain Gage

Figure 7-1. (Continued)

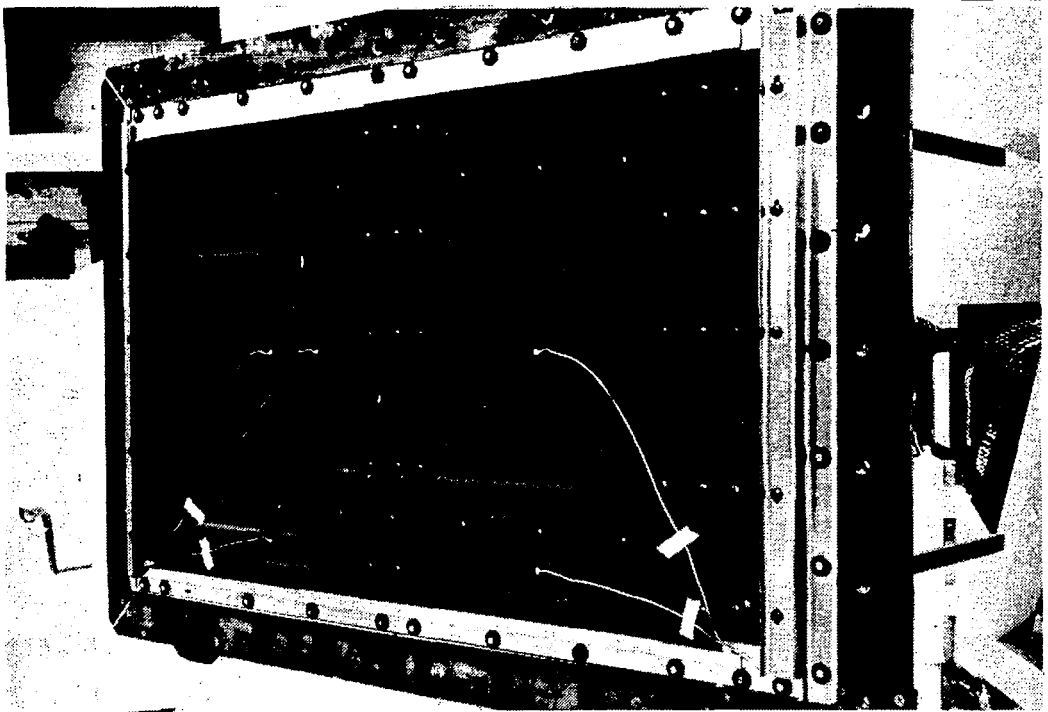
mission tests with a maximum temperature of 1,477°K (2,200°F) destroyed the strain gages. As shown in Figure 7-1, uniaxial strain gages were mounted on the external surface of the face sheets on both main test panels and on two of the side closeout panels, one of the instrumented side panels being the braze-reinforced panel. Similarly, uniaxial strain gages were placed on the interior sides of the panels on the corrugation crowns in positions directly beneath the exterior surface strain gage locations.

Control thermocouples were located in three transverse rows that corresponded to the approximate centers of the three groups of quartz lamps mounted in the lower half of the test fixture (see Figure 6-2). Data thermocouples were located in the main TD Ni-20Cr heat shields, the insulation packages, the side closeout panels, support beams, and a support strut. Locations for the data thermocouples were selected to provide temperature distribution data in several key areas, including the support beams and struts.

## 7.2 PRELIMINARY TESTS

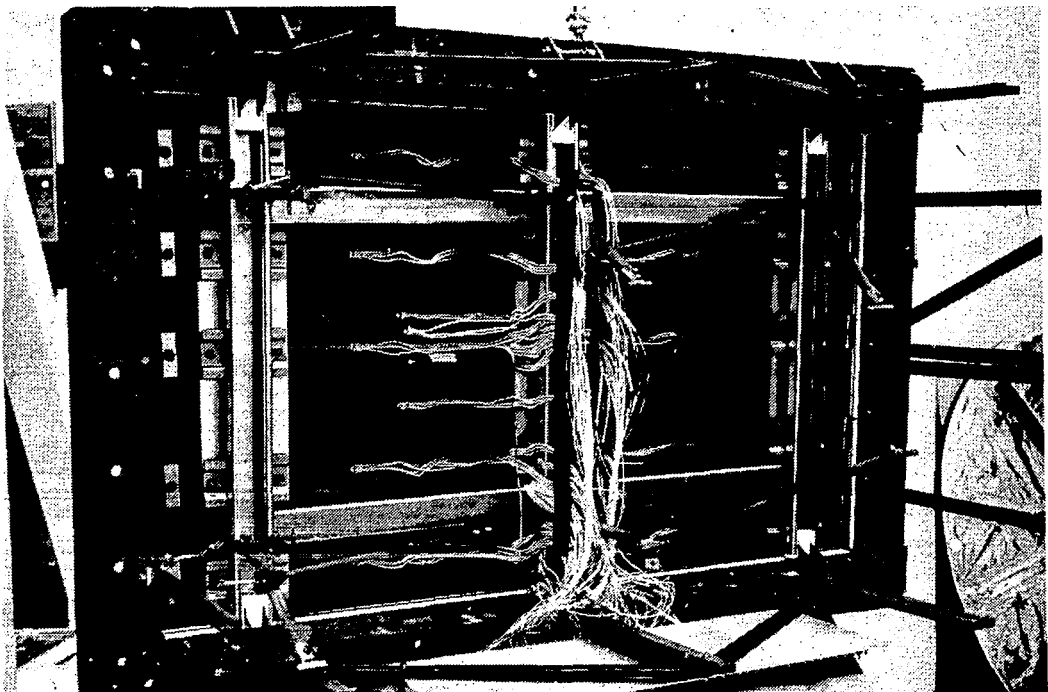
The heat shield test array is shown installed in the test fixture upper frame in Figures 7-2 and 7-3 before initiation of tests. The outer surfaces of the instrumented panels are shown in Figure 7-2 and the rear surfaces are shown in Figure 7-3. Insulation packages and the simulated substructure were installed after the photographs of Figures 7-2 and 7-3 were taken.

The TPS array was subjected initially to modal response tests to determine resonant frequencies and modal response shapes of the heat shield array. One of the main panels was excited near its center by an oscillating point force that produced panel accelerations normal to the plane of the array. Accelerometers located at 40 grid points on the array measured the response of the panels as noted in Figures 7-4 through 7-7. A frequency sweep was conducted first to determine the resonant frequencies by observing the phase and magnitude responses of the accelerometers at the various grid points. The first four resonant frequencies were identified and detailed response shapes were defined by recording the accelerations at each grid position. The first



CR60

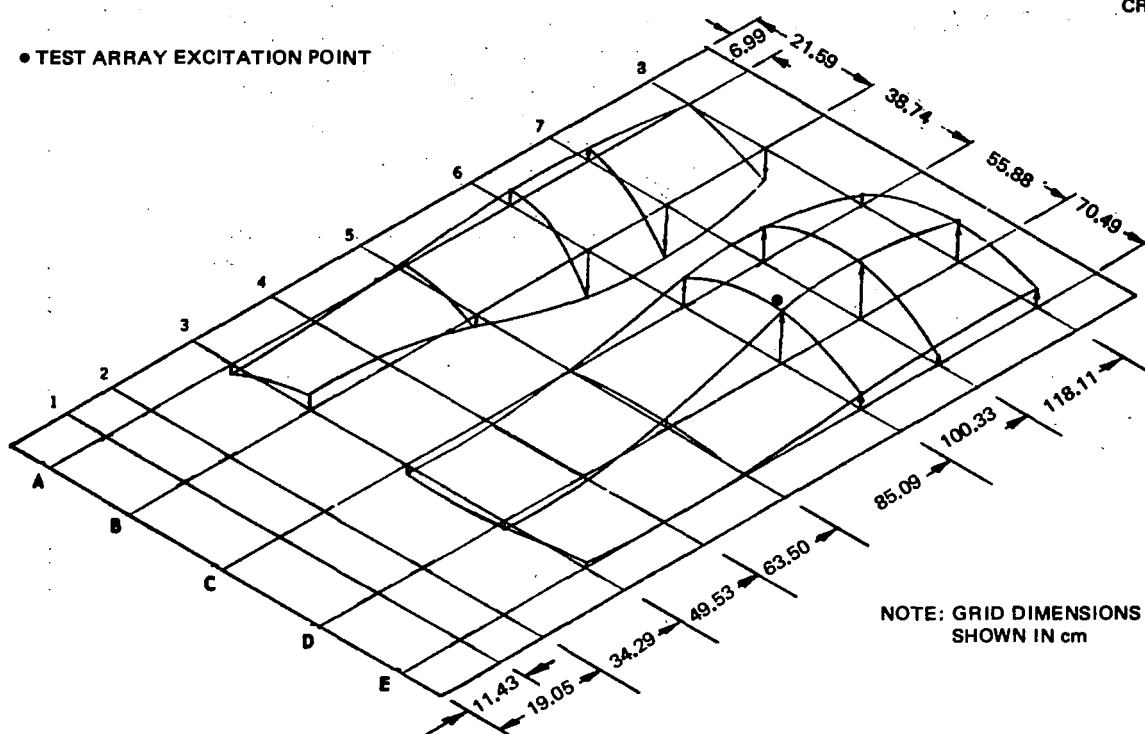
**Figure 7-2. External Surface of Test Array Before Test Initiation**



CR60

**Figure 7-3. Internal Surface of Heat Shield Panels Before Testing**

• TEST ARRAY EXCITATION POINT



- Test Array Excitation Point

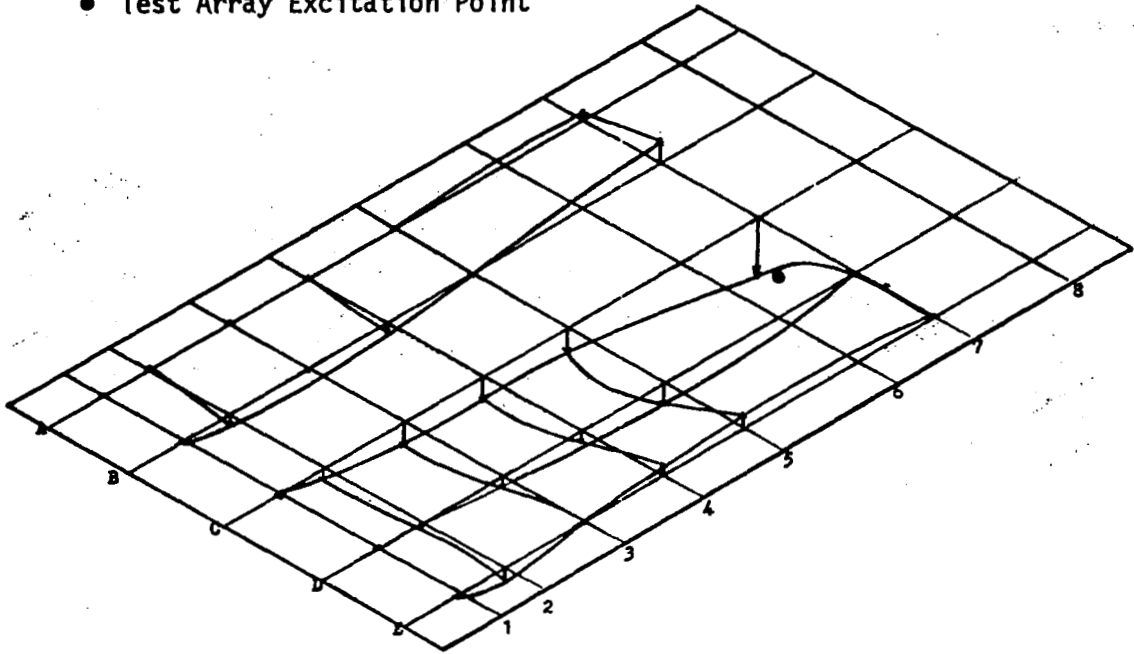


Figure 7-6. Test Array Normalized Modal Response at 322 Hz

CR60

- Test Array Excitation Point

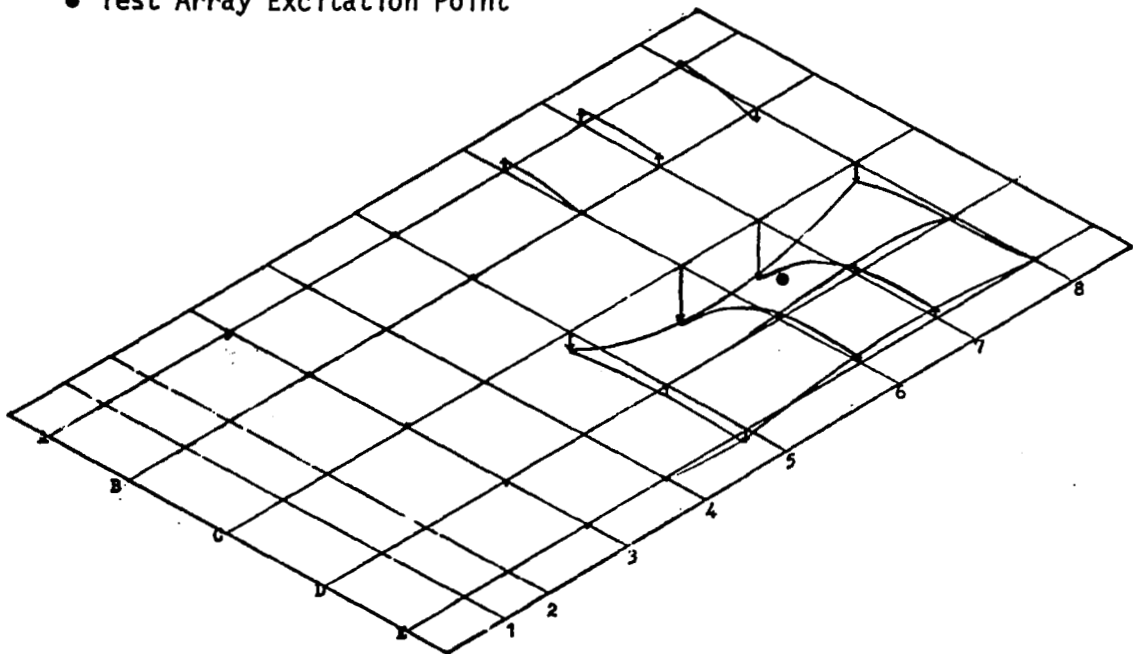


Figure 7-7. Test Array Normalized Modal Response at 330 Hz

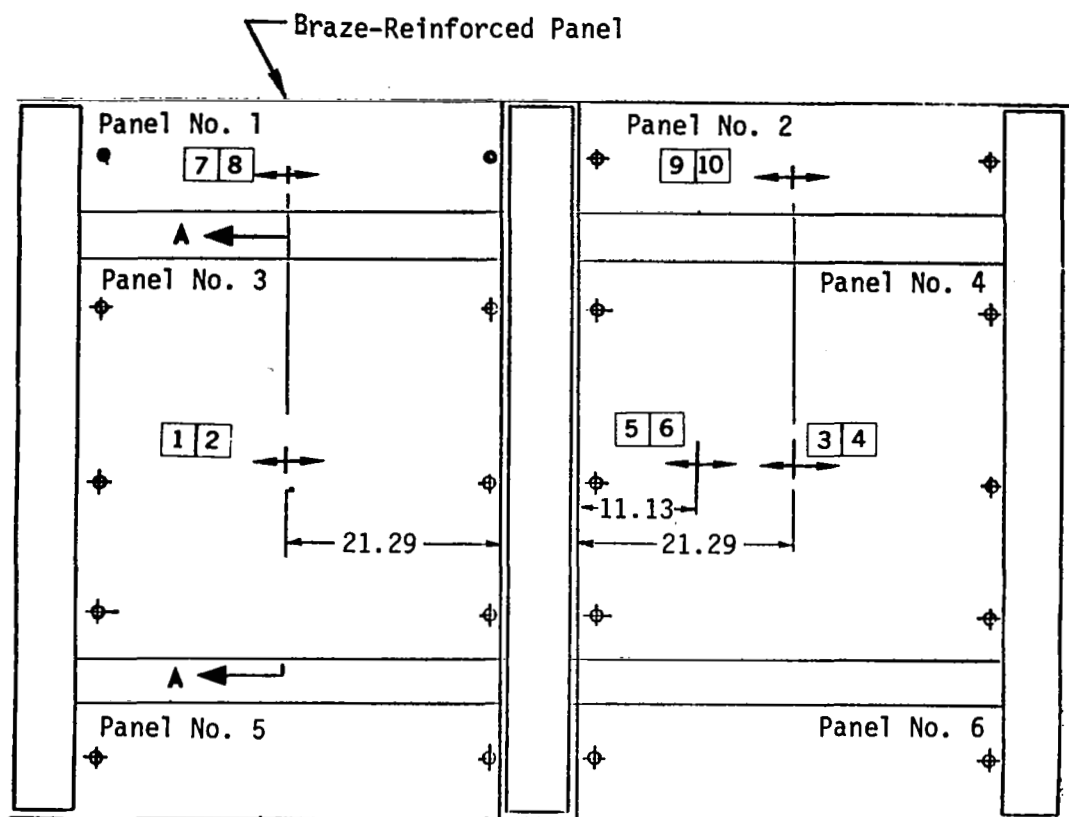
four resonant frequencies occurred at 228 Hz, 233 Hz, 322 Hz, and 330 Hz. The test array normalized mode shapes at each frequency are shown to scale in the perspective sketches in Figures 7-4 through 7-7.

After completion of the initial panel modal response tests in the Vibration and Acoustic facility the test array was moved back to the Space Simulation Laboratory for preliminary stress and thermal tests. The panel stresses caused by differential pressure at room temperature were checked in two separate runs, and both runs resulted in similar stress levels being recorded. The maximum tensile stress at the panel midspan position with a differential pressure of  $22.7 \text{ kN/m}^2$  (3.30 psi) was approximately  $109.0 \text{ MN/m}^2$  (15,800 psi), which compares favorably with the analytical prediction of  $109.8 \text{ MN/m}^2$  (15,900 psi). The maximum compression stress at the midspan point was  $7.61 \text{ MN/m}^2$  (11,050 psi) compared to a predicted stress of  $7.07 \text{ MN/m}^2$  (10,250 psi). Measured strains were converted to stresses using a static modulus of elasticity of  $167.8 \times 10^3 \text{ MN/m}^2$  ( $24.3 \times 10^6$  psi).

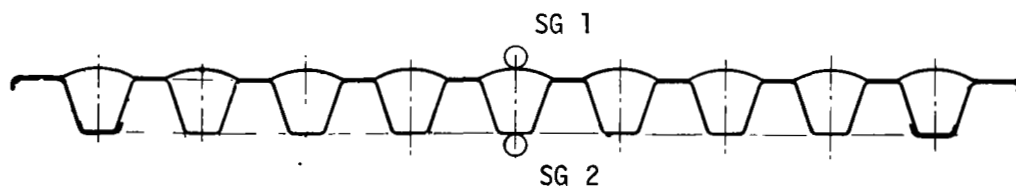
The preliminary strain survey on the panels was conducted with the heat shield array mounted in the test fixture and installed in the Space Simulation Chamber. The chamber was vacuum pumped while air at 1 atmosphere pressure was admitted to the pressure box portion of the test fixture so that differential pressure was applied to the heat shield array with the higher (1 atm.) pressure being on the external surface of the array. The pressure in the main test chamber was lowered in steps to permit strain readings to be recorded at approximate intervals of  $3.457 \text{ kN/m}^2$  (0.5 psi) differential pressure.

Strain gage locations are shown again in Figure 7-8 to indicate the detailed placement of the gages. Stresses derived from the first strain survey test are presented in Figures 7-9 through 7-11 as a function of differential pressure loads. Stresses at the midspan position on a main panel and at the same position on the braze-reinforced panel are shown in Figure 7-9. The data of Figure 7-9 indicate slightly lower stresses occurred on the braze-reinforced panel when compared to similar stresses on the main panel. Less





View of External Surface  
(Dimensions Shown in cm)



Section A-A (Rotated 90° CW)

Strain Gage Placement Typical for All Locations; Odd Numbered Gages on External Surface, Even Numbered Gages on Internal Surface

Figure 7-8. Strain Gage Locations

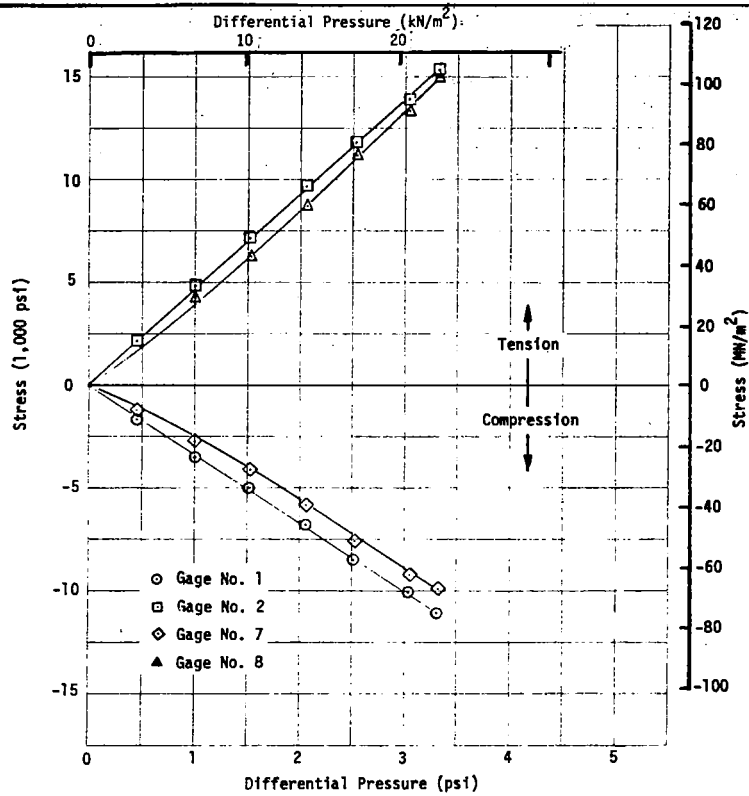


Figure 7-9. Panel Stresses as a Function of Differential Pressure

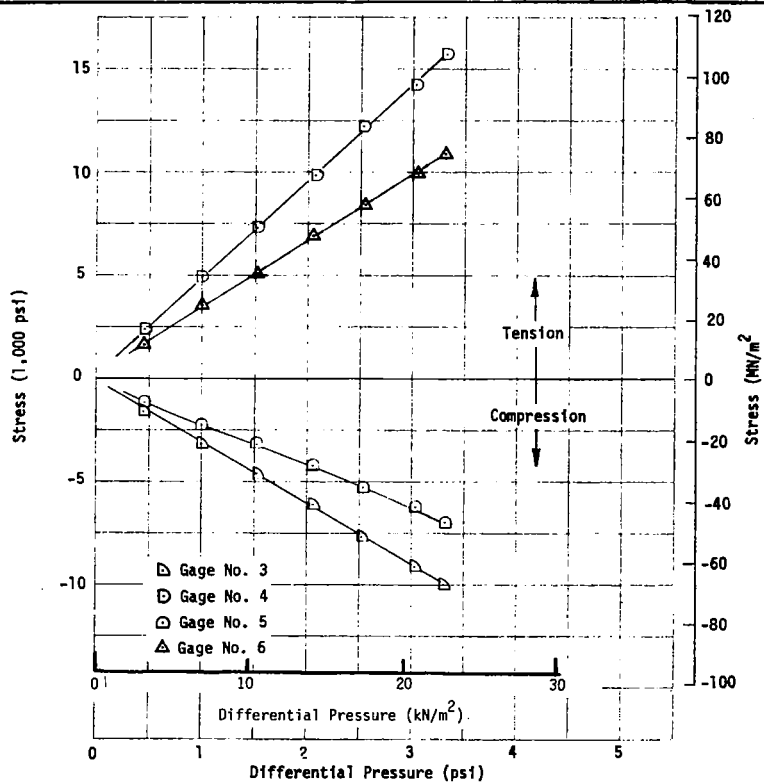


Figure 7-10. Panel Stresses as a Function of Differential Pressure

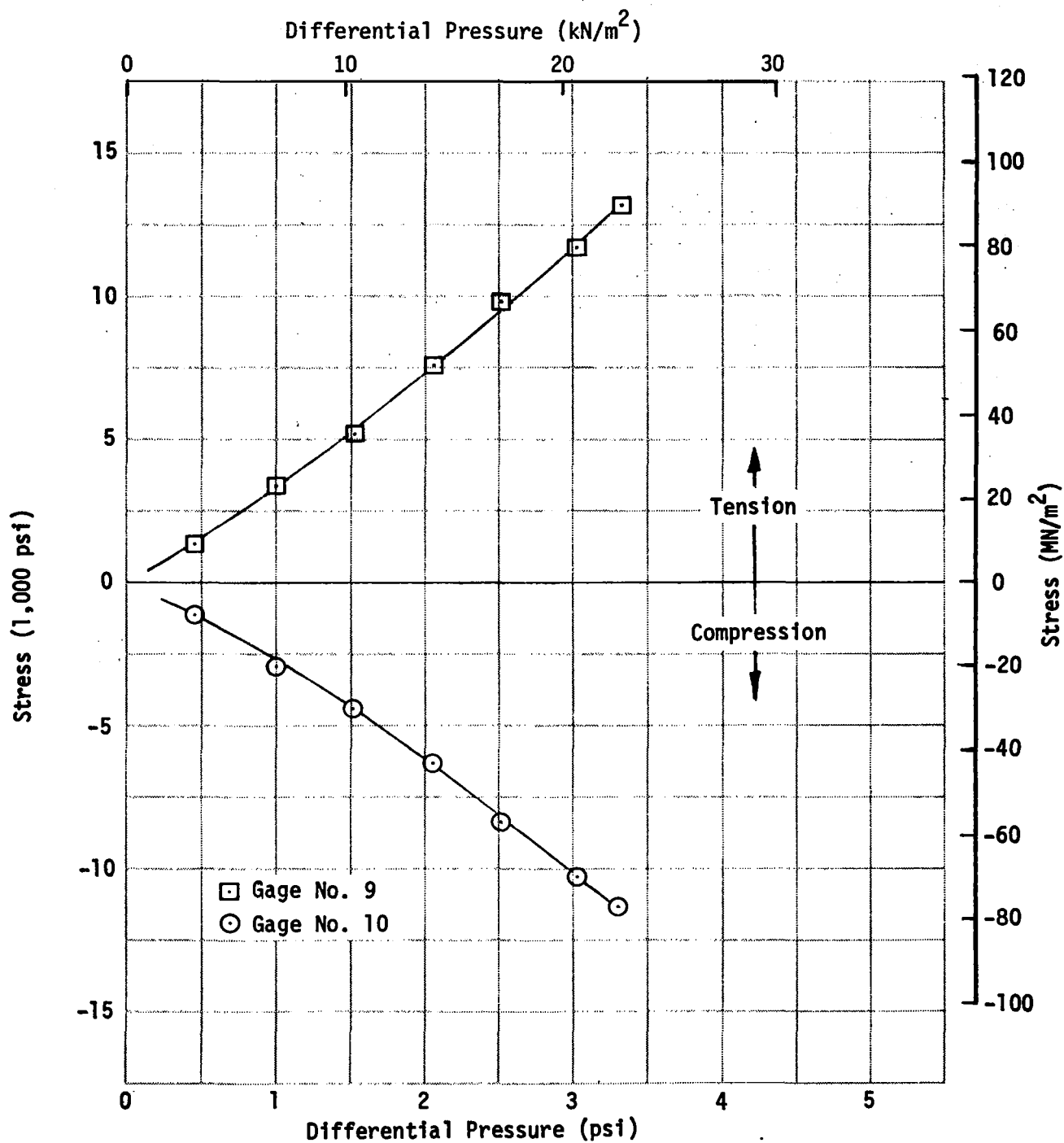


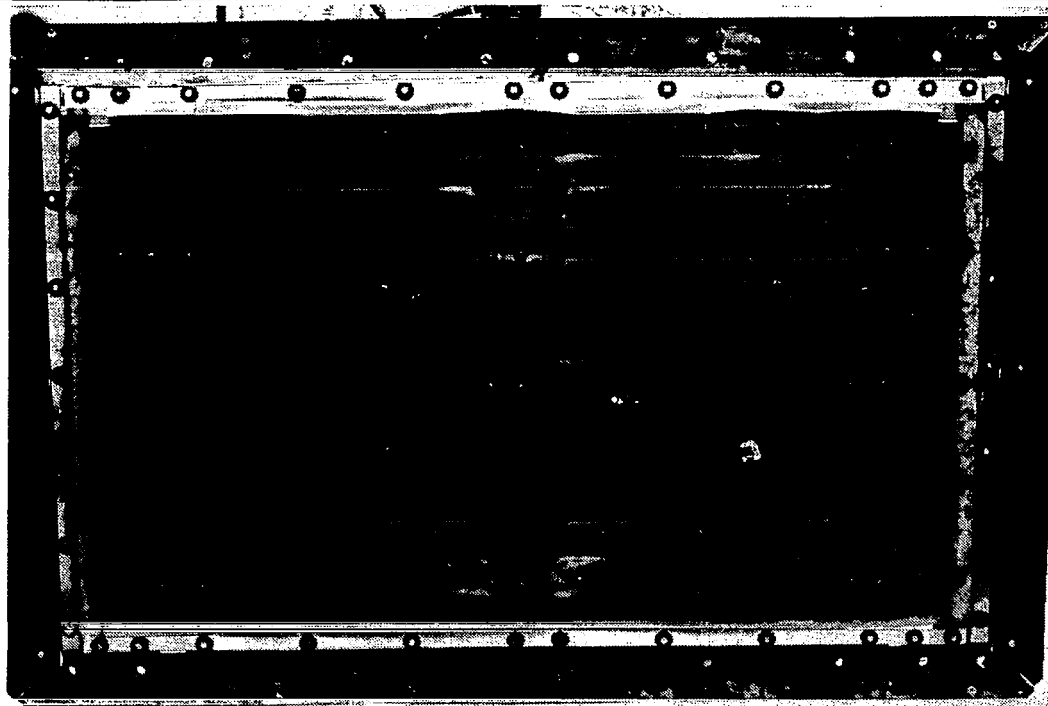
Figure 7-11. Panel Stresses as a Function of Differential Pressure – Gages 9 and 10

difference was noted in the compression stresses of the second main panel and its adjoining close-out panel, as can be observed in comparing the stress levels at gage 3 (Figure 7-10) with those of gage 9 (Figure 7-11). However, comparison of the tensile stresses measured at gages 4 and 10 show the main panel to have experienced somewhat higher tensile stresses in the reinforcing corrugation than experienced by the close-out panel.

A preliminary thermal test was next conducted using the full mission temperature profile with a maximum temperature of 1,477°K (2,200°F) without differential pressure loads. The preliminary thermal test caused a sine-wave shaped buckle to occur at one end of the center transverse cover strip due to restricted expansion space at the side edge seals. The cover strip buckle in turn caused some deformation of the edges of the two side close-out panels upon which the cover strip rested. Maximum deformation of the cover strip was estimated to be approximately 0.508-cm (0.20-in.) in a posttest visual examination of the test array. Figure 7-12 shows an overall view of the outer surface of the test array in which noticeable buckling of the lateral edge seals may be seen. The sine-wave shaped buckle in the end of the center transverse cover strip is shown clearly in Figure 7-13 in a photograph taken after the edge seals had been removed along the sides of the test array. Examination of the side close-out panels revealed several fine cracks in the panel face sheets where local bending was induced in the panels when the cover strip buckled. To conduct further examinations of the panel edges and to trim and straighten the cover strip end, the bolts attaching the center cover strip were removed. Figure 7-14 shows the cover strip partially detached. All of the transverse cover strips were then examined for interference with the edge seals, and the ends of the strips were trimmed where necessary. The strips and edge seals were reinstalled, and testing was continued with initiation of combined differential pressure and thermal cycles simulating the Shuttle Orbiter mission profile.

### 7.3 SIMULATED MISSION CYCLIC TESTS

The first mission test cycle was conducted with the objective of checking the control of the programmed pressure and temperature profiles when both were applied simultaneously. Minor difficulty was encountered in portions of the



CR60

**Figure 7-12.** Overall View of Test Array After Preliminary Thermal Test



CR60

**Figure 7-13.** Cover Strip Deformation After Preliminary Thermal Test

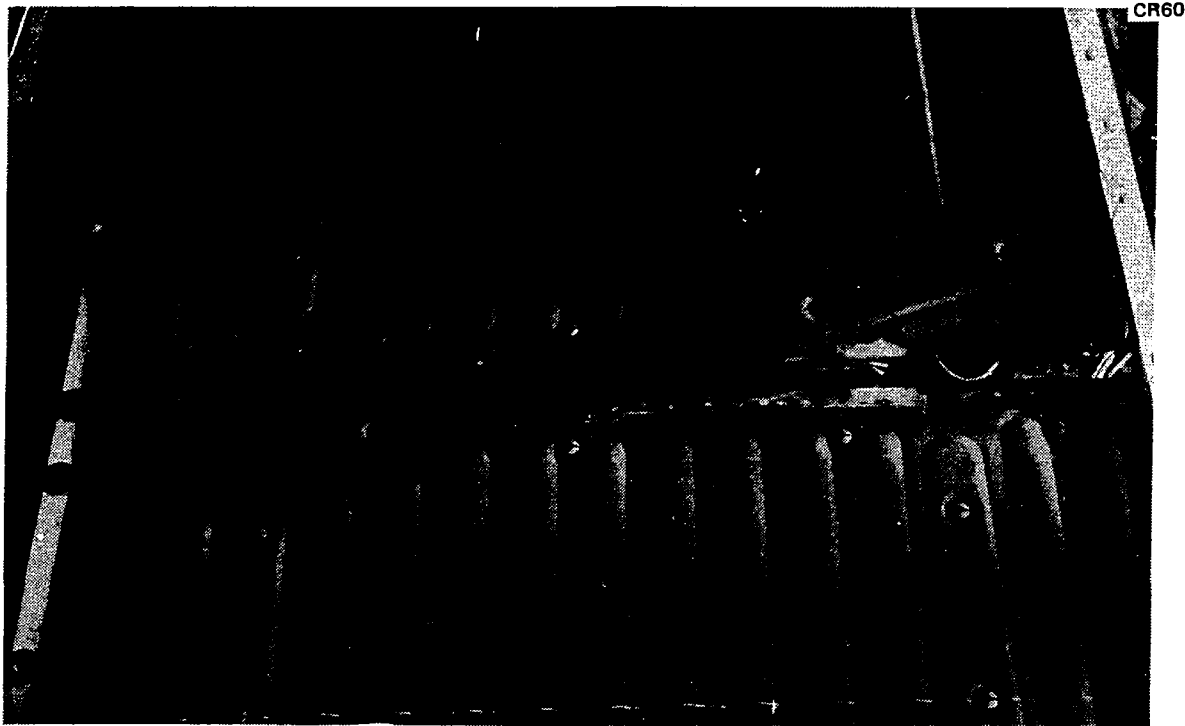


Figure 7-14. Cover Strip Partially Removed After Preliminary Thermal Test

temperature profile due to failure of some of the control thermocouples. After the first complete mission cycle the test array was removed from the test chamber and the failed thermocouples were replaced. Sufficient space was available to allow the necessary expansion of the transverse cover strips and no further deformations of the cover strip ends were noted. Examination of the panel areas where initial cracking had occurred during the preliminary thermal test showed some additional crack growth. Figure 7-15 presents an overall view of the test array after the first simulated mission cycle, and the areas where face sheet cracks were noted are indicated. Close-up views of two of the areas are shown in Figures 7-16 and 7-17. Several additional face sheet cracks were observed in the main panels at the ends of beads near a panel attach position. The latter cracks, shown in Figure 7-18, were approximately 0.63-cm (0.25-in.) in length. After inspection and thermocouple replacement, the test array was reinstalled in the Space Simulation Chamber and simulated mission test cycles were resumed.

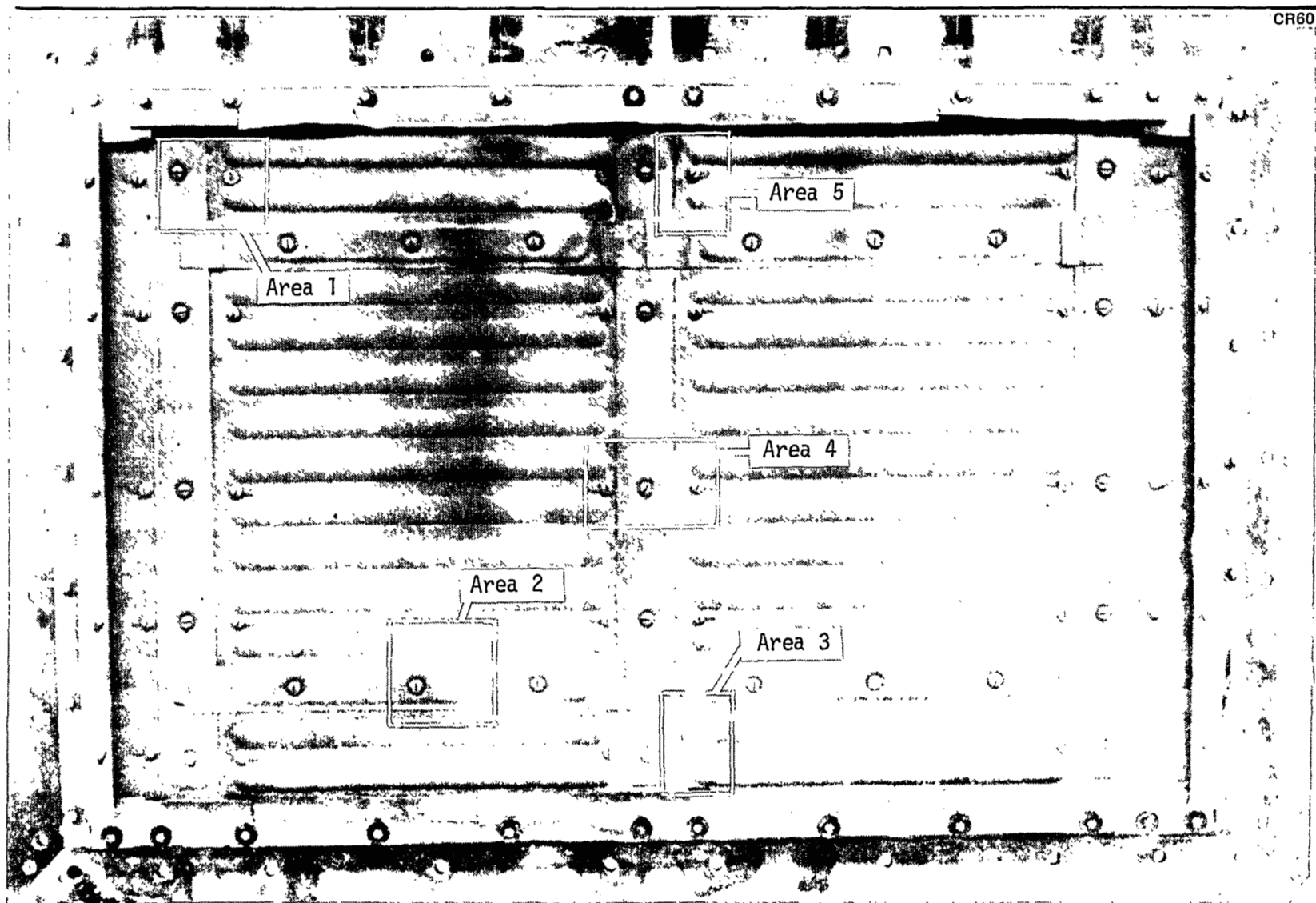


Figure 7-15. Overall View of Test Array After First Mission Test Cycle

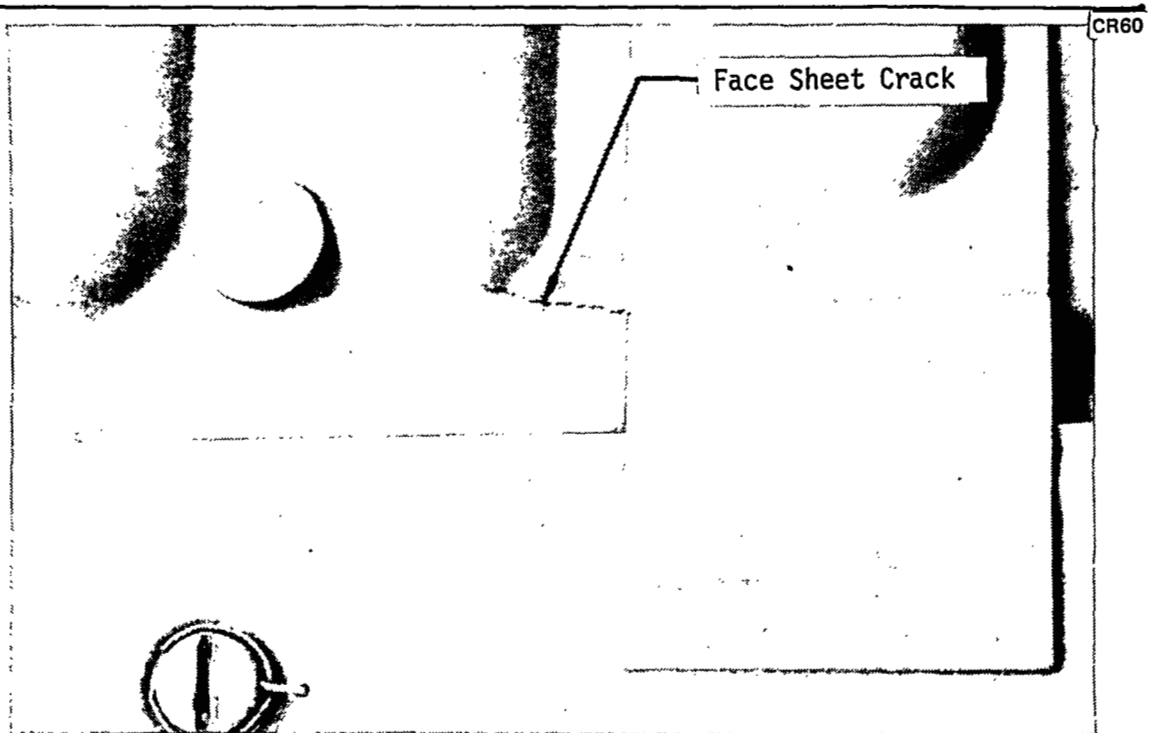


Figure 7-16. Damage in Braze-Reinforced Panel After First Mission Test Cycle

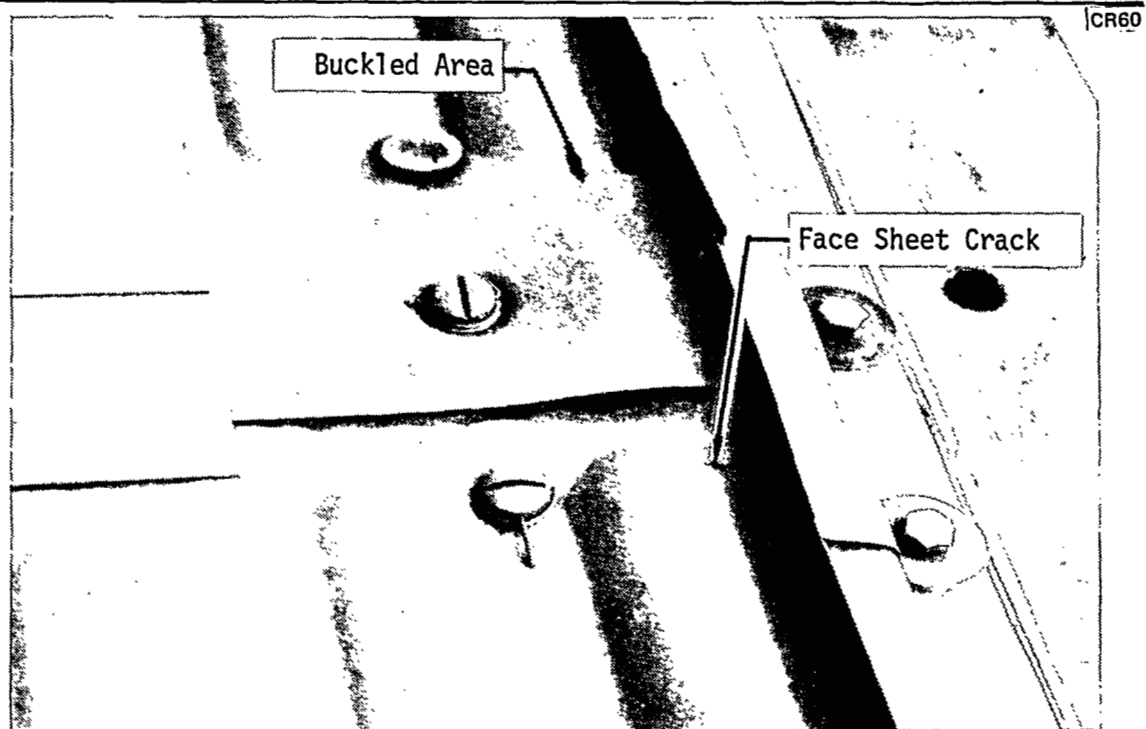


Figure 7-17. Close-up View of Center Transverse Cover Strip (Area 5)



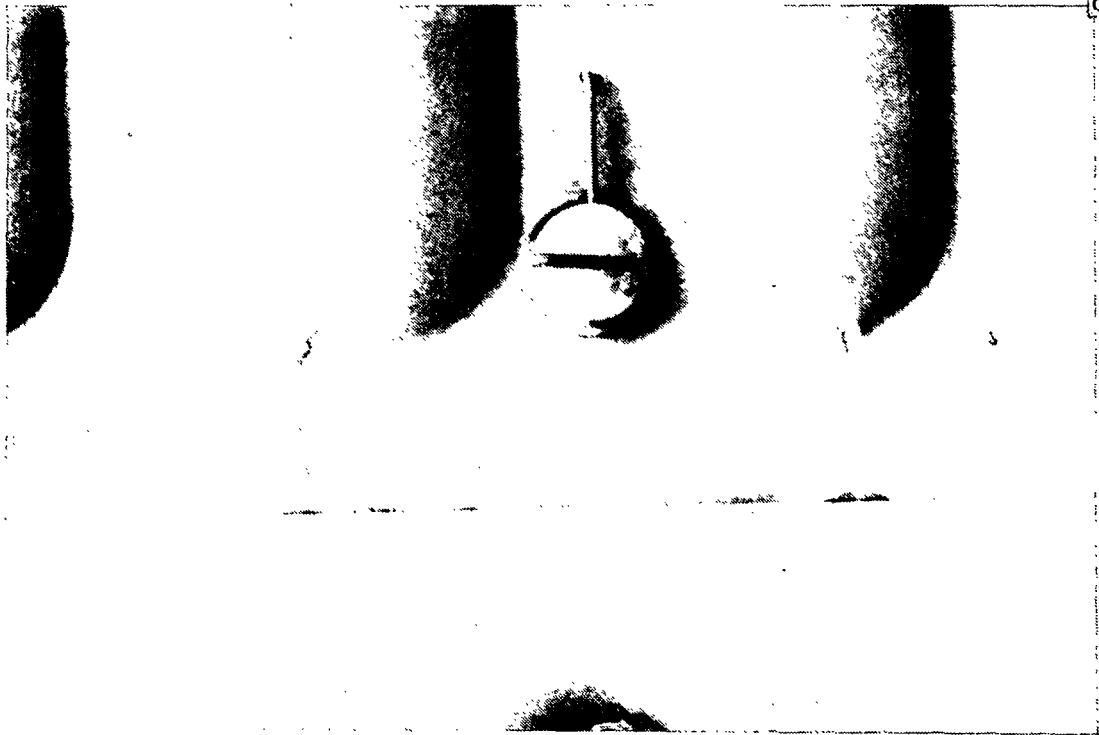


Figure 7-18. Cracks at Bead Ends on Main Panels (Area 4)

Another inspection of the test array was conducted at the end of the tenth cycle. Some additional growth was noted at existing crack locations as shown in Figure 7-19. The growth that occurred between test cycles 1 and 10 may be noted by comparing Figures 7-16 and 7-19. The maximum damage noted after the tenth test cycle occurred at the end of a side close-out panel. A crack approximately 7.62-cm (3.0-in.) in length, shown in Figure 7-20, was observed across the end of the panel. Smaller cracks, also shown in Figure 7-20, occurred around the ends of the two beads in the panel face sheet. The damage shown in Figure 7-20 was judged to be caused by excessive pressure from the transverse cover strip. Such pressure from the cover strip resulted in local bending in the panel end with high tensile stresses in the face sheet. The inspection conducted at the end of the tenth cycle indicated all damage was local, and therefore additional testing was scheduled.

Testing was continued in the Space Simulation Chamber by applying an additional fifteen test cycles to bring the total number of simulated mission cycles to twenty-five. At this point the test array was removed once again for

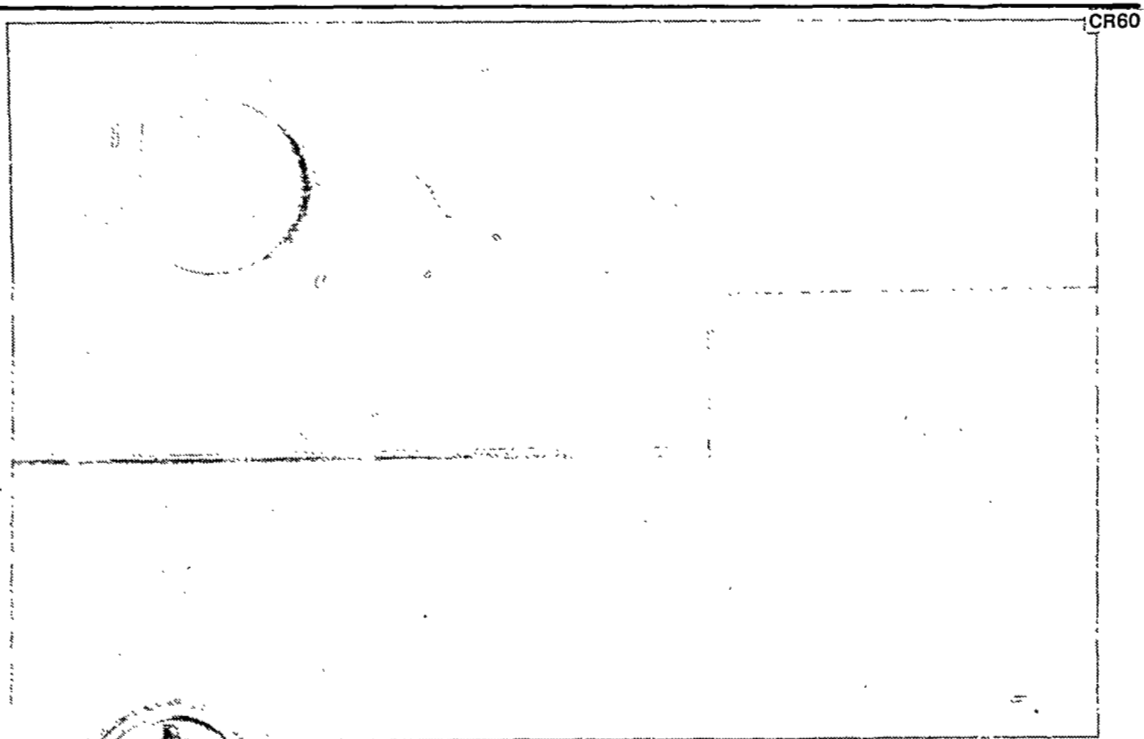


Figure 7-19. Damage in Braze-Reinforced Panel After Tenth Mission Cycle (Area 1)

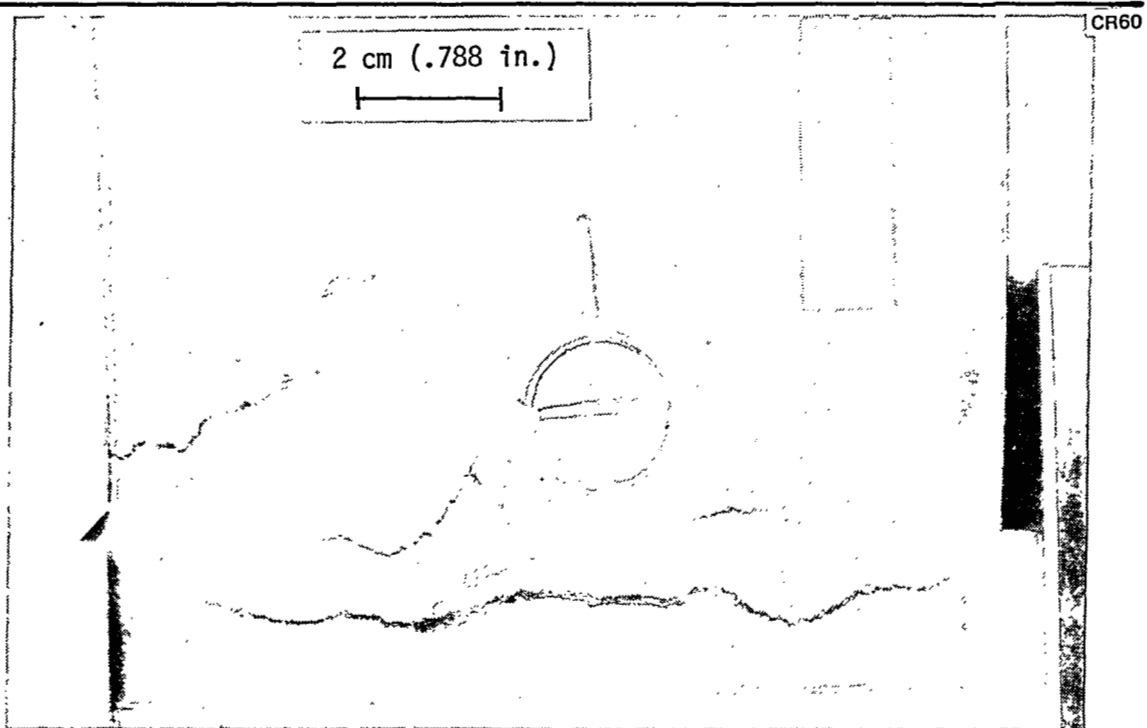


Figure 7-20. Damage in Panel No. 6 After Tenth Mission Test Cycle (Area 3)

inspection of the heat shields and instrumentation. Little additional crack growth was noted on the main panels at the end of the twenty-fifth cycle. Examination of the side close-out panels showed only a minimum additional damage in the fracture areas on those panels.

Typical temperature time-histories recorded during tests in the Space Simulation Laboratory are presented in Figures 7-21 through 7-26. Temperatures in the noted figures were recorded during test run number 10, and the values shown are typical of the temperatures recorded in simulated mission pressure and temperature tests conducted with the contractor test array. Comparison of the programmed surface temperature profile with the values of thermocouple 1 and other thermocouples mounted on test array's surface shows close adherence of the test array surface temperatures with the test profile. In other comparisons, the test temperature on the inner surface of the insulation peaked earlier and at a slightly higher value than predicted by analysis. Similar temperature responses occurred at the center of the second full-size heat shield. The temperature gradient through the heat shield thickness is shown in Figure 7-23 for a position near the center of panel No. 3 (Reference Figure 7-1). The maximum gradient through the panel occurs during initial heating, during which time a gradient of approximately  $198^{\circ}\text{K}$  ( $355^{\circ}\text{F}$ ) was recorded.

The differential pressure recorded in run 10, shown in Figure 7-27, indicates good agreement was maintained with the programmed test profile during a majority of the test run. Pressure drops occurred at two points near the end of the run, both deviations being in non-critical portions of the profile. The data of Figure 7-27 are typical of all test runs conducted in the Space Simulation Chamber during Phase II tests.

After inspection of the heat shields following the twenty-fifth thermal and differential pressure cycle, the test array was moved intact to the Acoustics Laboratory where it was mounted in the test chamber for simulated lift-off acoustic environment tests. The acoustic spectra, shown in Figure 5-14, simulated the projected engine noise at liftoff with an overall sound pressure level of 160 db. The duration of the simulated liftoff acoustic level was selected as 30 seconds for each mission.

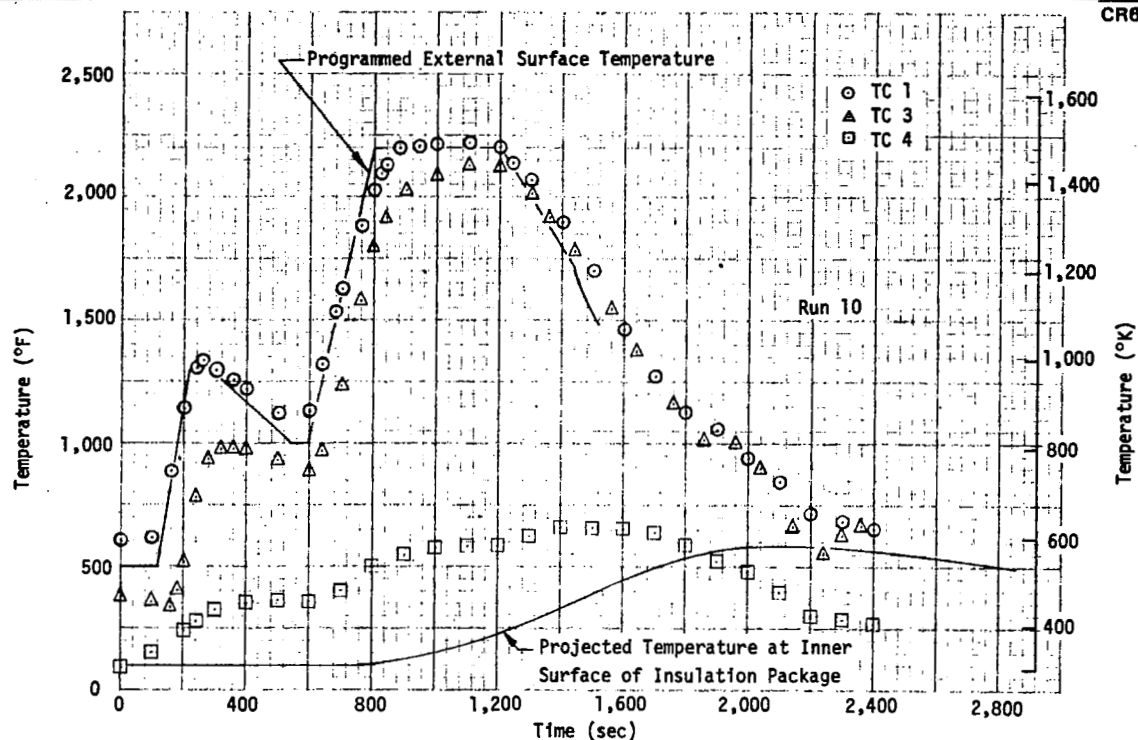


Figure 7-21. Temperature Time-Histories, Thermocouples 1, 3, 4

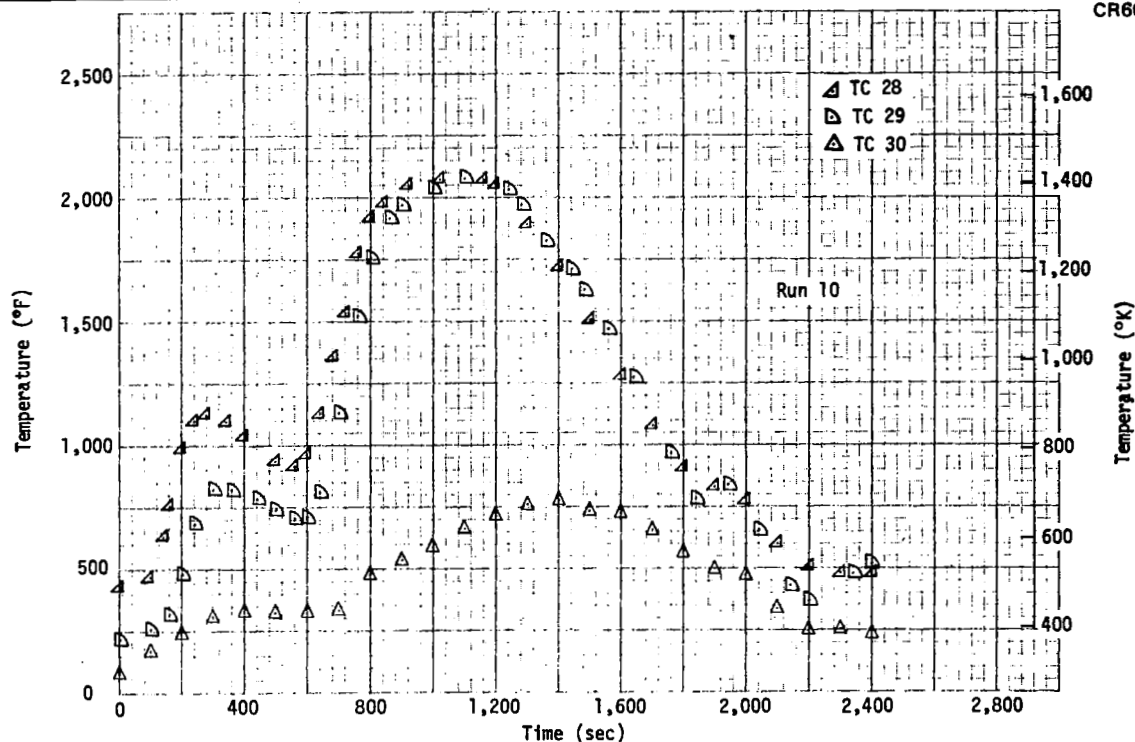


Figure 7-22. Temperature Time-Histories, Thermocouples 28, 29, 30

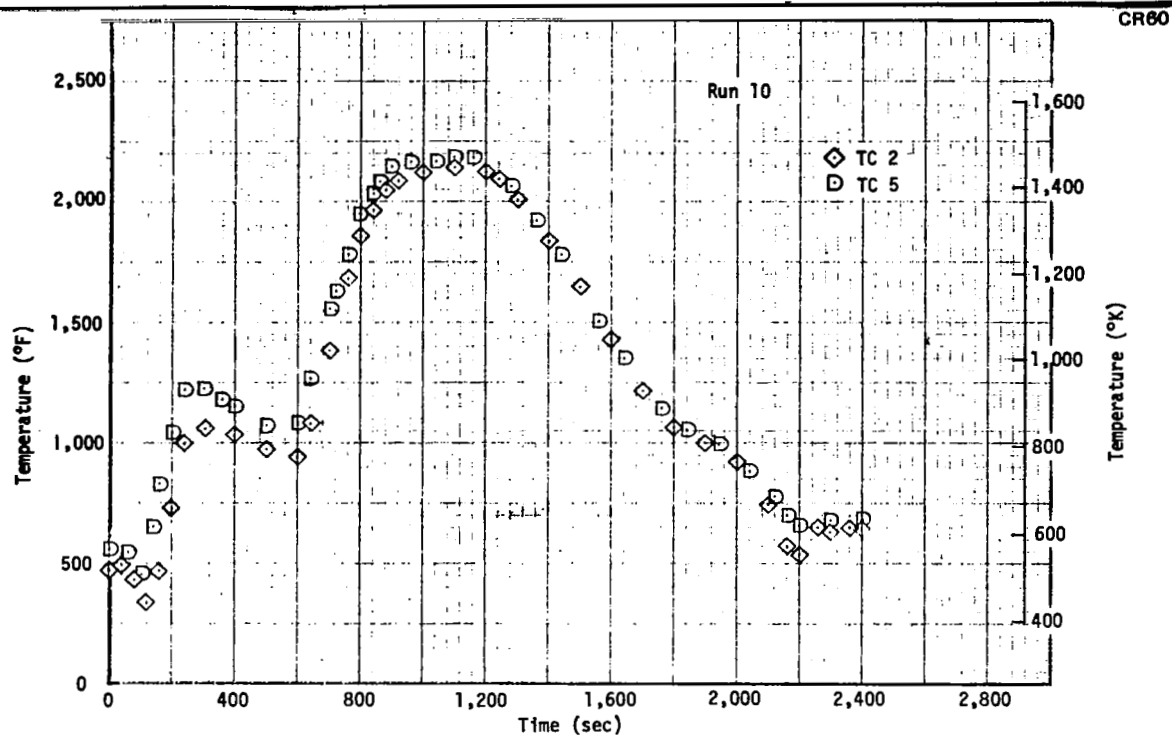


Figure 7-23. Temperature Time-Histories, Thermocouples 2, 5

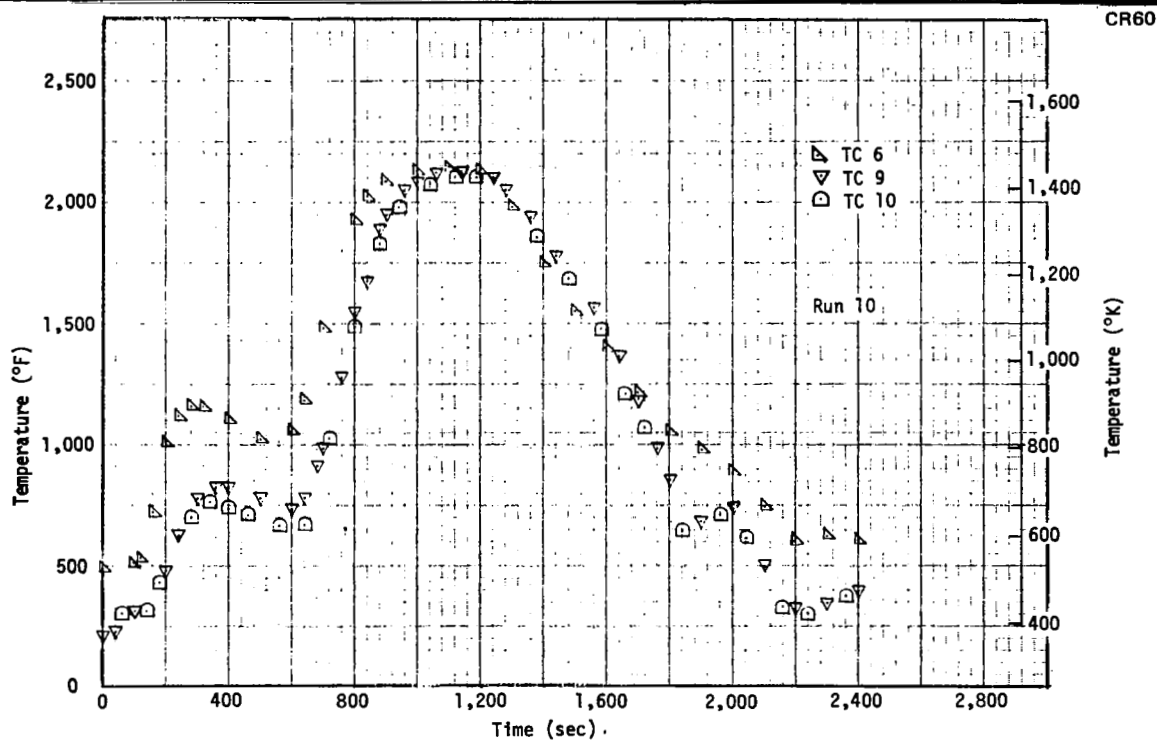


Figure 7-24. Temperature Time-Histories, Thermocouples 6, 9, 10

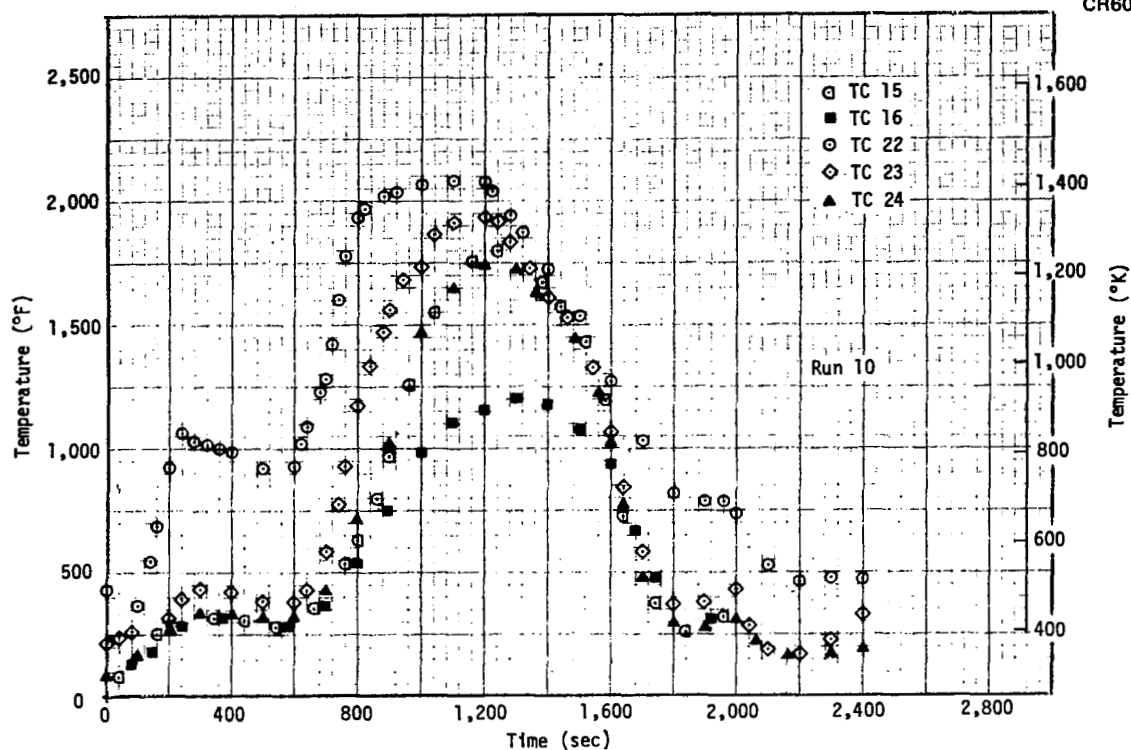


Figure 7-25. Temperature Time-Histories, Thermocouples 15, 16, 22, 23, 24

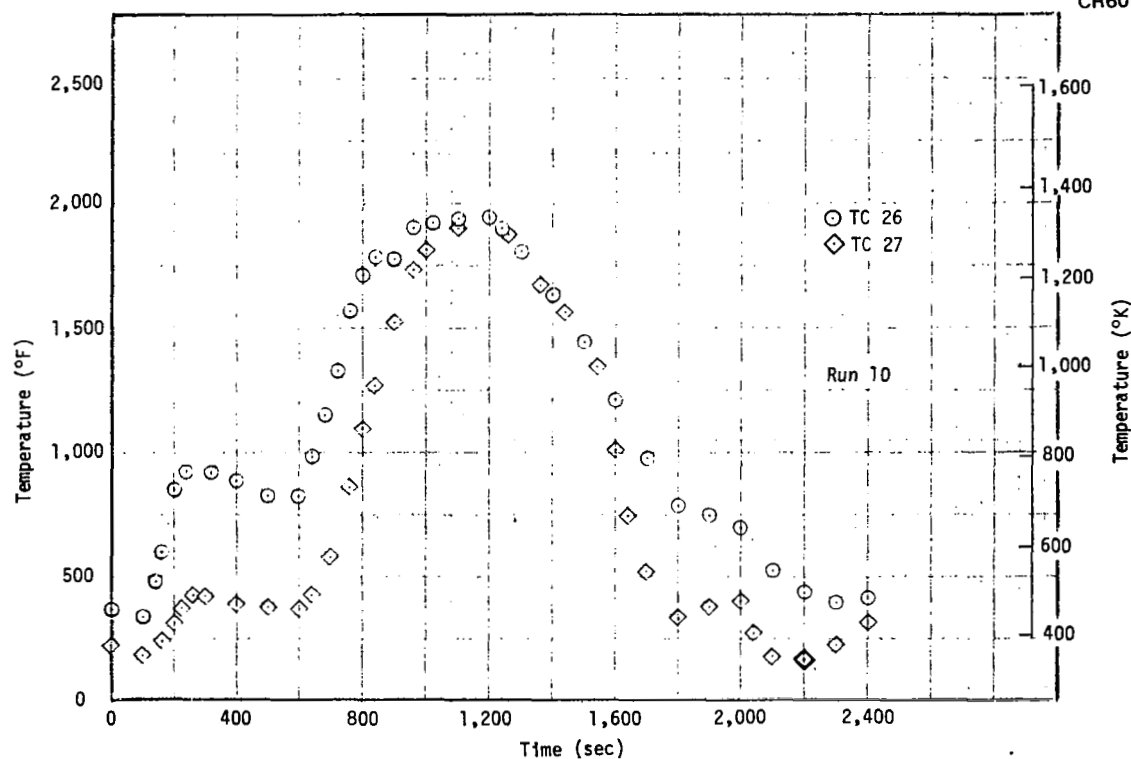


Figure 7-26. Temperature Time-Histories, Thermocouples 26, 27

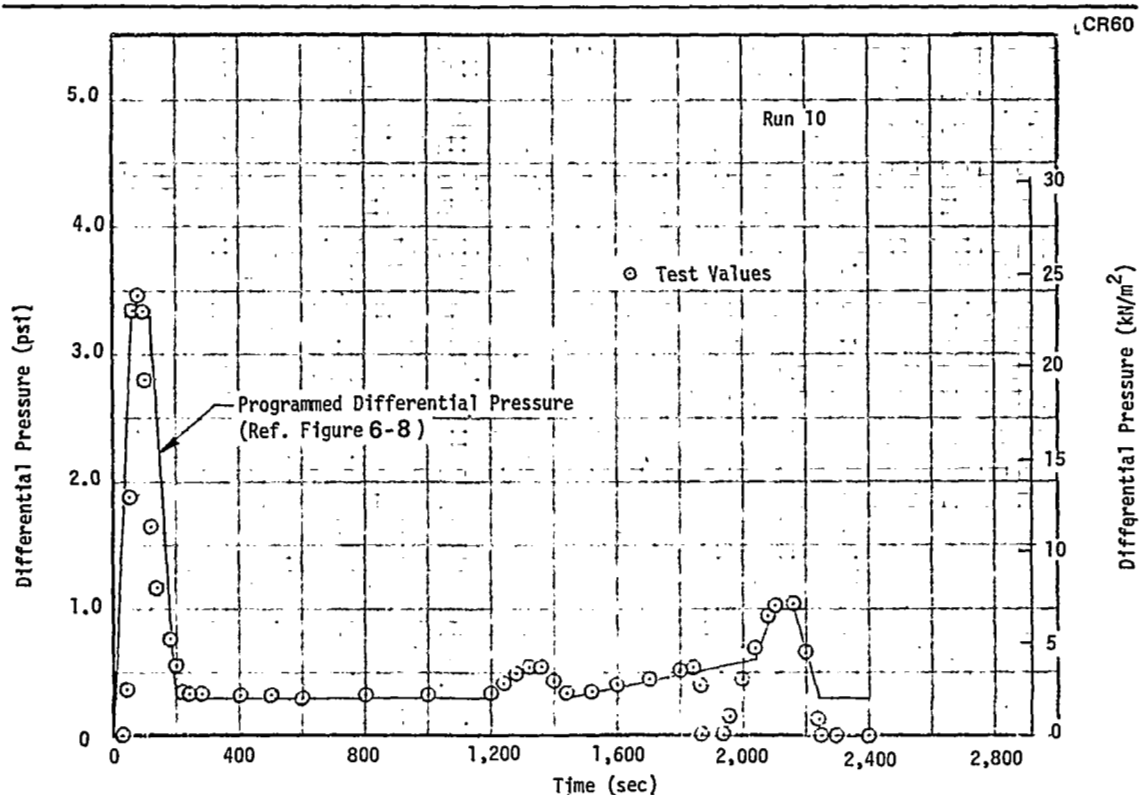


Figure 7-27. Differential Pressure Time-History

The test array, including its holding fixture, was mounted in the acoustic test chamber so that it formed one of the side walls in a rectangular chamber which was open at one end and attached to two exponential horns at the other end. The test chamber was approximately 2.14 m (7.0 ft.) in length, 1.22 m (4.0 ft.) in height, and .61 m (2.0 ft.) in width. Existing cracks in the heat shields were marked at their ends so that increases in fracture damage during the acoustic tests could be easily noted.

The initial test at 160 db was conducted for 1.5 minutes, after which the test was stopped and the test array was inspected. No additional damage could be detected in the visual inspection, and testing was resumed. An additional 11.5 minutes of acoustic test time was applied to the test array to simulate a total of 12.5 minutes, the equivalent of 25 missions. Inspection of the array was again made, and no further crack growth could be noted in the heat shields. The tests were continued until a total of 25 minutes of acoustic exposure at 160 db had been reached. Inspections at that point again showed no visible increase in crack lengths on the panels. An additional 25 minutes

of testing at 160 db overall sound pressure level was conducted to provide a total of 50 minutes of simulated liftoff acoustic noise levels. Thus, 100 missions were simulated in the acoustic tests. Inspection of the test array was made again, and one of the spring-loaded covers for the recessed fasteners on the braze-reinforced panels was found to have vibrated free and fallen from the assembly. Examination of the cover showed no failure in the part. The areas that had been damaged during testing in the Space Simulation Laboratory were examined visually at the termination of the acoustic tests, and crack lengths were compared with the markings made at the crack tips prior to the start of the acoustic tests. From the examinations made, no crack progression could be detected at any of the previously damaged areas.

#### 7.4 COST STUDIES

Cost studies were conducted to develop projected initial TPS costs, refurbishment rates, and overall TPS unit cost for 100 missions. Refurbishment and cost data were developed for several replacement rates, and results from contractor tests of the full-scale, full-size TPS array were then reviewed to select projected refurbishment requirements and overall costs. TPS cost studies were based upon fabrication of a TD Ni-20Cr metallic shield system of the same range as produced in Phase II for tests in the Langley 8-ft. HTST and the TPS test facility. The TPS arrays for Langley test facilities incorporated single-face corrugation-stiffened TD Ni-20Cr heat shields attached to TD Ni-20Cr pylon supports. TD Ni-20Cr fasteners were used to attach the panels and cover strips, and packaged low-density fibrous insulation was installed between the heat shields and the substructure. The panel face sheets, corrugations, and edge members were joined by resistance spot welding to form the assembled heat shields. Similarly, resistance spot welding was employed in joining the panel support members. All cost studies included heat shield panels, panel supports, fasteners, panel cover strips, and insulation packages. The primary structure was not included in the cost studies.

To define costs peculiar to a TD Ni-20Cr radiative thermal protection system, a nominal surface area of  $122.5 \text{ m}^2$  ( $1,320 \text{ ft}^2$ ) was selected as the vehicle area sustaining temperatures requiring TD Ni-20Cr shields. A nominal size of 50.8 by 50.8-cm (20 by 20-inches) was selected for the heat shields, a size that corresponded to the full-scale, full-size test array panel size. Thus,



470 TD Ni-20Cr panels were required per vehicle. Six orbiter vehicles were considered as the initial quantity produced, with heat shield requirements for six vehicles being 2,820 panels. A spare panel inventory of 10 percent was assumed, bringing total initial heat shield production to 3,102 panels.

Projected initial TPS costs included the recurring fabrication costs of labor and materials plus non-recurring tooling costs attributable to tooling design, materials and tooling fabrication. No engineering design, development, test, and evaluation costs were included in the cost studies. TD Ni-20Cr material costs were based upon the most recent commercial prices charged for sheet and bar material. Such prices ranged from \$100 per pound to \$125 per pound, with the higher price being charged for thin gage sheet material such as 0.0254-cm (0.010-inch) thick sheet. A scrappage rate of 25 percent was applied to all TD Ni-20Cr parts. Thus, a factor of 1.25 was applied to weights of finished components to determine the required purchased material.

Refurbishment cost studies were also conducted to define total costs over the span of 100 missions. Refurbishment costs included manhour costs for inspection and replacement of heat shields, replacement of other TPS parts (fasteners, supports, insulation), and additional costs for fabricating the required replacement panels and parts. Manhours required for TPS inspection were based on study results presented in Reference 10 for metallic radiative thermal protection systems. Removal and replacement manhours were based upon observed times in initial assembly and check-out operations of the full-size test arrays combined with disassembly operations during tests. As described subsequently, removal and replacement manhours observed in this program agreed closely with those presented in Reference 10. Repair of the TD Ni-20Cr heat shields was not considered feasible since the panel damage observed in both subsize and full-size panel tests occurred predominantly as cracks in the 0.0254-cm (0.010-inch) thick face sheets or edge members. Consequently, replacement of panels or other TPS components was considered as the only refurbishment operation for the TD Ni-20Cr TPS.

Refurbishment costs were defined for heat shield replacement rates per mission of 1 percent, 2 percent, 4 percent, and 6 percent. For an assumed replacement rate of 1 percent per mission, each vehicle would have 470 TD-Ni-20Cr heat

shields replaced by the end of 100 missions. For a 2 percent replacement rate, an entire set of 470 panels would be used as replacements by the end of 50 missions. Panel requirements per vehicle are presented in Figure 7-28 as a function of replacement rate and number of missions. The initial complement of panels in Figure 7-28 reflects the assumed 10 percent spares inventory. Results from contractor tests of both subsize and full-size TD Ni-20Cr TPS arrays showed a minimum replacement requirement for components other than the external heat shields. Consequently, a replacement rate for support structures, insulation, and fasteners was selected as one-tenth the rate for heat shield panel replacement.

The assumptions made in projecting the initial TPS costs and the ensuing refurbishment costs are summarized as follows:

- A. TD Ni-20Cr heat shields cover an area of  $122.5 \text{ m}^2$  ( $1,320 \text{ ft}^2$ ) on each of six orbiter vehicles. An individual heat shield planform size of 50.8 by 50.8-cm (20 by 20-inches) was assumed.

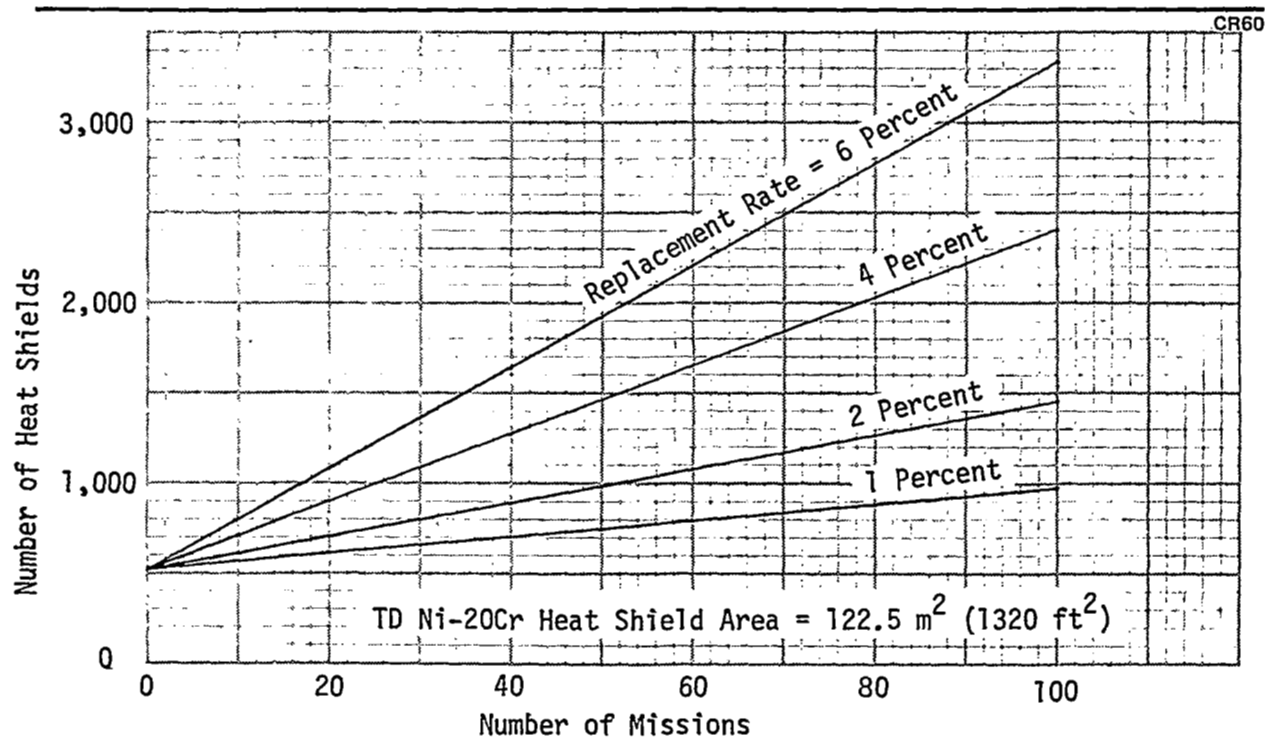


Figure 7-28. TD Ni-20Cr Heat Shield Requirements Per Vehicle

- B. The TPS configuration and fabrication approaches used for cost studies were the same as those applied to the full-scale, full-size test arrays designed for the Langley 8-ft HTST and the TPS test facility.
- C. Projected initial cost was based on recurring fabrication costs and non-recurring tooling costs. Design, development, test and evaluation costs were not included in cost projections.
- D. A 10 percent heat shield spares inventory is maintained.
- E. Refurbishment manhour requirements are based on study results presented in Reference 7.
- F. Replacement of support structures, fasteners, and insulation occurs at one-tenth the rate of panel replacement.

The TD Ni-20Cr TPS costs per vehicle are shown in Figure 7-29 as a function of number of missions and replacement rate of heat shields. Figure 7-30 presents the TD Ni-20Cr TPS costs per vehicle in terms of unit costs, or dollars per unit surface area.

Test results from both phases of the program were reviewed to define a projected replacement rate for heat shields in a TD Ni-20Cr thermal protection system applicable to the Shuttle Orbiter. Design deficiencies in the attachment design of the Phase I subsize test panels were considered significant in a majority of the damage incurred during the early portion of Phase I testing. Similarly, test fixture restrictions were considered to have contributed largely to the early damage incurred by the full-scale, full-size contractor test array in Phase II tests. As a result of test evaluations, a replacement rate of four percent was selected as a projected rate for the TD Ni-20Cr TPS. The criterion for panel replacement was detection of cracking in the panel. A replacement rate of four percent per flight would require 2,397 panels to be manufactured per vehicle, or a total of 14,382 heat shields for six vehicles.

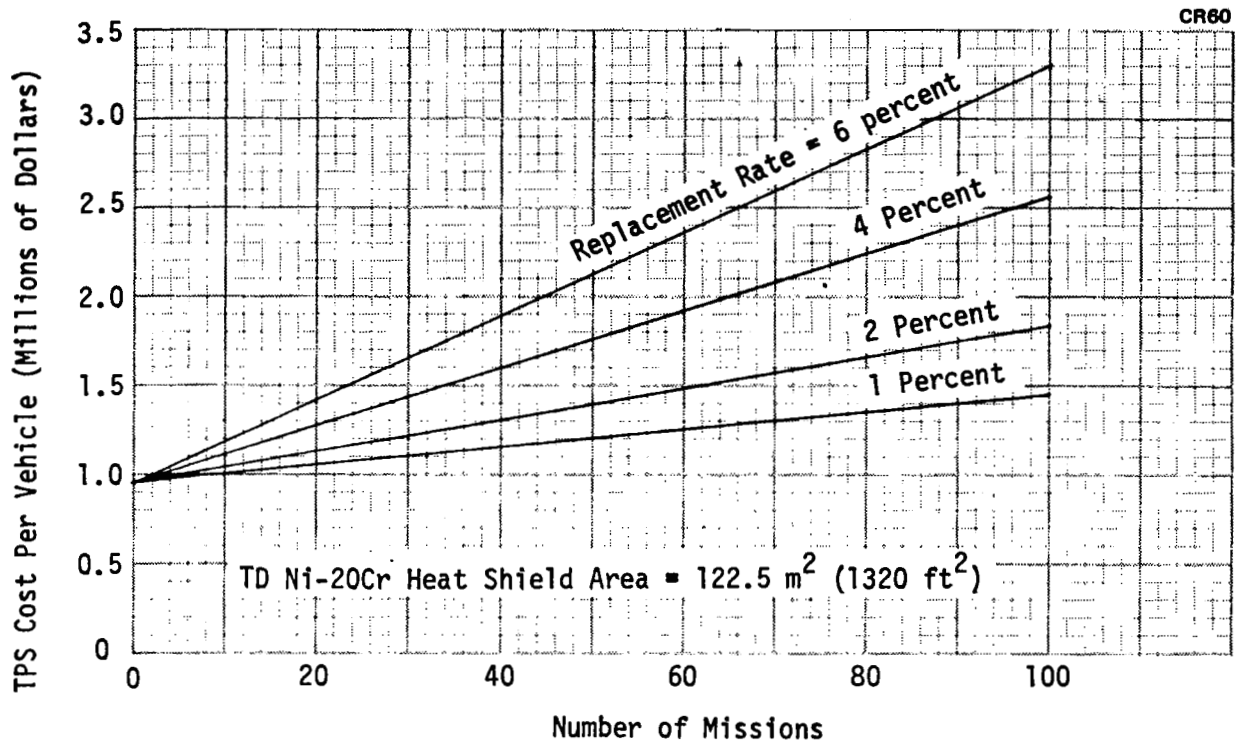


Figure 7-29. TD Ni-20Cr TPS Costs Per Vehicle

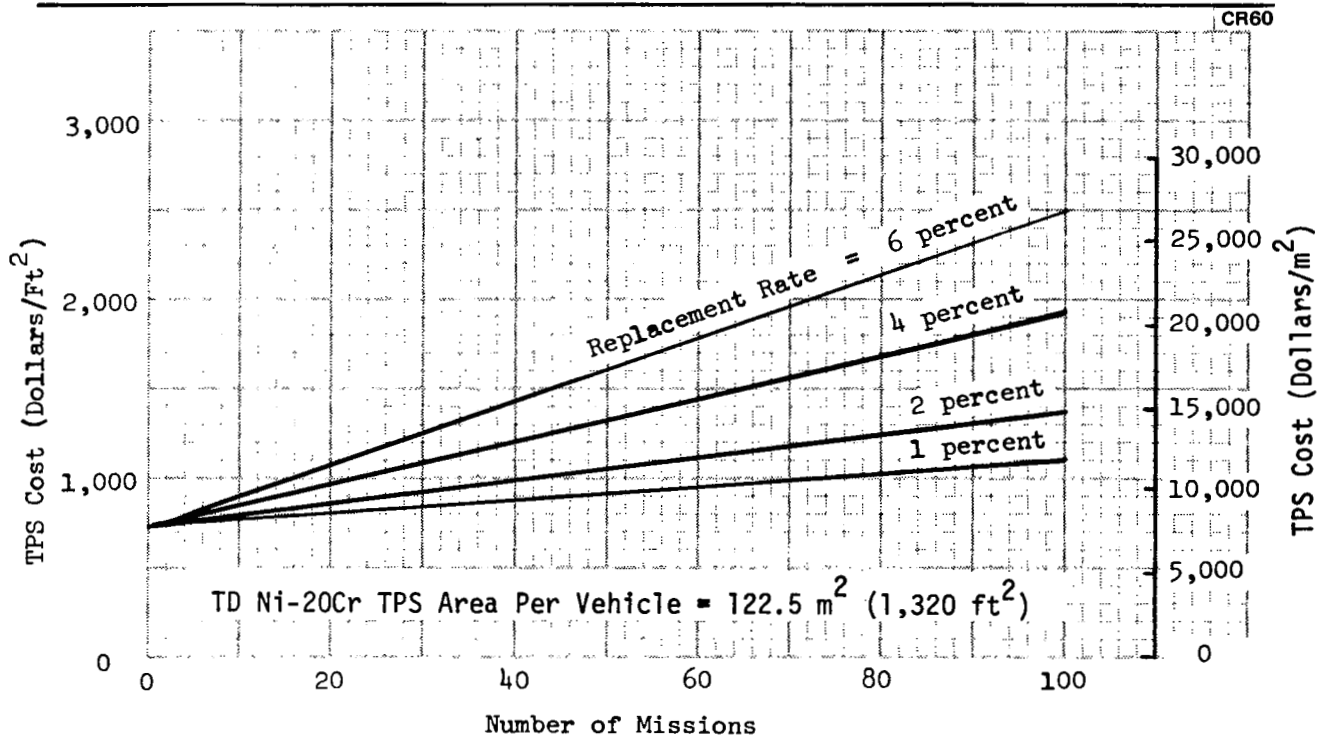


Figure 7-30. TPS Unit Cost Per Vehicle

Initial costs were independent of replacement rate, and from Figure 7-30 the initial unit cost is projected as \$721 per square foot of TPS surface area. The projected initial cost, as well as refurbishment cost projections, are based on 1974 dollars. As also shown in Figure 7-30, the unit cost per vehicle for 100 missions would be \$1,943 per square foot for the projected refurbishment rate of four percent per flight.

#### 7.5 DESIGN ADEQUACY AND LIFE EXPECTANCY

Results from Phase II tests conducted by MDAC were used to assess the adequacy of the TPS design and to evaluate life expectancy for TD Ni-20Cr heat shields in Shuttle applications. The evaluations for design adequacy and life expectancy were both closely related to assessment of refurbishment costs discussed in Section 7.4.

The TD Ni-20Cr heat shield design developed in this program was considered to be a viable basic approach that has the following desirable features:

- A. Removal and replacement of any individual panel may be made without loosening or removing adjacent panels.
- B. The surface heat shields are relatively low in weight with high stiffness in bending and torsion. Unit weight for the panels in the contractor test array was  $7.09 \text{ kg/m}^2$  ( $1.45 \text{ lb/ft}^2$ ) including closure strips and fasteners.
- C. The fasteners were secured externally. This approach eliminated the need for locknuts or internal lockwiring, both of which were considered to cause higher maintenance and refurbishment costs.

Improvements to the heat shield design were considered desirable in two specific areas. First, an improved method of positioning the cover strips should be incorporated in the design to prevent inducing bending moments near the panel edges where the cover strips are seated on the heat shield's external surface. Second, an improved fastener design is required that would incorporate a self-locking feature and would be shorter in length to reduce

fastener weight. Additional studies and tests should also be conducted with the objective of decreasing the number of fasteners per unit area. Such a reduction could reduce weight, initial cost, and refurbishment costs.

Average life expectancy for the TD Ni-20Cr heat shields was based on the performance of the main panels in tests conducted at the McDonnell Douglas Space Simulation and Acoustic Laboratories. In such tests the main panels showed significantly less deterioration than exhibited by the side close-out panels. The poorer performance of the close-out panels was due primarily to deformation of the cover strips near their ends that resulted from interference by the test fixture seals. In contrast, the cover strips in the area of the main test panels appeared to suffer no deformation, and consequently the main heat shields showed only minor degradation during tests. Coinciding with a replacement rate of four percent, the average heat shield life expectancy was projected as 12 to 15 missions.

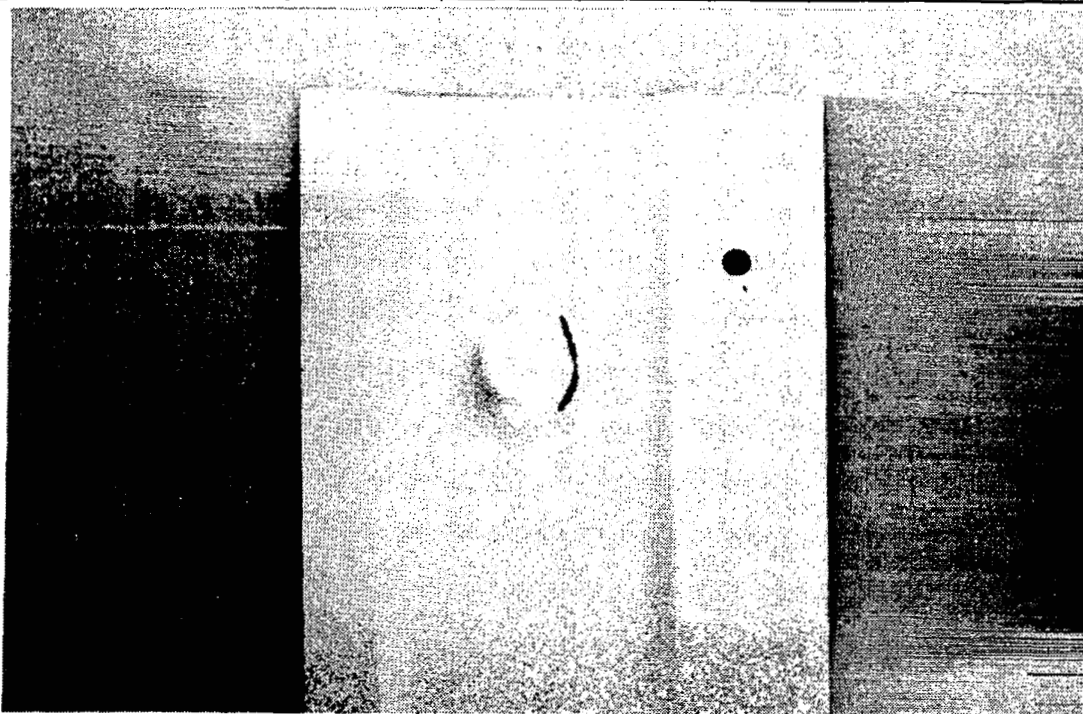
#### 7.6 INSTALLATION AND INSPECTION EVALUATIONS

Installation requirements and ease of replacement were assessed for the full size, full scale heat shield design and attachment system. Evaluations of panel installation were based on experience in the initial assembly of the three test arrays and in disassembly and reassembly operations conducted with the contractor test array during testing at the Space Simulation Laboratory.

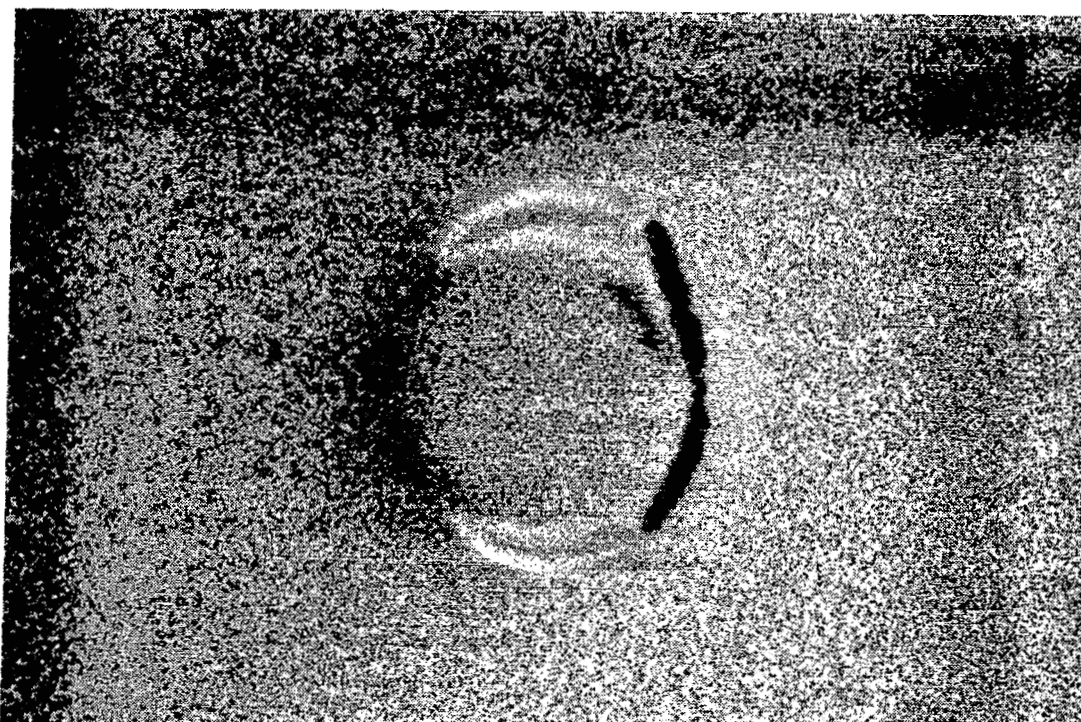
Installation of the heat shields was considered to be relatively simple, the basic steps being placement of the panel on the heat shield supports, alignment of the retaining nuts with the panel holes, installation of six retaining bolts, and lockwiring the bolts externally. Installation time ranged from 25 to 30 minutes per panel. Cover strips were then added to close the expansion space between panels, each cover strip requiring three bolts that were also lockwired externally. For flight vehicle installation, an average of two cover strips per heat shield would be required. Installation time per cover strip ranged from 4 to 5 minutes in the observed assembly operations with the test array. Total installation time per panel, including cover strip installation, ranged from 33 to 40 minutes. Panel removal time was more difficult to assess because removal operations involved other

components such as edge seals or close-out panels. Also, only partial removal of some components was required in most instances. Estimates for panel removal times, while not as firmly defined as those for installation, were judged to be in the same range as installation times. The total time for removal and replacement of the TD Ni-20Cr heat shields ranged from 66 to 80 minutes (1.10 to 1.33 hr.). In terms of manhours per square foot, the removal and replacement time ranged from 0.42 to 0.51 hr/ft<sup>2</sup>. The panel removal and replacement times observed in this program compare favorably with those reported in the studies of Reference 10, in which the projected removal and replacement time for 20-in. by 20-in. metallic radiative panels was 0.47 manhours/ft<sup>2</sup>.

Inspections of panels and other components were performed at various stages during fabrication and assembly of the test arrays. Basic inspection procedures included visual inspection of the detail parts to find obvious defects and dimensional checks to assure accuracy within specified tolerances. In addition to the basic inspection procedures, NDT techniques were evaluated for effectiveness in finding defects and in assessing the suitability of parts and assemblies containing minor defects. Three types of defective parts were noted during early fabrication efforts in building the three full-size, full-scale test arrays. The first type consisted of out-of-tolerance parts that were easily detected by basic inspection procedures. The second type of defect consisted of fine cracks that occurred in the early development stages of some formed parts. During development of the formed parts, a number of fine cracks were detected by visual inspection with the use of a 10X magnifying glass. More extensive examinations were also conducted with dye-penetrant checks of areas that are particularly susceptible to cracking in TD Ni-20Cr formed parts, such areas being the heel lines of contours on hydropress-formed parts and the external surfaces of brake-formed straight bends. A sample development part checked by dye-penetrant inspection is shown in Figure 7-31. Dye-penetrant inspection proved to be an exceptionally good technique for detecting very fine cracks in formed TD Ni-20Cr parts. Forming tools were changed where necessary during development work by increasing the radii at bead edges and other critical areas to eliminate cracks in the parts.



a. Overall View of Area with Crack



b. Closeup of Crack Shown by Dye-Penetrant

Figure 7-31. Dye-Penetrant Inspection of Formed Cover Strip



The third type of defect consisted of material expulsion at spot welds on the main heat shield panels and on the closeout panels. This condition can be caused by slight changes in spotweld machine settings or by changes in material thicknesses within a sheet of material. Tests were previously conducted to evaluate radiography as an NDT method for detecting expulsion at spot weld positions in panel assemblies. Defective spot welds were produced by intermittantly using above normal current settings on the spot welder so that expulsion occurred on some of the spot weld positions. The defective panel was x-rayed and the resulting x-ray was examined for indications of defective positions on the panel. Sections which appeared to show expulsion were subsequently cut from the panel and micrographs of the mounted spot welds were made to confirm the defect. A sample of the panel x-ray is shown in Figure 7-32. The lighter areas at spot weld positions in the panel x-ray indicate a thinning of the spot welds caused by greater transverse compression in the material where above-normal current was used. Such areas were visually confirmed by noting excessive indentation on the surface of the panel at spot weld positions that appear as lighter areas in the x-ray of Figure 7-32.

The x-ray NDT method has proven to be a satisfactory method for checking spot-welded components for material expulsion at the welds. In addition to evaluation of radiography as an NDT method, spot weld machine settings were checked regularly during panel fabrication by testing sample spot-welded single lap-shear test specimens using the same settings as those employed for assembly of the panels. Minimum strength values were established for each combination of sheet thicknesses, and test samples were strength checked intermittantly during spot welding operations to assure satisfactory machine settings.

As described in Section 6, braze-reinforcement of a spot-welded panel was used on only one close-out panel in the contractor test array. Consequently, evaluations of NDT methods for the braze-reinforced panel were not made during Phase II. However, the differences in coloration shown in Figure 6-7 indicate the possibility of using normal photography or visual inspection to evaluate the extent of braze alloy flow in braze-reinforced spot-welded panels.

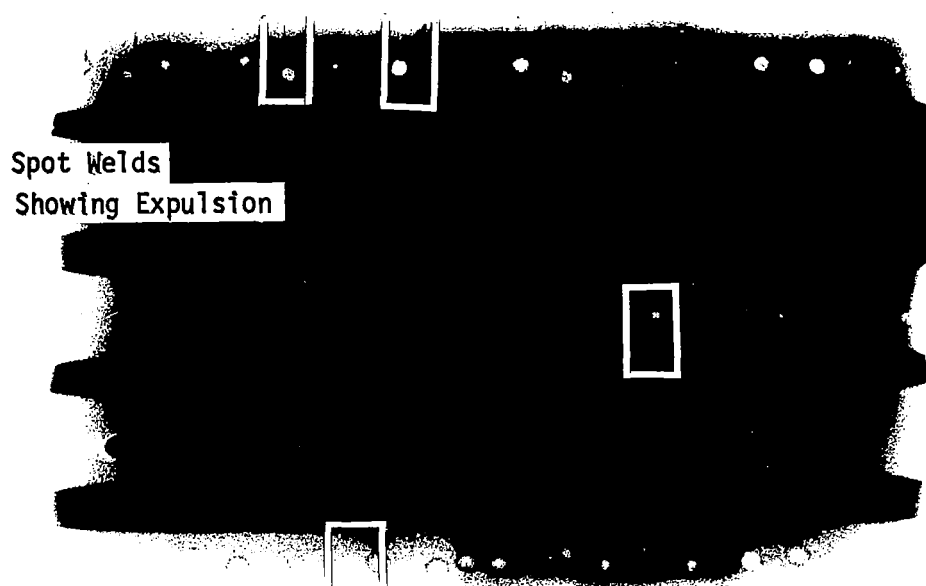


Figure 7-32. X-ray of Spot Welds

## Section 8

### CONCLUSIONS

The present program was conducted to evaluate dispersion-strengthened nickel-base alloys for use as heat shields in a Shuttle Orbiter thermal protection system. The specific alloy selected for evaluation was TD Ni-20Cr, a nickel-base alloy with 20 percent chromium and approximately 2.0-2.5 percent thoria. A two-phase program was conducted, the first phase covering the definition of critical mission environments, evaluation of TD Ni-20Cr material characteristics, comparative studies of thermal protection system designs, and evaluation tests of full scale subsize TPS components of two selected designs. The second phase of the program was devoted to evaluation of a full scale, full size TPS test array under tests that simulated the Orbiter critical environments. Test simulation included application of programmed temperature and differential pressure loads in a reduced atmosphere test chamber plus the separate application of acoustic loads in a second test chamber. Program objectives were to evaluate the application of TD Ni-20Cr heat shields in terms of reuse, refurbishment requirements, weight, and cost. Specific objectives of Phase II efforts included assessment of safe life expectancy, adequacy of design and unit weight of the total TPS, the projected initial cost, overall TPS unit cost for 100 missions, installation requirements and ease of replacement, degree of adequacy of available NDT techniques, and the projected frequency of refurbishment required.

The overall program results led to the following conclusions:

- A. Based on program results, TD Ni-20Cr heat shields provide a viable approach for a Shuttle thermal protection system in areas of the vehicle sustaining operating temperatures up to 1,478°K (2,200°F).
- B. Program test results showed that TD Ni-20Cr heat shields weighing approximately  $7.4 \text{ kg/m}^2$  ( $1.51 \text{ lb/ft}^2$ ) can be used for Shuttle thermal protection systems, with a total TPS weight of  $18.0 \text{ kg/m}^2$  ( $3.69 \text{ lb/ft}^2$ ).

Initial cost of a TD Ni-20Cr metallic radiative thermal protection system is projected as \$7,760 per square meter (\$721/ft<sup>2</sup>) of TPS surface area in terms of 1974 dollars.

- C. Refurbishment costs, based on a heat shield replacement rate of four percent per mission, were added to the projected initial cost to yield a projected total TD Ni-20Cr TPS cost of \$20,950 per square meter (\$1,943/ft<sup>2</sup>) for 100 Shuttle missions. Additional design development could reduce replacement rates to approximately 2 percent, thereby reducing total costs for 100 missions to \$14,860 per square meter (\$1,380/ft<sup>2</sup>).
- D. Flowing air tests conducted with TD Ni-20Cr sample heat shield designs in a plasma-arc stream showed that both overlapping panel edge designs and closure strip designs prevented hot gas ingestion at panel edge joints. Such tests also showed that panels previously subjected to simulated meteoroid impact tests did not suffer additional degradation in the impact areas when exposed to a plasma stream air flow simulating entry conditions.
- E. Properties of the TD Ni-20Cr sheet material used in this program were similar to those of previous quantities of TD Ni-20Cr with the exception that lower tensile elongation at failure was observed from tests of sheet TD Ni-20Cr used in this program for test temperatures of 921°K (1,200°F) and higher. Degradation of tensile properties resulting from programmed cycles of stress, temperature, and low environmental air pressure were more pronounced in the long transverse direction than in the longitudinal (rolling) direction. Observed tensile strength degradations did not significantly affect heat shield weights because compressive buckling stresses in the thin gage panels were critical for design strength. Braze-reinforcement of spot-welded, seam-welded, or diffusion-bonded joints provided significant improvement in fatigue, stress-rupture, and short-time joint strengths.

- F. Cracking in thin gage TD Ni-20Cr sheet material from thermal stresses and mechanical loads at heat shield attachment points proved to be the largest design problem for subsize test panels. Design improvements were incorporated in full size test panels, but small cracks in heat shield face sheets persisted at attach points in the full size panels. Correction of this problem is expected through design refinements that minimize thermal stresses at attachment points by recessing and shortening the attachment bolts and by providing greater accomodation at attachment positions for panel expansion and distortions at elevated temperatures.



## REFERENCES

1. Klingler, L. J., W. R. Weinberger, P. G. Bailey, and S. Baranow. Development of Dispersion-Strengthened Nickel-Chromium Alloy (Ni-Cr-ThO<sub>2</sub>) Sheet for Space Shuttle Vehicles. NASA CR-120796, December 1971.
2. Johnson, R., Jr., and D. H. Killpatrick. Evaluation of Dispersion Strengthened Nickel-Base Alloy Heat Shields for Shuttle Application. Phase I Summary Report, NASA CR-132360, May 1973.
3. Johnson, R., Jr., and D. H. Killpatrick. Evaluation of Dispersion Strengthened Nickel-Base Alloy Heat Shields for Shuttle Application. Phase II Summary Report, NASA CR-132615, May 1975.
4. Anon. Meteoroid Environmental Model-1969 (Near Earth to Lunar Surface). NASA SP-8013, March 1969.
5. Anon. Meteoroid Damage Assessment. NASA SP-8042, May 1970.
6. Anon. Space and Planetary Environment Criteria Guidelines for Use in Space Vehicle Development (1971 Revision). NASA TMX-64627, 15 November 1971.
7. Fritz, L. J. Characterization of Mechanical and Physical Properties of TD Ni-Cr (Ni-20Cr-2ThO<sub>2</sub>) Alloy. NASA CR-121221, 1973.
8. Gulbransen, E. A., and W. R. McMillan. Oxide Film on Nickel-Chromium Alloys. Industrial and Engineering Chemistry, Vol. 45, No. 8, August 1953, pp. 1734-1744.
9. Deveikis, W. D., and L. R. Hunt. Loading and Heating of a Large Flat Plate at Mach 7 in the Langley 8-Foot High Temperature Structures Tunnel. NASA TN-D-7275, September 1973.
10. Haas, D. W. Refurbishment Cost Study of the Thermal Protection System of a Space Shuttle Vehicle. NASA Report CR-111832, 1 March 1971.